

Reconstructing ~~land temperature~~hydroclimate changes of ~~the~~ past 2,500 years using speleothems from Pyrenean caves (NE Spain)

Miguel Bartolomé^{1,2,3*}, Ana ~~Moreno~~⁴Moreno⁴, Carlos ~~Sancho~~⁵Sancho^{5†}, Isabel ~~Cacho~~⁶Cacho⁶, Heather ~~Stoll~~³Stoll³, Negar ~~Haghipour~~^{5,6}Haghipour^{3,7}, Ánchel ~~Belmonte~~⁷Belmonte⁸, Christoph ~~Spöth~~⁸Spöth⁹, John ~~Hellstrom~~⁹Hellstrom¹⁰, R. Lawrence ~~Edwards~~¹⁰Edwards¹¹ and Hai ~~Cheng~~^{11,12}Cheng^{12,13,14}

¹ Departamento de Geología, Museo Nacional de Ciencias Naturales (CSIC), C. de José Gutiérrez Abascal, 2, 28006 Madrid, Spain.

² Swiss Institute for Speleology and Karst Studies (SISKA), Rue de la Serre 68 2300 La Chaux-de-Fonds, Switzerland.

³ Geological Institute, NO G59, Department of Earth Sciences, Sonneggstrasse 5, ETH, 8092 Zurich, Switzerland.

⁴ Department of Geoenvironmental Processes and Global Change, Pyrenean Institute of Ecology (IPE-CSIC), Avda. Montañana 1005, 50059 Zaragoza, Spain,

⁵ Universität zu Köln, Institut für Geologie und Mineralogie, Zùlpicher Str. 49b, 50674 Köln, Germany.

⁶ Earth Sciences Department, University of Zaragoza, C/Pedro Cerbuna 12, 50009 Zaragoza, Spain. Deceased.

⁷ CRG Geociències Marines, Dept. Dinàmica de la Terra i de l'Oceà, Universitat de Barcelona, 08028 Barcelona, Spain

⁸ Geological Institute, NO G59, Department of Earth Sciences, Sonneggstrasse 5, ETH, 8092 Zurich, Switzerland.

⁹ Laboratory for Ion Beam Physics, Department of Physics, ETH Zurich, Switzerland

¹⁰ Sobrarbe-Pirineos UNESCO Global Geopark. Boltaña. Spain.

¹¹ Institute of Geology, University of Innsbruck, 6020, Innsbruck, Austria

¹² School of Earth Sciences, The University of Melbourne, VIC 3010, Australia

¹³ Department of Earth and Environmental Sciences, University of Minnesota, Minneapolis, MN, 55455, USA

¹⁴ Institute of Global Environmental Change, Xi'an Jiaotong University, Xi'an, 710049, China.

¹⁵ State Key Laboratory of Loess and Quaternary Geology, Institute of Earth Environment, 11 Chinese Academy of Sciences, Xi'an, 710061, China.

¹⁶ Key Laboratory of Karst Dynamics, MLR, Institute of Karst Geology, CAGS, Guilin, 541004, China.

* Both authors have contributed equally to this manuscript

Corresponding author: Ana Moreno (amoreno@ipe.csic.es)

Abstract. Reconstructing of past ~~temperatures~~hydroclimates at regional scales during the Common Era (CE) is necessary to place the current warming in the context of natural climate variability. Here we present a composite record of oxygen isotope variations during last 2500 years based on eight stalagmites from four caves in the central Pyrenees (NE Spain) dominated by temperature variations, with precipitation playing a minor role. The dataset is compared with other Iberian reconstructions that show a high degree of internal coherence with respect to variability at the centennial scale. The Roman Period (RP) (especially 0-200 ADCE), the Medieval Climate Anomaly (MCA), and part of the Little Ice Age (LIA) represent the warmest periods, while the coldest decades occurred during the Dark Ages (DA) and most of the Little Ice Age (LIA) intervals (e.g., 520-550 ADCE and 1800-1850 ADCE). Importantly, the LIA cooling or the MCA warming were not continuous or uniform and exhibited high decadal variability. The Industrial Era (IE) shows an overall warming trend although with marked cycles and partial stabilization during the last two

Con formato: Inglés (Estados Unidos)

Con formato: Izquierda, Espacio Después: 10 pto, No agregar espacio entre párrafos del mismo estilo

Con formato: Fuente: +Cuerpo (Calibri), 11 pto

Con formato: Fuente: 10 pto

Con formato: Izquierda

Código de campo cambiado

48 decades (1990-2010). The strong coherence between the speleothem data, European temperature
49 reconstructions and global tree-ring data informs about the regional representativeness of this new record
50 as Pyrenean past [temperature/climate](#) variations. Solar variability, [likely through its impact on the North](#)
51 [Atlantic Oscillation](#), and major volcanic eruptions appear to be the two main drivers of climate in
52 southwestern Europe during the past 2.5 millennia.

53 **Keywords.** Iberian Peninsula, Central Pyrenees, late Holocene, stalagmite, temperature reconstruction

54 1. Introduction

55 Global surface temperatures in the first two decades of the 21st century (2001–2020) were 0.84 to 1.10 °C
56 warmer than 1850–1900 [ADCE](#) (IPCC, 2021). There is strong evidence that anthropogenic global warming
57 is unprecedented in terms of absolute temperatures and spatial consistency over the past 2000 yr ([Ahmed](#)
58 [et al., 2013](#); [Konecky et al., 2020](#)) ([Ahmed et al., 2013](#); [Konecky et al., 2020](#)). On the contrary, pre-industrial
59 temperatures were less spatially coherent, and further work is needed to explain the regional expression of
60 climate change ([Mann, 2021](#); [Neukom et al., 2019](#)) ([Mann, 2021](#); [Neukom et al., 2019](#)). Obtaining new and
61 high-quality records in terms of resolution, dating and regional representativeness is thus critical for
62 characterizing natural climate variability on decadal to centennial scales (PAGES2k Consortium et al.,
63 2017).

64 High mountains are particularly sensitive regions to climate change and among them the Pyrenees occupy
65 a crucial frontier position in southern Europe, influenced by both Mediterranean and Atlantic climates. In
66 the Pyrenees, the temperature has increased by more than 1.5°C since 1882, as shown by the longest time
67 series from the Pic du Midi observatory (Bücher and Dessens, 1991; Dessens and Bücher, 1995). Recent
68 studies confirm this warming trend, showing an increase of 0.1 °C per decade during the last century in
69 Central Pyrenees (Pérez-Zanón et al., 2017), or even 0.28°C per decade if only the 1959-2015 period is
70 considered (Observatorio Pirenaico de Cambio Global, 2018). Long-term snow depth observations (starting
71 in 1955) show a statistically significant decline, especially at elevations above 2000 m a.s.l. (López-Moreno
72 et al., 2020). This fact, together with the increase in temperature, has caused the glaciated area in the
73 Pyrenees to decrease by 21.9% in the last decade (Vidaller et al., 2021), changing from 2060 ha during the
74 [Little Ice Age \(LIA\)](#) to 242 ha in 2016 (Rico et al., 2017). Recent studies on one of the emblematic glaciers
75 in the Pyrenees, the Monte Perdido glacier, show that the current ice retreat is unprecedented in the last 2000
76 years, as this glacier survived previous warm periods such as the [Medieval Climate Anomaly \(MCA\)](#) and
77 the [Roman Period \(RP\)](#) (Moreno et al., 2021b).

78 The study of sediment records from lakes in the Pyrenees, where considerable variations in water level,
79 water chemistry, and biological processes have occurred due to changes in effective moisture and
80 temperature, is an excellent approach to reconstruct past climate variability (González-Sampéiz et al.,
81 2017). Recently, a comprehensive study in six high altitude Pyrenean lakes indicates unprecedented
82 changes in the lithogenic and organic carbon fluxes since 1950 CE, suggesting an increase in algal
83 productivity likely favoured by warmer temperatures and higher nutrient deposition associated to the Great
84 Acceleration (Vicente de Vera García et al., 2023). [Atlantic, a period when human-driven global, social,](#)
85 [technological, and environmental changes intensifying dramatically](#) (Steffen et al., 2015). [Marine](#) records
86 off the Iberian coast show a clear long-term cooling trend, from 0 CE to the beginning of the 20th century,
87 probably reflecting the decline in Northern Hemisphere summer insolation that began after the Holocene
88 optimum (Abrantes et al., 2017). Unfortunately, it is not possible to record [decadal temperature](#) ~~decadal~~
89 changes from the studied proxies of these lake or marine records, so other archives allowing higher
90 chronological robustness and larger resolution are required.

91 The Central Pyrenees are largely composed of limestones and host numerous caves, some of which are rich
92 in speleothems, thus making it possible to reconstruct the past climate by studying stalagmites from
93 different caves. Unfortunately, despite the high potential of stalagmite with annually to sub-annual
94 resolution in the [Common Era \(CE\)](#), it is extremely difficult to obtain high-resolution and well-replicated
95 records. In most cases, the CE period spans only a few centimetres, limiting the number of samples drilled

96 for high-precision U-Th dating (PAGES Hydro2k Consortium, 2017). In addition to this chronological
97 challenge, the interpretation of oxygen isotopes of speleothems ($\delta^{18}\text{O}_c$) from southern Europe is also
98 complex (Moreno et al., 2021a)(Moreno et al., 2021a). Recent studies of Pyrenean stalagmites covering the
99 last deglaciation indicate the important role of changes in annual temperature in the variability of $\delta^{48}\text{O}_c\delta^{18}\text{O}_c$
100 (Bartolomé et al., 2015a; Bernal-Wormull et al., 2021). However, correct interpretation of $\delta^{48}\text{O}_c\delta^{18}\text{O}_c$
101 proxies requires a sound understanding of the influence of climate variables on carbonate deposition in
102 caves through monitoring (e.g. Pérez-Mejías et al., 2018) and calibration to the instrumental period
103 (Mangini et al., 2005; Tadros et al., 2022).

104 In this study, we provide high-resolution $\delta^{48}\text{O}_c\delta^{18}\text{O}_c$ data for eight stalagmites from four different caves in
105 the Central Pyrenees, allowing us to construct a stacked curve of climate variability for the last 2500 years
106 with potential regional representativeness. These eight stalagmites allow climate changes during the CE to
107 be studied in reasonably robust chronological framework. Monitoring and calibration of $\delta^{48}\text{O}_c\delta^{18}\text{O}_c$ with
108 instrumental data for the two youngest stalagmites suggests that the $\delta^{48}\text{O}_c\delta^{18}\text{O}_c$ variability as primarily
109 reflects annual temperatures, while precipitation played a role during certain periods. This new record
110 represents an excellent opportunity to characterize natural temperature changes in this region on decadal to
111 centennial scales for the last 2500 years and compare them with other approaches to examine their regional
112 representativeness.

113 2. Study sites

114 2.1. Geological setting, climate and vegetation

115 This study of speleothems is located in the central sector of the Pyrenees, in northeastern Iberia (Fig.
116 4A, B1a,b). All caves are located in the Sobrarbe Geopark, close to or at the borders of the Ordesa and
117 Monte Perdido National Park, formed in Mesozoic and Cenozoic limestones and at different altitudes (Fig.
118 4C1c). This area has a steep topography due to the high altitudinal gradient and constitutes the largest
119 limestone massif in Europe (with 22 peaks above 3000 m a.s.l.).

120 The climate is Mediterranean according to the Köppen classification. However, the high relief influences
121 the climate of this high-altitude area which is accurately described as humid sub-Mediterranean because of
122 higher rainfall than the typically Mediterranean climate, particularly for the caves above 1000 m a.s.l. where
123 annual precipitation is above 1000-1200mm and falls mostly as snow. In lower altitude caves (e.g. Seso
124 Cave) mean annual precipitation is 900 mm, concentrated in spring and fall. Mean air temperatures range
125 from 0.5 to 15°C, depending on the altitude.

126 Around the caves, in the valleys, there are mid-mountain forests dominated by *Pinus sylvestris* and *Quercus*
127 *ilex*, as well as shrublands, whereas the highlands are characterized by exposed rock with sparse vegetation
128 such as meadows.

129 2.2. Cave locations

130 Seso cave (42°27'23.08"N; 0°02'23.18"E, 794 m a.s.l.) is formed in the eastern flank of the Boltaña
131 Anticline, close to Boltaña village. The cave developed in insoluble marly strata between limestone beds
132 of Eocene age. The cave system consists of two longitudinal shallow galleries (2-33m of limestone
133 thickness over the cave) controlled by the bedding and the main set of joints. Formation of this shallow
134 cave involved the mechanical removal of large amounts of marl under vadose conditions which took place
135 about 60-40 ka BP (Bartolomé et al., 2015b). Subsequently, calcite speleothems formed which became
136 more abundant during the Holocene. Average annual temperature inside Seso cave is ~11.8°C.

137 Las Gloces cave (42°35'40" N, 0°1'41" W, 44001243 m a.s.l.) is located on the border of the Ordesa
138 National Park, next to Fanlo village. The cave formed in limestones of Early Eocene age. The limestone's
139 thickness above the cave is ~20-30 m. Two galleries form the cave. The upper one preserves phreatic

140 features and hosts the majority of speleothems located in a small room, while vadose morphologies
141 characterize the lower gallery. [Average annual temperature where the stalagmites were taken is ~9.8 °C](#)

142 [B-1 cave](#) (42°36'0.2"N; 0°7'46"E; 1090 m a.s.l.) is the lower entrance of the Las Fuentes de Escuaín
143 karstic system, and acts as the collector of all water drained by the system. This system comprises more
144 than 40 km of galleries and shows a vertical extension of -1150 m. It drains an area of ~15 km² and
145 developed mostly in Eocene limestones. Since a river runs through the cave, several detrital sequences
146 appear, as well as speleothems, affected by floods. The cave is then well ventilated and shows annual
147 temperature variations in response to the seasonal ventilation changes and seasonal flooding. The studied
148 sample was obtained in a fossil gallery, not currently influenced by flooding- [and with an average annual](#)
149 [temperature of ~9.5°C](#).

150 [Pot au Feu cave](#) (42°31.48' N; 0°14.26' W; 996 m a.s.l.) is located in the Irués river valley in the Cotiella
151 massif. The host rock is an Upper Cretaceous limestone. Hydrogeologically, the cave belongs to the high
152 mountain unconfined karst Cotiella-Turbón aquifer but located in a non-active level. The cave comprises
153 horizontal galleries and small rooms connected by shafts formed by phreatic circulation. Some rooms are
154 well-decorated by large speleothems. The limestone thickness over the gallery where the stalagmite was
155 collected is approximately 800 m.

156 2.3. Cave climate

157 Understanding the modern microclimatic and hydrological conditions of caves is import for a sound
158 interpretation of speleothem proxy data (Genty et al., 2014; Lachniet, 2009; Moreno et al., 2014).
159 Particularly, the transfer of the stable isotopic signal from the rainfall to the dripwater and, eventually, to
160 the studied stalagmite is influenced by different processes in the atmosphere, soil and epikarst. Our
161 preliminary results for the Pyrenees show a seasonal pattern of precipitation isotopes consistent with the
162 annual temperature cycle ([Moreno et al., 2021b](#)); [Moreno et al., 2021b](#)). These data also suggest [an](#)
163 [interannual](#) temperature- $\delta^{18}\text{O}$ relationship of 0.47‰/°C (Giménez et al., 2021) that is only partially
164 compensated by the -0.18 ‰/°C due to the water-calcite isotope fractionation (Tremaine et al., 2011) thus
165 allowing to use $\delta^{18}\text{O}$ in speleothems as a temperature indicator in this region (see also Bartolomé et al.,
166 2015a; Bernal-Wormull et al., 2021).

167 From the four studied caves, the best monitored one is Seso cave where a detailed monitoring survey was
168 conducted including analyses of $\delta^{18}\text{O}$ variability in rainfall, soil water, dripwater and farmed calcite
169 (Bartolomé, 2016). Seso cave developed under just few metres of rock, while the other caves are much
170 deeper, allowing a faster response to rainfall variability in Seso dripwaters and speleothems. Monitoring
171 carried out in Seso cave indicates a relationship -between temperature and $\delta^{18}\text{O}$ of rainfall observed at
172 seasonal scale [and while rainfall isotopic composition is](#) slightly modulated by the precipitation (Bartolomé
173 et al., 2015a).

174 3. Methods

175 3.1. Speleothem samples

176 This study is based on eight stalagmites from four different caves in Central Pyrenees (Fig. [4C1c](#), Table 1).
177 The specimens were cut parallel to the growth axis and the central segment was sampled for U-Th dating,
178 stable isotopes ($\delta^{18}\text{O}$ and $\delta^{13}\text{C}$) and Mg/Ca. Furthermore, the ¹⁴C-activity of multiple samples from the top
179 of stalagmites MIC and XEV (both from Seso cave and underneath active drips) was determined in order
180 to detect the atmospheric bomb peak induced by the nuclear tests in 1945-1963.

181 Four small stalagmites were obtained from Seso cave, all showing fine laminations consisting of pairs of
182 dark-compact and light-porous laminae, but difficult to count due to their irregular pattern. The four Seso
183 stalagmites show medium to high porosity in some intervals, usually more frequent towards the top. MIC
184 (8.5 cm long) and XEV (26 cm long, composed of two stacked stalagmites - [Appendix Fig. S1-A1.a](#))
185 were sampled from base to top. In stalagmites CHA (8.5 cm long) and in CLA (10.5 cm long), the

186 uppermost interval was discarded due to the poor chronological control and associated to a possible hiatus
187 above a macroscopic discontinuity (Fig. [S1-A1.a](#)).

188 Stalagmites ISA (13.5 cm long, with a visual hiatus at 7 cm above the base) and LUC (23.3 cm long, also
189 with a hiatus at 12.5 cm above the base) were sampled in Las Gloces cave (Fig. [S1-B1.b](#)). Both are candle-
190 shaped with a slight tilt in the growth axis above their respective hiatus. One stalagmite, TAR, was obtained
191 from B1 cave which is an overgrowth over an older stalagmite composed of 7.5 cm of white carbonate that
192 is slightly laminated towards the top (Fig. [S1-C1.c](#)). Finally, a 80 cm-long stalagmite (JAR) was obtained
193 from Pot au Feu cave. It is candle-shaped, laminated and ~~lacks~~ macroscopic hiatuses (Fig. [S1-D1.d](#)).

194 3.2. Stable isotope and Mg/Ca analyses

195 Samples for stable isotopic ($\delta^{18}\text{O}$ and $\delta^{13}\text{C}$) analyses were microdrilled at 1-mm resolution along the growth
196 axis of seven of the eight speleothems (JAR from Pot au Feu was sampled every 5 mm) using a 0.5 mm
197 tungsten carbide dental bur. [One](#)The first batch of the isotopic analyses was analysed at the University of
198 Barcelona (Scientific-Technical Services), Spain, using a Finnigan-MAT 252 mass spectrometer, linked to
199 a Kiel Carbonate Device III, with a reproducibility of 0.02‰ for $\delta^{13}\text{C}$ and 0.06‰ for $\delta^{18}\text{O}$. Calibration to
200 Vienna Pee Dee Belemnite (VPDB) was carried out by means of the NBS-19 standard. A second batch was
201 analysed at the University of Innsbruck using a ThermoFisher Delta V Plus isotope ratio mass spectrometer
202 coupled to a ThermoFisher GasBench II. Calibration of the instrument was accomplished using
203 international reference materials and the results are also reported relative to VPDB. Long-term precision
204 on the 1-sigma level is 0.06‰ and 0.08‰ for $\delta^{13}\text{C}$ and $\delta^{18}\text{O}$, respectively (Spötl, 2011).

205 The elemental chemical composition was analysed in the eight stalagmites (every 1 mm in Las Gloces,
206 Seso and B1 stalagmites and every 5 mm in JAR from Pot au Feu cave) using matrix-matched standards on
207 an inductively coupled plasma-atomic emission spectrometer (Thermo ICAP DUO 6300 at the Pyrenean
208 Institute of Ecology) following the procedure described in Moreno et al. (2010). Reported ratios are from
209 measurement of Ca (315.8 nm) and Mg (279.5 nm), all in radial mode.

210 3.3. U-Th dating and ^{14}C bomb peak

211 A total of 55 samples were prepared for U-Th dating, according to the U and Th chemical procedures
212 described in Edwards et al. (1987). Sample portions characterized by high porosity and voids were avoided
213 to minimize the effect of open system behaviour and possible age inversions. From those 55 samples, 45
214 were measured at the University of Minnesota (USA) and at the Xian' Jiaotong University (China) while
215 10 samples were analysed at the University of Melbourne (Australia) (samples of JAR) using the
216 methodology described in Hellstrom (2006). In the three laboratories, measurements were performed using
217 a MC-ICP-MS (Thermo-Finnigan Neptune or Nu Instruments) following previously described methods
218 (Cheng et al., 2013).

219 Due to the low U content (Table 2), the U-Th ages are not precise enough to obtain an accurate chronology
220 for the recent speleothem growth (see large errors in top samples in Fig. [S1-A1](#)). Therefore, the ^{14}C “bomb
221 peak” method was applied to the MIC and XEV stalagmites that were actively growing in Seso cave at the
222 time of collection (2010 and 2013, respectively), confirmed by U/Th ages, albeit of low precision. We
223 drilled 10 and 8 subsamples for MIC and XEV, respectively (Fig. 2a and b), and ^{14}C activities were
224 measured using a novel online sampling and analysis method combining laser ablation with accelerator
225 mass spectrometry (LA-AMS) at the ETH Zurich (Welte et al., 2016). LA-AMS allows to produce spatially
226 resolved ^{14}C profiles of carbonate minerals with a precision of 1% for modern samples. The background
227 measured on ^{14}C -free marble ($F^{14}\text{C} = 0.011 \pm 0.002$) is low and reference carbonate material is well
228 reproduced. This method relies on the exploitation of the global anthropogenic increase in atmospheric ^{14}C
229 resulting from nuclear testing predominately in the 1950s and 1960s CE as a chronological marker in the
230 mid to late 20th Century (e.g., Genty et al., 1998; Hua et al., 2012). [Atmospheric \$^{14}\text{C}\$ concentrations began
231 to rise in 1955 CE, peaking in the Northern Hemisphere \(NH\) in 1963 AD. Atmospheric \$^{14}\text{C}\$ concentrations
232 began to rise in 1955 CE, peaking in the Northern Hemisphere \(NH\) in 1963 CE \(Reimer, 2004\).](#) Because

233 80 to 90% of the carbon found in most speleothems comes from soil CO₂, this being linked to atmosphere
234 CO₂, it is likely that speleothem ¹⁴C activity is close to the atmospheric ¹⁴C activity or at least to the soil
235 activity (Markowska et al., 2019). Thus, the point where the ¹⁴C concentration begins to rise, the highest
236 concentration point, and the date when the speleothem was removed from the cave (if actively dripping)
237 [waswere](#) used as chronological anchor points (Fig. 2a and b).

238 3.4. Age model

239 Age models were produced using StalAge [software](#) (Scholz and Hoffmann, 2011) for the eight speleothems
240 (Fig. [S4A1](#)) using the U-Th dates presented in Table 2. In the ISA stalagmite, one date was discarded due
241 to the large error (indicated in red in Table 2). During several intervals, two or more stalagmites grew
242 contemporaneously, allowing to test the reproducibility of the proxy records. We made the a priori
243 assumption that the δ¹⁸O data of the selected stalagmites record a common rainfall and temperature signal,
244 given that these caves [arewere](#) only 20 km apart (Fig. [4C1c](#)). Then, the records are combined with *Iscam*
245 (Fohlmeister, 2012), a method that correlates dated proxy signals from several stalagmites, determines the
246 most probable age-depth model, and calculates the age uncertainty for the combined record.

247 In order to minimize the effect of different absolute isotopic values and ranges of individual stalagmite data
248 series, we detrended and normalized the δ¹⁸O series using *Iscam*. Doing so, the interpretation of absolute
249 values will be precluded. Regarding the other parameters that can be changed in *Iscam*, we used point-wise
250 linear interpolation, 1000 Monte Carlo simulations and the smoothing window was fixed at 10 years. The
251 stalagmites were included in [the *Iscam* composite record](#) from the oldest to the youngest one as was the
252 order that provided the highest correlation coefficients: JAR- LUC – ISA -TAR – CHA – CLA -XEV and
253 MIC. The ISA sample was treated as two parts (ISA top and ISA base) to account for the hiatus, while LUC
254 was regarded as only one as StalAge does not suggest a hiatus in this stalagmite (Fig. [S4A1.b](#)). For the two
255 stalagmites that were active when collected, MIC and XEV, we also produced a composite record for the
256 last 200 years using *Iscam* (Fig. 2c).

257 In order to explore correlations among stalagmites from the same caves, we repeated the procedure to obtain
258 a composite record for the four stalagmites from Seso cave (CHA, CLA, XEV and MIC) (Fig. [S2](#)) and the
259 ~~two from Las Gloces cave (ISA and LUC) (Fig. S3). In those two cases, we did not detrend or normalize~~
260 ~~the individual records since they belong to the same cave and show the same range of δ¹⁸O values. These~~
261 ~~four records (composite records from Las Gloces and Seso caves, and individual stalagmites from Pot au~~
262 ~~Feu and B1 caves) are show in Fig. 3 and compared to the final composite record. The composite δ¹⁸O~~
263 ~~record is used in this article as a proxy record for the Central Pyrenees climate of last 2500 years. A2) and~~
264 ~~the two from Las Gloces cave (ISA and LUC) (Fig. A3). In those two cases, we did not detrend or normalize~~
265 ~~the individual records since they belong to the same cave and show the same range of δ¹⁸O values. These~~
266 ~~four records (composite records from Las Gloces and Seso caves, and individual stalagmites from Pot au~~
267 ~~Feu and B1 caves) are show in Fig. 3 and compared to the final composite record. The composite δ¹⁸O~~
268 ~~record is used in this article as a proxy record for the Central Pyrenees climate of last 2500 years. We have~~
269 ~~used approximate onset and end of five time subperiods, following previous literature (eg. Sánchez-López~~
270 ~~et al., 2016): the end of the RP at 450 CE; DA (450-850 CE), MCA (850-1250 CE), LIA (1250-1950 CE)~~
271 ~~and IE (since 1850 CE).~~

272 3.5. Statistical analyses

273 [Statistical analyses were carried out using PAST software \(Hammer et al., 2001\). The δ¹⁸O series and the](#)
274 [instrumental climatic series were first resampled \(linear interpolation\) to obtain the same regular spacing](#)
275 [\(annual\). Then, correlation was computed using Spearman's rank correlation analysis, a nonparametric](#)
276 [measure as an alternative to Pearson correlation analysis. This analysis was preferred to account for](#)
277 [nonlinear relationships, with r indicating the correlation coefficient and p-value, the probability value of](#)
278 [that correlation. The Bonferroni test was applied to prevent data from spuriously appearing as statistically](#)
279 [significant by making an adjustment during comparison testing \(PAST software; Hammer et al. 2001\).](#)

280

281 4. Results

282 4.1. Age models and composite record

283 4.1.1. Detection of the bomb peak and composite record of the last 200 years

284 Stalagmites MIC and XEV from Seso cave were actively dripping when removed from the cave (in 2010
285 and 2013, respectively). Calcite deposited on glass plates placed below the two dripping points and
286 collected seasonally until 2021 demonstrates that the drip water is supersaturated with respect to calcite and
287 suggests that the top layer of both stalagmites was formed during the respective collection year (Fig. 2).
288 Therefore, these two stalagmites were analysed for their ^{14}C activity to identify the “bomb peak” and
289 improve the age model.

290 A strong increase in the ^{14}C activity is registered in the MIC and XEV stalagmites at 16 mm and 40 mm
291 depth from top (dft), respectively (Fig. 2a and b) with a rise in [the fraction modern](#) $F^{14}\text{C}$, interpreted as the
292 start of the mid-20th century atmospheric bomb peak. This allows ~~to define~~[defining](#) the year 1955 [ADCE](#),
293 within $\pm 2\text{yr}$ uncertainties, at 16 mm dft in MIC and 40 mm dft in XEV (Fig. 2). All radiocarbon bomb
294 peaks published from speleothems show that the response of speleothem ^{14}C activity to the increase in
295 atmospheric radiocarbon activity occurred nearly simultaneously. However, whether the ^{14}C activity peak
296 in a speleothem can be assigned to the year 1963 [ADCE](#) depends on the soil properties and the thickness
297 of the rock above the cave, as well as the delay in the transfer of the atmospheric ^{14}C signal to the speleothem
298 (Fohlmeister et al., 2011; Hua et al., 2017). In the case of Seso cave, which is just 2-3 m below the surface
299 and the soils are patchy and thin (Bartolomé, 2016), the transfer of the ^{14}C signal was likely fast. We
300 therefore place the year 1963 [ADCE](#), within $\pm 2\text{yr}$ uncertainties, at 11 mm dft in MIC and at 25 mm dft in
301 XEV (Fig. 2a and b).

302 Since the two stalagmites MIC and XEV are the only ones in this study whose records extend to modern
303 times, we compare them with the instrumental record in order to improve the interpretation of the stable
304 isotope data. Thus, MIC and XEV $\delta^{18}\text{O}$ data were first combined using *Iscam* (Fig. 2c). Using the
305 parameters indicated in Methods (section 3.3), but without normalizing the records (both stalagmites belong
306 to the same cave and show the same [range of](#) $\delta^{18}\text{O}$ values) the correlation of stalagmites MIC and XEV
307 [provided by Iscam software](#) (r) is 0.81 (95% significance). This composite $\delta^{18}\text{O}$ record covers the last 200
308 years and has an amplitude of 0.9 ‰. The main feature (Fig. 2c) is a trend towards less negative values
309 (indicated by a polynomial line in Fig. 2c).

310 4.1.2. StalAge models and Iscam stack

311 Age models obtained by StalAge for individual stalagmites indicate that the growth rate was quite stable,
312 except of ISA and LUC, both from Las Gloces cave, where the growth rate changed after hiatuses (Fig.
313 [S4A1.B](#)). The temporal resolution of the stable isotope data allows to explore changes occurring on a
314 decadal scale (Table 1).

315 Using the parameters for constructing a composite record using *Iscam* (see Methods), correlation (r) value
316 (95% significance) of stalagmite JAR and LUC is 0.48, 0.67 between ISA_base and the combined stack of
317 JAR-LUC, 0.65 between ISA_top and the previous stack, 0.74 between TAR and the previous stack, 0.79
318 between CHA and the previous stack, 0.95 between CLA and the previous stack, 0.71 between XEV and
319 the previous stack and finally, 0.53 between MIC and the previous stack. These values demonstrate a
320 statistically significant correlation among the individual stalagmites and a higher correlation than between
321 the original time series. The composite $\delta^{18}\text{O}$ record was compared to the composite records from Seso (Fig.
322 [S3A3](#)) and Las Gloces (Fig. [S4A4](#)) caves and the two individual stalagmites from the other two caves (Fig.
323 3). This comparison shows that many of the main features of the original records are also well recorded in
324 the composite (Fig. 3). One example is the interval 530-550 [ADCE](#) during the Dark Ages characterized by
325 relatively low $\delta^{18}\text{O}$ values in Las Gloces and Pot au Feu cave records (black arrows in Fig. 3), or the interval

326 at the end of the LIA (1675-1750 [ADCE](#)) with less negative $\delta^{18}\text{O}$ values in Seso, B1 and Las Gloces cave
327 records (this interval is recorded in five stalagmites: CHA, XEV, TAR, LUC and ISA, Figs. [S4A1](#)).

328 4.2. Individual isotopic and Mg/Ca profiles and composite $\delta^{18}\text{O}$ record

329 The isotopic ($\delta^{18}\text{O}$ and $\delta^{13}\text{C}$) and Mg/Ca profiles are shown for the eight stalagmites, using their StalAge
330 models (Fig. [S4A1](#)) for the four caves studied (Seso, Las Gloces, B1 and Pot au Feu). In general, $\delta^{18}\text{O}$ and
331 $\delta^{13}\text{C}$ are not well correlated ($r=-0.23-0.34$; p-values indicating no significant correlation) with the exception
332 of TAR ($r > 0.8$) and CHA ($r=0.5$). Generally, $\delta^{13}\text{C}$ is better correlated with Mg/Ca pointing to a
333 hydrological link of these proxies, via changes in prior calcite precipitation (PCP) associated with the longer
334 residence time of the water in the soil and epikarst during dry periods (Genty et al., 2006; Moreno et al.,
335 2010). ~~A similar interpretation was suggested for other Holocene records from northeastern Spanish caves,~~
336 ~~such as speleothems from Molinos-Ejulte caves in the Iberian Range (Moreno et al., 2017)~~ ~~A similar~~
337 ~~interpretation was suggested for other Holocene records from northeastern Spanish caves, such as~~
338 ~~speleothems from Molinos-Ejulte caves in the Iberian Range (Moreno et al., 2017)~~ and records covering
339 the last deglaciation in the Pyrenees (Bartolomé et al., 2015a). However, $\delta^{13}\text{C}$ and Mg/Ca are highly
340 variable in absolute values and patterns among caves, and further studies are required to better constrain
341 the climate-proxy transfer functions for two parameters. Therefore, we base our paleoclimate interpretations
342 on the oxygen isotopes which are known to show a more robust response to regional climate change.

343 The composite $\delta^{18}\text{O}$ record for the Central Pyrenees of the last 2500 years is shown in Fig. 3. The highest
344 $\delta^{18}\text{O}$ values of last 2500 years were reached during the [Roman-Period \(RP\)](#) (50 [BCBCE](#)-250 [ADCE](#)). The
345 MCA is characterized by two intervals of relatively high values (900-950 [ADCE](#) and 1150-1250 [ADCE](#))
346 and also the LIA shows a one such interval (1675-1750 [ADCE](#)). In contrast, the Dark Ages are characterised
347 by consistently low values. In fact, the most negative interval of last 2500 years is reached at ~520 [ADCE](#),
348 a well-known cold episode related to volcanic eruptions (see section 5.2). A long interval with low $\delta^{18}\text{O}$
349 values corresponds to the onset of the LIA (1250-1500 [ADCE](#), with two very negative excursions) as well
350 as the end of the LIA (1750-1850 [ADCE](#)). The most remarkable feature of the MCA and LIA is the large
351 centennial-scale variability. In fact, the LIA has a clear tripartite pattern, with two intervals of low values
352 at the onset and end and less negative values in between. In contrast, the MCA pattern, although also
353 tripartite, it is characterized by two intervals of less negative values at the onset and end, and a short period
354 of low values in between. An interval with high $\delta^{18}\text{O}$ values is observed since 1950 [ADCE](#) (Fig. 3).

355

356 5. Discussion

357 5.1. Interpretation of $\delta^{18}\text{O}$ data

358 Under equilibrium conditions, the $\delta^{18}\text{O}$ value of speleothem carbonate is related to just two variables: the
359 $\delta^{18}\text{O}$ value of the drip water, and the cave temperature through its control on equilibrium isotope
360 fractionation between water and calcite (Lachniet, 2009). Over the CE, air temperature in a given cave
361 likely changed very little ($< 1\text{ }^\circ\text{C}$ corresponding to $\sim 0.18\text{‰}$ in stalagmite $\delta^{18}\text{O}$, following Tremaine et al.,
362 2011) (PAGES Hydro2k Consortium, 2017) such that the observed $\delta^{18}\text{O}$ variations in these Pyrenean
363 speleothems of more than 1‰ are governed primarily by the $\delta^{18}\text{O}$ variability of the drip water.

364 ~~For a constant sea-surface $d^{18}\text{O}_{\text{sw}}$ value, as it is expected for this time period, event-scale monitoring of the~~
365 ~~isotopic composition of oxygen in the rainwater ($\delta^{18}\text{O}_r$) in different areas of the Iberian Peninsula constrains~~
366 ~~some of the drivers of rainfall isotopic fractionation (Moreno et al., 2021b). Recent rainfall monitoring~~
367 ~~surveys in the Central Pyrenees indicate that the values of $\delta^{18}\text{O}_r$ show a dependence on temperature~~
368 ~~equivalent to $0.47-0.52\text{‰}/^\circ\text{C}$, depending on the station (Giménez et al., 2021; Moreno et al., 2021a). This~~
369 ~~dependence is only partially offset by the empirical value of isotope fractionation during calcite~~
370 ~~precipitation ($-0.18\text{‰}/^\circ\text{C}$; Tremaine et al., 2011) thus allowing to consider temperature as one important~~
371 ~~factor controlling $\delta^{18}\text{O}$ variability over the last 2500 years. Thus, we consider that $\delta^{18}\text{O}_{\text{dw}}$ is driven the $\delta^{18}\text{O}_r$~~

372 signal in the stalagmites and, very likely, air temperature is the dominant factor in modulating its variability
373 along last 2500 years due to the $\delta^{18}\text{O}_c$ large dependence on temperature in this region.

374 The $\delta^{18}\text{O}$ composite record, based on the combination of MIC and XEV $\delta^{18}\text{O}$ data, provides the opportunity
375 to correlate with instrumental temperature data (Fig. S4). TemperatureFor a constant sea-surface $\delta^{18}\text{O}_{sw}$
376 value, as it is expected for this time period, event-scale monitoring of the isotopic composition of oxygen
377 in the rainwater ($\delta^{18}\text{O}_r$) in different areas of the Iberian Peninsula constrains some of the drivers of rainfall
378 isotopic fractionation (Moreno et al., 2021b). Recent rainfall monitoring surveys in the Central Pyrenees
379 indicate that the values of $\delta^{18}\text{O}_r$ show an interannual dependence on temperature equivalent to 0.47–
380 0.52‰/°C, depending on the site (Giménez et al., 2021; Moreno et al., 2021a). This dependence is only
381 partially offset by the empirical value of isotope fractionation during calcite precipitation (–0.18‰/°C;
382 Tremaine et al., 2011) thus allowing to consider temperature as one important factor driving $\delta^{18}\text{O}$
383 variability. Apparently, the rainfall amount does not strongly control the isotopic values at event-scale, but
384 analysing the $\delta^{18}\text{O}_r$ variation through time, added to the strong dependence on air temperature, it is clearly
385 observed how the most intense rainfall events together with the longest lasting rain events (several days)
386 resulted in an isotopic lightening (Giménez et al., 2021). Thus, we consider that dripwater $\delta^{18}\text{O}_{dw}$ is driving
387 the $\delta^{18}\text{O}_c$ signal in the stalagmites and, very likely, air temperature and precipitation amount will be
388 modulating its variability along last 2500 years.

389 The $\delta^{18}\text{O}$ composite record, based on the combination of MIC and XEV $\delta^{18}\text{O}$ data, provides the opportunity
390 to correlate with instrumental temperature and precipitation data (Fig. A4 and A5). It is worth to note that
391 the chronological control of $\delta^{18}\text{O}$ data is robust at decadal-scale, thus limiting an annual accurate
392 correlation. In spite temperature records in the region of the studied caves are, unfortunately, scarce and
393 short (e.g., the Goriz hut station covers only the last 50 years, Fig. S4b). ThereA4b) there are two
394 exceptions, however. First, the homogenized MAAT dataset since 1882 from the Pic du Midi de Bigorre
395 meteorological station (2860 m a.s.l. in the French Pyrenees) (Bücher and Dessens, 1991; Dessens and
396 Bücher, 1995), which started in 1882 ADCE, is the currently longest one from the Pyrenees (Fig. S4eA4c).
397 And, second, the temperature and precipitation reconstruction by Pérez-Zanón et al. (2017) based on 155
398 stations from the Central Pyrenees starting in 1910 ADCE (Fig. S4dA4d). Comparing the MIC and XEV
399 $\delta^{18}\text{O}$ data with those temperature datasets a significant correlation is found with Pic du Midi de Bigorre
400 mean annual minima temperature ($\sigma_s = 0.32$; p-value<0.005). Likely, the other temperature records were
401 too short to generate a significant correlation.

402 Additionally, when comparing our $\delta^{18}\text{O}$ stack with the HadCRU5 reconstruction for the mean Northern
403 Hemisphere temperatures (Morice et al., 2021) (Fig. S4eA4e), the correlation is higher and
404 significant ($\sigma_s = 0.49$; p-value<0.005). We suspect that the length of this last series (150 years)
405 together with a large spatial scale leads to a better correlation with the speleothem composite. However, a
406 large part of the variance remains to be explained by other factors (i.e. precipitation changes in source,
407 seasonality or amount). Using these relationships as a guide, a change and considering all the isotopic
408 change related to temperature change, the observed variation of 0.30 – 0.32 ‰ in $\delta^{18}\text{O}$ of our composite
409 would represent a change of 1°C (Fig. S4) whatA4), that appears quite plausible for the studied period.
410 Still, at least a small part of the isotopic change in the studied speleothems could be related to precipitation
411 and thus reducing the temperature effect.

412 The influence of precipitation variability on the $\delta^{18}\text{O}$ speleothem composite is evident from 1965/1970 to
413 1985 AD1980 CE, a relatively cool interval in the Pyrenees but characterized by lowcharacterized by a
414 sustained decrease in precipitation (Pérez-Zanón et al., 2017) (Fig. S5, note reversed axis for precipitation).
415 For this interval, the relationship between the $\delta^{18}\text{O}$ composite and temperature series is reversed, as the low
416 precipitation leads to higher $\delta^{18}\text{O}$ values (as if they represented higher air temperatures). This shows that,
417 in spite air temperature being an important factor influencing $\delta^{18}\text{O}$ variability in speleothems from the
418 Pyrenees, other processes such as the amount of precipitation or even its source(s) may be also a significant
419 controlling factor, especially when extreme values are reached (very dry or very wet time intervals). In any

420 ease, MIC and XEV $\delta^{18}\text{O}$ data are not significantly correlated with any of the precipitation data from Fig.
421 S5.

422 Finally, it is important to note that (Fig. A5, note reversed axis for precipitation). For this interval, the
423 relationship between the $\delta^{18}\text{O}$ composite and temperature series is reversed, as the low precipitation leads
424 to higher $\delta^{18}\text{O}$ values (as if they represented higher air temperatures). On the contrary, a rapid increase in
425 precipitation at ca. 1960 without any important change in temperature, results in a negative peak on the
426 $\delta^{18}\text{O}$ speleothem composite (Fig. A5). This shows that, in spite air temperature being an important factor
427 influencing $\delta^{18}\text{O}$ variability in speleothems from the Pyrenees, other processes such as the amount of
428 precipitation or even its source(s) may be also a significant controlling factor (Priestley et al., 2023; Treble
429 et al., 2022), especially when extreme values are reached (very dry or very wet time intervals), as was
430 indicated by rainfall studies in the Pyrenees (Giménez et al., 2021; Moreno et al., 2021a). In any case, MIC
431 and XEV $\delta^{18}\text{O}$ data are not significantly correlated with any of the precipitation data from Fig. A5.

432 Finally, it is important to note that the $\delta^{18}\text{O}$ values in the different caves varied at distinct range (Fig. 3).
433 Thus, when producing the composite record, the $\delta^{18}\text{O}$ profiles of the eight stalagmites were normalized and
434 detrended with the aim of combining different caves where $\delta^{18}\text{O}$ from the speleothems varies at distinct
435 range (Fig. 3). With such a procedure, it is really complicated to compare comparing relative temperature
436 changes coming from different time periods is not possible. Thus, for example, comparing the warming
437 magnitude of the RP with the MCA or with the IE is not feasible since data were obtained from different
438 caves and were previously normalized and detrended. Unfortunately, none of our stalagmites cover
439 continuously from a warm period, i.e. the MCA, to current conditions to compare values. Therefore, the
440 ability of current data to accurately quantify changes in temperature for last 2500 years in the Central
441 Pyrenees is limited. Normalized $\delta^{18}\text{O}$ composite record is evaluated in the context of previous local,
442 regional and global information.

443 5.2 TemperatureClimate reconstruction for the last 2500 years

444 The Pyrenees is a region threatened by global warming, where the impact on biodiversity, elements of the
445 mountain cryosphere such as glaciers or ice caves, and water resources has been increasing in recent
446 decades (<https://www.opcc-ctp.org>). In this context, it is of great importance to analyse archives of past
447 temperature to reconstruct natural variability and disentangle main driving mechanisms. The $\delta^{18}\text{O}$
448 composite constructed using eight speleothems represents the first climate reconstruction based on
449 speleothems for this region covering the last 2500 years and provides an excellent opportunity to
450 reconstruct natural variability and disentangle main driving mechanisms. We compare it first with other
451 climate series from the Pyrenees and northern Iberia (section 5.2.1) and, then, with available speleothems
452 from Europe and western Mediterranean to obtain a regional overview (section 5.2.2). Finally, a short
453 discussion about the potential drivers of main observed changes is provided (section 5.2.3).

454 5.2.1. The last 2500 years in the context of the Iberian Peninsula

455 Previous climate reconstructions for the CE from the Pyrenees were mostly based on lake records (e.g.,
456 González-Sampérez et al., 2017), tree-ring data (e.g., Büntgen et al., 2017), and few data from glaciers or
457 ice caves (Moreno et al., 2021b; Oliva et al., 2018; Sancho et al., 2018; Leunda et al., 2019). Despite large
458 variability, these records reveal a clear distinction between relatively cold (DA, LIA) and warm (RP, MCA)
459 periods, which were generally characterized by high and low lake levels, respectively. The differences and
460 similarities among Pyrenean records merit a more detailed evaluation, organized by chronological
461 periods. (Moreno et al., 2021b; Oliva et al., 2018; Sancho et al., 2018). Observations from four of the best
462 studied lakes in the Southern Pyrenees (Basa de la Mora, 1914 m a.s.l., Pérez-Sanz et al., 2011; Estanya,
463 670 m a.s.l., Morellón et al., 2011; Riera et al., 2006; Redon, 2240 m a.s.l., Pla and Catalan, 2005 and
464 Monteortès, 1027 m a.s.l., (Corella et al., 2016, 2014, 2012, 2011; Rull et al., 2011; Scussolini et al., 2011;
465 Vegas-Vilarrúbia et al., 2022) were compiled by González-Sampérez et al. (2017). Despite large variability,
466 these records reveal a clear distinction between relatively cold (Dark Ages, LIA) and warm (RP, MCA)

467 periods, which were generally characterized by high and low lake levels, respectively. Interestingly, a
468 record of heavy precipitation obtained from the abundance of detrital layers in the laminated record of
469 Monteortés lake shows a good correspondence with the Pyrenean speleothems during some intervals (Fig.
470 4b), highlighting the link between precipitation and $\delta^{18}\text{O}$. This similarity is specially marked during the
471 MCA and the LIA where, although with a slight asynchrony (likely related to age model uncertainties), low
472 values in $\delta^{18}\text{O}$ correlate with higher precipitation and vice versa. Therefore, it is expected that an increase
473 in precipitation in the Pyrenees, as deduced from the Monteortés lake record, would have had a significant
474 influence on the $\delta^{18}\text{O}$ values. The other lake record we compared to the speleothem record is Estanya lake,
475 whose palaeo-salinity data provide a clue to the hydroclimate in the Pre-Pyrenees (Morellón et al., 2012;
476 2009) (Fig. 4c). The Estanya record indicates a general increase in salinity during the second part of the
477 MCA (and thus a comparably warm and dry climate), while low salinity prevailed during the LIA
478 (corresponding to a cooler and more humid climate). This pattern is also well reproduced in the
479 speleothems, albeit with a different short-term variability.

480 There are no data from ice caves in the Pyrenees spanning the CE, with the exception of the last ice
481 accumulation phase in the A298 ice cave (Cotiella massif) (Fig. 4d) (Sancho et al., 2018) that stopped at
482 the thermal maximum of the Roman Period, in spite it may continue growing during following cold periods.
483 Tree-ring records spans the period 1186–2014 AD and reveal overall warmer conditions around 1200 AD
484 (Büntgen et al., 2017) coinciding with the speleothem composite presented here, and again around 1400
485 AD (Fig. 4c). ~~The differences and similarities among Pyrenean records merit a more detailed evaluation,~~
486 ~~organized by chronological periods.~~

487 **A. The Iberian - Roman period in the Pyrenees.** Considering the last 2500 years, the Roman Period (RP)
488 stands out as ~~the warmest a clear warm~~ period from the speleothem composite record (Fig. 4a). In the Eastern
489 Pyrenees, Redon Lake records low winter-spring temperatures with a warming trend at the end (Pla and
490 Catalan, 2005; Pla-Rabes and Catalan, 2011), whereas the summer-autumn temperatures show a transition
491 from cold to warm (Catalan et al., 2009). ~~Only very few~~ ~~Not many high-resolution~~ Pyrenean
492 ~~temperature lake~~ records exist, ~~because lacustrine proxies are more sensitive to humidity than in temperature~~
493 ~~changes for this period~~ (e.g. Corella et al., 2016; Vegas-Vilarrúbia et al., 2022) and dendrochronological
494 studies in this mountain range do not cover this time period. Thus, an interesting record to compare with is
495 the A294 ice cave in the Cotiella massif (Sancho et al., 2018). This 9-m thick ice is divided into intervals
496 of low and high snow accumulation, requiring moist and cold conditions to form. The fourth (and last) stage
497 of this ice deposit indicates a high accumulation rate (Fig. 4d), thus a relatively humid and cold period,
498 from 500 BC to 62 ADCE. Afterwards, the record stopped reflecting the onset of a warmer and drier climate
499 (Sancho et al., 2018) associated with the RP thermal maximum (Fig 4a), ~~in spite recent~~. ~~Recently, not yet~~
500 ~~published~~ observations indicate the ice deposit grew during the ~~cold/wet years associated to the~~ DA (M.
501 Bartolomé, personal communication). In our speleothem composite, the RP is represented by Las Gloces
502 and Pot au Feu stalagmites that show less negative values (Fig. 3), which suggest rather warm, and probably
503 dry conditions in the Central Pyrenees during the RP, particularly ~~during from between~~ 0 to 200 ADCE (Fig.
504 4). This is supported by data showing retreating glaciers in the Pyrenees at that time (Moreno et al., 2021b).

505 **B. The Dark Ages in the Pyrenees.** ~~This period after the fall of the Western Roman Empire (Helama et al.,~~
506 ~~2017) is characterized in our~~ ~~speleothem composite by cold temperatures starting ca. 300 AD, with two~~
507 ~~particular cold events at 500-650 AD and 750-850 AD and a warmer interval in between (650-750 AD)~~
508 ~~(Fig. This period is characterized in our speleothem composite by cold-wet climates starting ca. 300 CE,~~
509 ~~with two particular cold events at 500-650 CE and 750-850 CE and a warmer-drier interval in between~~
510 ~~(650-750 CE) (Fig. 4a).~~ Pyrenean lake records also point to cold and wet conditions but with a high
511 heterogeneity and low resolution, thus preventing a detailed characterization of this time period (González-
512 Sampéris et al., 2017). For example, Estanya Lake recorded a dominant dry climate between 500 and 750
513 ADCE (Fig. 4c), changing to higher lake levels afterwards (Morellón et al., 2009), a pattern that is ~~quite~~
514 coherent with the speleothem composite. Proxy data from Redon Lake suggest cold winter-spring
515 temperatures in the Eastern Pyrenees during the DA (Pla and Catalan, 2005, 2011).

516 *C. The Medieval Climate Anomaly in the Pyrenees.* The large centennial-scale temperature variability
517 recorded by the speleothem composite is particularly well expressed for the MCA and the LIA, with three
518 distinct intervals of temperature changes (yellow and blue bands in Fig. 4a), thus revealing a more complex
519 pattern as previously inferred by lower resolution records (e.g., Moreno et al., 2012; Sánchez-López et al.,
520 2016). The MCA has been interpreted as a “warm and dry” climate regime in the Southern Pyrenees
521 (Morellón et al., 2012) (Fig. 4c), characterized by low lake levels and more abundant xerophytic vegetation.
522 Our new data show, however, that a colder (~~maybe wetter~~) interval between 950 and 1050 ADCE separated
523 two clear warm periods before (900-950 ADCE) and after (1150-1250 ADCE; Fig. 3); ~~this intervening cold~~
524 ~~phase was one of the coldest ones in the last 2500 years (Fig. 4a).~~ This cold interval was also identified in
525 the Redon Lake record as a sudden cooling about 1000 years ago (Pla and Catalan, 2005). Interestingly,
526 this cold century was not observed by an increase in precipitation in the Montcortés lake record (Fig. 4b).

527 *D. The Little Ice Age in the Pyrenees.* The LIA climate variability is well-characterized in the Pyrenees
528 thanks to records from glaciers, such as moraines associated with glacier advances, but also due to historical
529 documents such as pictures or old photographs (Oliva et al., 2018). The available information indicates that
530 the LIA glaciers in the Pyrenees occupied 3366 ha in 1876, just 810 ha in 1984 and these glaciers have lost
531 23.2% of their volume considering only from 2011 to 2020 (Hughes, 2018; Vidaller et al., 2021). In many
532 Pyrenean valleys, more than one moraine belt was assigned to the LIA (García-Ruiz et al., 2014) but,
533 unfortunately, the discontinuous character of these landforms and difficulties in dating them does not allow
534 to resolve the internal pattern of the LIA in the Pyrenees. A recent compilation of records across the Iberian
535 mountains proposed several climate phases during the LIA (Oliva et al., 2018), which are well-correlated
536 with our speleothem composite (Fig. 4a): A first cooling phase lasted from the onset of the LIA (ca. 1200
537 ADCE) until 1480 ADCE, followed by relatively warmer conditions from 1480 to 1570 ADCE. A second
538 phase of gradual cooling occurred until 1600 ADCE followed by very cool conditions lasting until 1715
539 ADCE and coinciding with the Maunder Minimum (1645 – 1715AD1715CE). In our speleothem
540 composite, this interval is well defined as a cold period but it was not the ~~coldest one~~ ~~one with minimum~~
541 ~~$\delta^{18}\text{O}$ values~~ of the LIA (Fig. 4a). The first half of the 18th century was characterized by warm conditions,
542 supported by many records compiled by Oliva et al. (2018). After 1760 and until the end of the LIA (ca.
543 1850 ADCE), a climate deterioration and more frequent extreme climate events were described. This last
544 cold phase is also captured by the speleothem composite and may correspond to the Dalton Minimum (1790
545 – 1830 ADCE). It is characterised by ~~high~~ ~~large~~ ~~climate~~ variability and lasted until about 1850 ADCE.

546 *E. The Industrial Era in the Pyrenees.* The Industrial Era (IE), defined as the last 150 years, is characterized
547 in the Pyrenean speleothem composite by low temperatures that started to increase at about 1950 ADCE
548 (Fig. 4a), in response to the Great Acceleration (Steffen et al., 2015) (yellow band in Fig.4). This increase
549 of temperature is well recorded in other Pyrenean climate archives, such as glaciers or lake records. Thus,
550 the last 150 years were marked by a gradual glacier retreat since 1850 ADCE that accelerated specially
551 after 1980 ADCE, considered as a “tipping point” in glacier retreat not only on a Pyrenean scale (López-
552 Moreno et al., 2016) but also on a global scale (Beniston et al., 2018). ~~For the last 150 years, in spite it is~~
553 ~~difficult to disentangle among climate change and human impact on the lacustrine records, a~~ decrease in
554 heavy rainfall (Fig. 4b) and an increase in salinity (Fig. 4c) are well defined in Montcortés and Estanya lake
555 records, respectively, ~~during the IE, indicating a decrease in precipitation in a, likely, drier scenario.~~
556 Besides, ~~recent high-resolution these two lake records obtained from, high-altitude lakes indicates~~ ~~show~~ a
557 significant increase in lake primary productivity during the last decades ~~as the result of combined impacts~~
558 ~~of climate change and increased human pressure in the Pyrenees~~ (Vicente de Vera García et al., 2023). ~~In~~
559 ~~spite~~ ~~These recent results demonstrate the combined impacts of climate change and increased human~~
560 ~~pressure in the Pyrenees. Coherently,~~ last 50 years are characterized ~~as one of the warmest intervals by~~
561 ~~generally enriched $\delta^{18}\text{O}$ values~~ in our speleothem record (yellow bands in Fig. 4a). ~~However,~~ the last two
562 decades (our record ends in 2013, the year XEV sample was collected) are not the ones with the highest
563 $\delta^{18}\text{O}$ values (Fig. 4a) as also observed in tree-ring data from the Spanish Central Pyrenees (Büntgen et al.,
564 2017) (Fig. 4c). ~~In general, all available records from the Pyrenees isolate last 70–80 years as a period with~~
565 ~~a notable increase in temperature in the context of last 2500 years~~ ~~One potential explanation for the lack of~~
566 ~~exceptionally high $\delta^{18}\text{O}$ values would be a slight increase in precipitation amount. Thus, precipitation~~

reconstruction for the Pyrenees during the last two decades indicate slightly higher values than those of previous decades (Pérez-Zanón et al., 2017, Fig. A.5). Other factors, such as changes in the precipitation source or type (eg. dominance of Atlantic frontal rainfall versus Mediterranean convective episodes) may be also behind the recorded $\delta^{18}\text{O}$ values of last decades.

5.2.2. Temperature variability in W Europe and the W Mediterranean during last 2500 years

The PAGES2k European temperature record is the most recent compilation of the last two millennia at European scale (PAGES 2k Consortium, 2013) and it is coherent with our speleothem composite for the Central Pyrenees (Fig. 6). This comparison shows a synchronicity for several of the warmest intervals of the CE, such as the first centuries CE in the RP, the 1150-1250 CE period within the MCA, and the last decades (marked as orange bars in Fig. 6). There are very few high-resolution speleothem records in Europe covering the CE (Comas-Bru et al., 2020). We compare the Central Pyrenean speleothem composite with nine selected; we selected nine speleothems records in Europe and northern Africa which cover with robust chronology and decadal resolution the last 2500 years (Fig. 5). One of these records is interpreted as NAO variability (Baker et al., 2015), three are paleo-precipitation reconstructions (Ait Brahim et al., 2019; Cisneros et al., 2021; Thatcher et al., 2022) and the other five are reflecting paleo-temperature variations (Affolter et al., 2019; Fohlmeister et al., 2012; Mangini et al., 2005; Martín-Chivelet et al., 2011; Sundqvist et al., 2010). Considering these differences in the interpretation and the fact these records are from different regions with different climates (from Sweden to Morocco), dissimilar profiles of paleoclimate variability can be expected. Still, some features are comparable and can be discussed to obtain a super-regional picture.

A. The Roman period in Europe-W Mediterranean. In Europe, and particularly in the Mediterranean region, the RP is well-known as a warm period (e.g., McCormick et al., 2012). The average sea-surface temperature in the western Mediterranean Sea was 2°C higher than the average temperature of the late centuries (Margaritelli et al., 2020). Our composite, with high values of normalized $\delta^{18}\text{O}$ values during the whole RP, and particularly from 0-200 ADCE, agrees with the scenario of warm temperatures (Fig. 5i). Speleothem data from the Balearic Islands (Cisneros et al., 2021) indicate a transition from humid to dry conditions along the Iberian-RP (Fig. 5c). The dry period at the end of the RP in the Balearic record, appears in agreement with a new speleothem record from northern Italy (Hu et al., 2022), suggesting that the observed drying trend was a possible contribution to the collapse of the Roman Empire in 476 ADCE. Record from Morocco (Ait Brahim et al., 2019), contrarily, marks a humid trend at the end of the RP (Fig. 5d). Similarly, an increase in humidity was observed in southern Iberia during the Iberian-Roman Period RP (Jiménez-Moreno et al., 2013; Martín-Puertas et al., 2009) thus reflecting a large spatial heterogeneity in precipitation during the RP when comparing records from the north and south of the Mediterranean basin.

B. The Dark Ages in Europe-W Mediterranean. After the RP, the cold Dark Ages started (450-850 ADCE). Part of this period is known as the “Late Antique Little Ice Age” (LALIA), lasting from 536 ADCE to 670 ADCE, characterized by specially cold conditions in Europe (Büntgen et al., 2016). Our speleothem composite shows in general cold-wet conditions, but with centennial-scale variability during the DA (Fig. 5). Three clear intervals can be defined in terms of temperature, following the $\delta^{18}\text{O}$ pattern of our composite, as well as speleothem records from the Alps (Mangini et al., 2005) and Central Europe (Affolter et al., 2019; Fohlmeister et al., 2012): an initial cooling phase corresponding to the LALIA (ca. 500-650 ADCE), a warming phase (ca. 650-750 ADCE) and a final cooling phase right before the onset of the warming associated with the MCA (ca 750-850 ADCE). A $\delta^{13}\text{C}$ speleothem record from three N Iberian caves (Martín-Chivelet et al., 2011) shows a warming trend in the DA period but with internal variability that, within dating uncertainties, can be related to the three phases defined above (Fig. 5i). It is worth noting that the coldest period with the most negative $\delta^{18}\text{O}$ values recorded in the speleothem composite from the Pyrenees corresponds to the LALIA decades, a cooling period which provoked widespread social disruption in Europe, famine, and episodes of epidemic diseases (Peregrine, 2020).

C. The Medieval Climate Anomaly in Europe-W Mediterranean. The MCA was one of the warmest periods in continental Europe (and the W Mediterranean, Lüning et al., 2019) of the CE, usually dated to 900 ADCE

615 to 1300 ADCE and characterized by warm (Goosse et al., 2012) and relatively dry conditions (Helama et
616 al., 2009). The MCA was also characterized by a general glacier retreat, mainly associated with a decline
617 in precipitation in the Alps (Holzhauser et al., 2016) and the Pyrenees (Moreno et al., 2021b). This scenario
618 is supported by speleothem records from Europe and the W Mediterranean (Fig. 5), which all point to
619 generally warm (Affolter et al., 2019; Fohlmeister et al., 2012; Mangini et al., 2005; Martín-Chivelet et al.,
620 2011; Sundqvist et al., 2010) and/or dry conditions (Ait Brahim et al., 2019; Baker et al., 2015; Thatcher et
621 al., 2022), even leading to speleothem growth stops as for example seen in the Balearic record (Cisneros et
622 al., 2021). Previous studies have emphasized the complexity of the spatial and seasonal structure of the
623 MCA in Europe (Goosse et al., 2012). The selected speleothem records underscore this complexity,
624 particularly considering that in our Pyrenean composite one of the ~~coldest periods of the last 2500~~
625 ~~years marked as cold-wet~~ occurred during the MCA, ca. 950-1050 ADCE (Fig. 5). We propose that this
626 cold interval represents the climate response to the Oort solar minimum in the Pyrenees, a time period
627 characterized by low number of sunspots covering spanning 1010 to 1050 ADCE (Bard et al., 2000).

628 ~~It has been widely debated if the MCA was warmer than current conditions. This controversy has not totally~~
629 ~~been resolved using proxy records, especially since comparisons with modern conditions are difficult due~~
630 ~~to the small number of high quality records covering continuously the last 1500 years (e.g., Bradley et al.,~~
631 ~~2003). In our case, none of the studied speleothems cover continuously from the MCA to current times~~
632 ~~(Fig. 3) and, since records were detrended and normalized to construct the composite profile, that~~
633 ~~comparison among the MCA and the IE is precluded.~~

634 *D. The Little Ice Age in Europe-W Mediterranean.* The LIA is well known in Europe and the W
635 Mediterranean region, characterized by cold temperatures and relatively humid conditions as recorded, for
636 example, in chironomid-inferred summer temperatures (Ilyashuk et al., 2019), Mediterranean SSTs
637 (Cisneros et al., 2016), the advance of alpine glaciers (Holzhauser et al., 2016) and the rise of lake levels
638 (Magny, 2013). The LIA cooling, however, was not continuous and uniform in space and time. Regarding
639 temperatures, many of the available reconstructions from the Alps (Trachsel et al., 2012), Scandinavia
640 (Zawiska et al., 2017), and other regions of Europe (Luterbacher et al., 2016), provide evidence for a main
641 LIA cooling phase which was divided into three parts: two cold intervals with a slightly warmer episode in
642 between, with the most severe cooling during the 18th century (Ilyashuk et al., 2019). This pattern is also
643 found in the two temperature records from Iberian speleothems (this study and the one from Martín-
644 Chivelet et al., 2011) and a temperature record from the Alps (Mangini et al., 2005) (Fig. 5, marked by
645 arrows). The other European speleothem records show only two phases during the LIA: a longer and intense
646 cooling period followed by a warming (Fig. 5, Affolter et al., 2019; Fohlmeister et al., 2012; Sundqvist
647 et al., 2010). A tripartite pattern is recorded by humidity-sensitive speleothems from Portugal, with wet-dry-
648 wet conditions in excellent agreement with the cold-warm-cold pattern in the Pyrenean record (this study),
649 supporting the concept that this pattern is controlled by changes in intensity and N-S migration of the Azores
650 High (Thatcher et al., 2022).

651 *E. The Industrial Era in Europe-W Mediterranean.* Between about 1870 ADCE and today, an increase in
652 temperature is detected by European speleothem records (Fig. 5), as previously shown by the retreat of
653 European glaciers (Beniston et al., 2018) and tree-ring summer temperature records (Büntgen et al., 2011)
654 as well as drought reconstructions (Büntgen et al., 2021). The impacts in Europe and the W Mediterranean
655 of the current global warming trend, accelerated during last 50 years, are becoming more and more evident
656 (Jacob et al., 2018; Naumann et al., 2021).

657 5.2.3 Drivers of past temperature variability in the Pyrenees

658 ~~Although there is a good agreement among the continental records of the last two millennia in terms of~~
659 ~~temperature variability, providing widespread evidence of a warm RP and MCA and a cold DA and LIA, a~~
660 ~~detailed comparison highlights regional differences at multi-decadal to centennial time scales (PAGES 2k~~
661 ~~Consortium, 2013). As an example, by using an extended proxy data set, the PAGES 2k Consortium~~
662 ~~confirmed that the MCA was not globally synchronous (PAGES2k Consortium et al., 2017). Still, in~~

663 Europe, the record produced in the PAGES2k exercise is coherent with our speleothem composite for the
664 Central Pyrenees, particularly for some periods (Fig. 6).

665 This comparison shows a synchronicity between the PAGES2k European record and the Pyrenean
666 composite for several of the warmest intervals of the CE, such as the first centuries AD in the RP, the 1150-
667 1250 AD period within the MCA, and the last decades (marked as orange bars in Fig. 6). The good
668 correlation and synchronicity between the PAGES2k European record and the Pyrenean composite (marked
669 as orange bars in Fig. 6) supports the interpretation of temperature being the dominant factor in controlling
670 the speleothem record. This centennial-scale correlation can be extended to a worldwide tree-ring
671 compilation (Sigl et al., 2015) pointing to the presence of common warm periods in the Central Pyrenees.
672 Similarly, interestingly, if precipitation was the dominant factor controlling the $\delta^{18}\text{O}$ speleothem composite,
673 it would be difficult to find a common signal at regional or even continental scale, as indicated by the
674 overall good correlation shown in Fig. 6.

675 It is worth to mention also the good correlation with several especially cold periods at decadal scale (blue
676 bars in Fig. 6), such as the event at 540-550 ADCE (registered at 520 ADCE in the speleothem record) or
677 two cold spikes at 800-850 ADCE at the end of the DA. We proposed that the cold event at ca. 540
678 ADCE (the coldest of the speleothem record) may be related to a cataclysmic volcanic eruption that took
679 place in Iceland in 536 ADCE and spewed ash across the Northern Hemisphere, together with the effect of
680 two other massive eruptions in 540 and 547 AD (Sigl et al., 2015). CE (Fig. 6b, Sigl et al., 2015). An
681 unprecedented, long-lasting and spatially synchronized cooling was observed in European tree-ring records
682 associated with these large volcanic eruptions, corresponding to the LALIA period (Büntgen et al., 2016).
683 Therefore, volcanic events, at least the large ones such that from 536 CE in Iceland, have an effect driving
684 temperature variations in the Pyrenean region.

685 Besides, there is also an evident synchrony between the European record and the Pyrenean
686 speleothems in several of the more recent coldest intervals of the MCA and the LIA (dark blue bars in Fig.
687 6), probably a regional response to minima in solar irradiance as these events correspond to minima in
688 sunspot numbers: 1010-1050 AD (Oort minimum), 1280-1350 AD (Wolf minimum), 1450-1550 AD
689 (Spörer minimum), 1645-1715 AD (Maunder minimum) and 1790-1820 AD (Dalton minimum). (Fig. 6c,
690 (Usoskin et al., 2014, 2016): 1010-1050 CE (Oort minimum), 1280-1350 CE (Wolf minimum), 1450-1550
691 CE (Spörer minimum), 1645-1715 CE (Maunder minimum) and 1790-1820 CE (Dalton minimum).
692 Because variations in total solar irradiance are relatively small, on the order of a few tenths of Wm^{-2} , the
693 mechanism that could result in a detectable cooling remains uncertain (Gray et al., 2010). The most likely
694 connection is via changes in the large-scale atmospheric circulation of the Northern Hemisphere. While some
695 studies discarded the idea that there has been a strong direct radiative influence of solar forcing on Northern
696 Hemisphere temperatures in the past millennium (Schurer et al., 2014), other authors demonstrated a
697 connection among solar variability and climate throughout changes in the large-scale atmospheric
698 circulation of the Northern Hemisphere, such as the North Atlantic Oscillation (NAO) (Martin-Puertas et
699 al., 2012). These circulation changes occur primarily through a forced shift toward the low index state of
700 the Arctic Oscillation/North Atlantic Oscillation as solar irradiance decreases, leading to colder
701 temperatures over the Northern Hemisphere continents. The NAO was proposed as a plausible mechanism
702 to explain climate changes in Europe during the MCA vs LIA periods through the study in combination of
703 proxy records and model simulations (Trouet et al., 2009; Mann et al., 2009). Thus, it was postulated that
704 the MCA/LIA transition included a weakening of the Atlantic Meridional Overturning Circulation (AMOC)
705 and a transition to more negative NAO conditions, resulting in a strong cooling of the North Atlantic region
706 and an increase in the storm intensity (Trouet et al., 2012).

707 Such a connection among solar irradiance and temperature over Europe is then manifested through a change
708 in the pressure gradient in the Atlantic that resembles a negative phase of the NAO and results in lower
709 temperatures over Europe but also in a southward shift of the storm tracks enhancing precipitation over
710 central and southern Europe (Swingedouw et al., 2011). As solar irradiance decreases, colder temperatures
711 over the Northern Hemisphere continents are observed, especially in winter (1° to 2°C), in agreement with

712 historical records and proxy data for surface temperatures (Shindell et al., 2001). ~~A low NAO index may~~
713 ~~also be the driver of variations in the abundance and magnitude of floods in Europe~~ Coherently, most
714 episodes of flooding in northwest and northern Europe region match with multi-decadal periods of grand
715 solar minima and are thus also associated to the negative phase in the NAO index (Benito et al., 2015) (Fig.
716 6d), thus being also consistent with).

717 In Iberia, the solar irradiance record and NAO forcing was embraced to explain the dryness during the MCA
718 as observed in low resolution records (Moreno et al., 2012). Further studies based on proxy reconstructions
719 in Iberia explained those MCA - LIA differences by using interactions between the NAO and the East
720 Atlantic (EA) phases (Sánchez-López et al., 2016). In that line, the persistence of NAO phases, for example,
721 the dominance of positive index during Medieval times, has been questioned (Ortega et al., 2015) and the
722 interactions with other atmospheric modes, together with the non-stationary character of these atmospheric
723 patterns, are nowadays important issues to contemplate when providing a NAO reconstruction (Comas-Bru
724 and Hernández, 2018). In Fig. 6g, the NAO reconstruction provided using a lake record in NW Iberia
725 (Hernández et al., 2020) is compared with the speleothem Pyrenean speleothems (Fig. 6)-record
726 demonstrating a good connection. Not surprisingly, the lack of correlation for some periods could be
727 associated to i) chronological uncertainties of both records, ii) different season recorded by the analyzed
728 proxies and iii) distinct influence of NAO in W and E of the IP.

729 **6. Conclusions**

730 The eight stalagmites presented in this study document for the first-time significant climate changes on the
731 decadal scale in the Central Pyrenees during the last 2500 years. The $\delta^{18}\text{O}$ composite record is dominated
732 by regional temperature changes, as suggested by monitoring data and by the correlation with observational
733 temperature data from the Pyrenees and at a hemispheric scale. The precipitation amount may also play a
734 role as shown by the comparison with Pyrenean lake records.

735 On a regional scale, there is a good agreement with other Pyrenean and Iberian records (lake levels, tree
736 rings and glacier advances) indicating a regional representativity of this new record. The RP stands out as
737 one of the warmest periods of the last 2500 years a clear warm period, while the DA, MCA and LIA exhibit
738 a high centennial-scale variability with cold (e.g., 520-540 ADCE and 1750-1850 ADCE) and warm
739 intervals (e.g., 900-950 ADCE and 1150-1250 ADCE) modulated by increases and decreases in the
740 precipitation amount, respectively. In spite temperature increases since 1950 ADCE, known as the Great
741 Acceleration within the IE, the last two decades are not the ones with higher the highest $\delta^{18}\text{O}$ values in the
742 composite record, likely pointing to the secondary role played by precipitation amount.

743 On a European scale, the Pyrenean composite is in robust agreement with the PAGES2k temperature
744 reconstructions ~~and, particularly during warm events~~. It shows some similarities with other speleothem
745 reconstructions from the Alps, Central and Northern Europe, pointing to coherent patterns all over the
746 continent for cold/wet and warm/dry periods of last 2500 years. This coherence is supported by synchronous
747 changes with the sunspot number (low temperatures during solar minima), the North Atlantic Oscillation
748 index (low NAO correlates with cold and wet decades) and major volcanic eruptions (e.g., several eruptions
749 during LALIA).

750 **Author contribution.** MB, AM and CS designed the study; MB, AB and CS carried out the field work;
751 MB, JH, IC, HS and NH did the analyses. LE and HC provided the U-Th facilities. MB and AM prepared
752 the manuscript with contributions from all co-authors.

753 **Competing interests:** The authors declare that they have no conflict of interest.

754 **Acknowledgements.** We acknowledge the Spanish projects CTM2013-48639-C2-2-R (OPERA),
755 CGL2016-77479-R (SPYRIT), and PID2019-106050RB-I00 (PYCACHU) for funding. We thank the
756 Ordesa y Monte Perdido National Park (Spain) authorities and guards for their permission and help in
757 exploring and monitoring the studied caves. We also thank Jaime Mas and Xavier Fuertes (Free Caving

758 Team; and GEB), Ramón Queraltó and Carles Pons (Asociación Científica Espeleológica Cotiella), Maria
759 Leunda and the Palazio family (www.hotelpalazio.com) for their invaluable help during fieldwork. [Dr.](#)
760 [Miguel Sevilla \(IPE-CSIC\) is greatly acknowledge for his design and production of maps in Fig. 1.](#) The
761 authors would like to acknowledge the use of the Servicio General de Apoyo a la Investigación-SAI,
762 University of Zaragoza. This study contributes to the work carried out by the DGA research group Procesos
763 Geoambientales y Cambio Global (ref.: E02-20R). [Miguel Bartolomé is supported by the HORIZON TMA](#)
764 [MSCA Postdoctoral Fellowships - Global Fellowships 2022 MODKARST project \(n° 101107943\) funded](#)
765 [by the European Union.](#) Isabel Cacho thanks the Catalan Institution for Research and Advanced Studies
766 (ICREA) academia program from the Generalitat de Catalunya.

767 References

- 768 Abrantes, F., Rodrigues, T., Rufino, M., Salgueiro, E., Oliveira, D., Gomes, S., Oliveira, P., Costa, A., Mil-
769 Homens, M., Drago, T., and Naughton, F.: The climate of the Common Era off the Iberian Peninsula,
770 *Clim. Past*, 13, 1901–1918, <https://doi.org/10.5194/cp-13-1901-2017>, 2017.
- 771 Affolter, S., Häuselmann, A., Fleitmann, D., Edwards, R. L., Cheng, H., and Leuenberger, M.: Central
772 Europe temperature constrained by speleothem fluid inclusion water isotopes over the past 14,000
773 years, *Science Advances*, 5, eaav3809, <https://doi.org/10.1126/sciadv.aav3809>, 2019.
- 774 Ahmed, M., Anchukaitis, K. J., Asrat, A., Borgaonkar, H. P., Braid, M., Buckley, B. M., Büntgen, U., Chase,
775 B. M., Christie, D. A., Cook, E. R., Curran, M. A. J., Diaz, H. F., Esper, J., Fan, Z.-X., Gaire, N. P., Ge, Q.,
776 Gergis, J., González-Rouco, J. F., Goosse, H., Grab, S. W., Graham, N., Graham, R., Grosjean, M.,
777 Hanhijärvi, S. T., Kaufman, D. S., Kiefer, T., Kimura, K., Korhola, A. A., Krusic, P. J., Lara, A., Lézine, A.-M.,
778 Ljungqvist, F. C., Lorrey, A. M., Luterbacher, J., Masson-Delmotte, V., McCarroll, D., McConnell, J. R.,
779 McKay, N. P., Morales, M. S., Moy, A. D., Mulvaney, R., Mundo, I. A., Nakatsuka, T., Nash, D. J., Neukom,
780 R., Nicholson, S. E., Oerter, H., Palmer, J. G., Phipps, S. J., Prieto, M. R., Rivera, A., Sano, M., Severi, M.,
781 Shanahan, T. M., Shao, X., Shi, F., Sigl, M., Smerdon, J. E., Solomina, O. N., Steig, E. J., Stenni, B.,
782 Thamban, M., Trouet, V., Turney, C. S. M., Umer, M., van Ommen, T., Verschuren, D., Viau, A. E., Villalba,
783 R., Vinther, B. M., von Gunten, L., Wagner, S., Wahl, E. R., Wanner, H., Werner, J. P., White, J. W. C.,
784 Yasue, K., Zorita, E., and PAGES 2k Consortium: Continental-scale temperature variability during the past
785 two millennia, *Nature Geoscience*, 6, 339–346, <https://doi.org/10.1038/ngeo1797>, 2013.
- 786 Ait Brahim, Y., Wassenburg, J. A., Sha, L., Cruz, F. W., Deininger, M., Sifeddine, A., Bouchaou, L., Spötl, C.,
787 Edwards, R. L., and Cheng, H.: North Atlantic Ice-Rafting, Ocean and Atmospheric Circulation During the
788 Holocene: Insights From Western Mediterranean Speleothems, *Geophysical Research Letters*, 46, 7614–
789 7623, <https://doi.org/10.1029/2019GL082405>, 2019.
- 790 Baker, A., C. Hellstrom, J., Kelly, B. F. J., Mariethoz, G., and Trouet, V.: A composite annual-resolution
791 stalagmite record of North Atlantic climate over the last three millennia, *Sci Rep*, 5, 10307,
792 <https://doi.org/10.1038/srep10307>, 2015.
- 793 Bard, E., Raisbeck, G., Yiou, F., and Jouzel, J.: Solar irradiance during the last 1200 years based on
794 cosmogenic nuclides, *Tellus B*, 52, 985–992, <https://doi.org/10.1034/j.1600-0889.2000.d01-7.x>, 2000.
- 795 Bartolomé, M.: La Cueva del Caserío de Sesó (Pirineo Central): espeleogénesis, dinámica actual y
796 reconstrucción paleoambiental de los últimos 13.000 años, Universidad de Zaragoza, 276 pp., 2016.
- 797 Bartolomé, M., Moreno, A., Sancho, C., Stoll, H. M., Cacho, I., Spötl, C., Belmonte, Á., Edwards, R. L.,
798 Cheng, H., and Hellstrom, J. C.: Hydrological change in Southern Europe responding to increasing North
799 Atlantic overturning during Greenland Stadial 1, *PNAS*, 112, 6568–6572,
800 <https://doi.org/10.1073/pnas.1503990112>, 2015a.
- 801 Bartolomé, M., Sancho, C., Moreno, A., Oliva-Urcia, B., Belmonte, Á., Bastida, J., Cheng, H., and Edwards,
802 R. L.: Upper Pleistocene interstratal piping-cave speleogenesis: The Sesó Cave System (Central Pyrenees,
803 Northern Spain), *Geomorphology*, 228, 335–344, <https://doi.org/10.1016/j.geomorph.2014.09.007>,
804 2015b.

805 Beniston, M., Farinotti, D., Stoffel, M., Andreassen, L. M., Coppola, E., Eckert, N., Fantini, A., Giacona, F.,
806 Hauck, C., Huss, M., Huwald, H., Lehning, M., López-Moreno, J.-I., Magnusson, J., Marty, C., Morán-
807 Tejada, E., Morin, S., Naaim, M., Provenzale, A., Rabatel, A., Six, D., Stötter, J., Strasser, U., Terzago, S.,
808 and Vincent, C.: The European mountain cryosphere: a review of its current state, trends, and future
809 challenges, *The Cryosphere*, 12, 759–794, <https://doi.org/10.5194/tc-12-759-2018>, 2018.

810 Benito, G., Macklin, M. G., Panin, A., Rossato, S., Fontana, A., Jones, A. F., Machado, M. J., Matlakhova,
811 E., Mozzi, P., and Zielhofer, C.: Recurring flood distribution patterns related to short-term Holocene
812 climatic variability, *Sci Rep*, 5, 16398, <https://doi.org/10.1038/srep16398>, 2015.

813 Bernal-Wormull, J. L., Moreno, A., Pérez-Mejías, C., Bartolomé, M., Aranburu, A., Arriolabengoa, M.,
814 Iriarte, E., Cacho, I., Spötl, C., Edwards, R. L., and Cheng, H.: Immediate temperature response in
815 northern Iberia to last deglacial changes in the North Atlantic, *Geology*,
816 <https://doi.org/10.1130/G48660.1>, 2021.

817 ~~Bradley, R. S., Hughes, M. K., and Diaz, H. F.: Climate in Medieval Time, *Science*, 302, 404–405,
818 <https://doi.org/10.1126/science.1090372>, 2003.~~

819 Bücher, A. and Dessens, J.: Secular Trend of Surface Temperature at an Elevated Observatory in the
820 Pyrenees, *Journal of Climate*, 4, 859–868, [https://doi.org/10.1175/1520-0442\(1991\)004<0859:STOSTA>2.0.CO;2](https://doi.org/10.1175/1520-0442(1991)004<0859:STOSTA>2.0.CO;2), 1991.

822 Büntgen, U., Tegel, W., Nicolussi, K., McCormick, M., Frank, D., Trouet, V., Kaplan, J. O., Herzig, F.,
823 Heussner, K.-U., Wanner, H., Luterbacher, J., and Esper, J.: 2500 Years of European Climate Variability
824 and Human Susceptibility, *Science*, 2011.

825 Büntgen, U., Myglan, V. S., Ljungqvist, F. C., McCormick, M., Di Cosmo, N., Sigl, M., Jungclaus, J., Wagner,
826 S., Krusic, P. J., Esper, J., Kaplan, J. O., de Vaan, M. A. C., Luterbacher, J., Wacker, L., Tegel, W., and
827 Kirilyanov, A. V.: Cooling and societal change during the Late Antique Little Ice Age from 536 to around
828 660 AD, *Nature Geosci*, 9, 231–236, <https://doi.org/10.1038/ngeo2652>, 2016.

829 Büntgen, U., Krusic, P. J., Verstege, A., Sangüesa-Barreda, G., Wagner, S., Camarero, J. J., Ljungqvist, F.
830 C., Zorita, E., Oppenheimer, C., Konter, O., Tegel, W., Gärtner, H., Cherubini, P., Reinig, F., and Esper, J.:
831 New Tree-Ring Evidence from the Pyrenees Reveals Western Mediterranean Climate Variability since
832 Medieval Times, *J. Climate*, 30, 5295–5318, <https://doi.org/10.1175/JCLI-D-16-0526.1>, 2017.

833 Büntgen, U., Urban, O., Krusic, P. J., Rybníček, M., Kolář, T., Kyncl, T., Ač, A., Koňasová, E., Čáslavský, J.,
834 Esper, J., Wagner, S., Saurer, M., Tegel, W., Dobrovolný, P., Cherubini, P., Reinig, F., and Trnka, M.:
835 Recent European drought extremes beyond Common Era background variability, *Nat. Geosci.*, 14, 190–
836 196, <https://doi.org/10.1038/s41561-021-00698-0>, 2021.

837 ~~Cheng, H., Edwards, L. R., Hoff, J., Gallup, C. D., Richards, D. A., and Asmerom, Y.: The half-lives of
838 uranium-234 and thorium-230, *Chemical Geology*, 169, 17–33, 2000.~~

839 Cisneros, M., Cacho, I., Frigola, J., Canals, M., Masqué, P., Martrat, B., Casado, M., Grimalt, J. O., Pena, L.
840 D., Margaritelli, G., and Lirer, F.: Sea surface temperature variability in the central-western
841 Mediterranean Sea during the last 2700 years: a multi-proxy and multi-record approach, *Clim. Past*, 12,
842 849–869, <https://doi.org/10.5194/cp-12-849-2016>, 2016.

843 Cisneros, M., Cacho, I., Moreno, A., Stoll, H., Torner, J., Català, A., Edwards, R. L., Cheng, H., and Fornós,
844 J. J.: Hydroclimate variability during the last 2700 years based on stalagmite multi-proxy records in the
845 central-western Mediterranean, *Quaternary Science Reviews*, 269, 107137,
846 <https://doi.org/10.1016/j.quascirev.2021.107137>, 2021.

847 Comas-Bru, L. and Hernández, A.: [Reconciling North Atlantic climate modes: revised monthly indices for
848 the East Atlantic and the Scandinavian patterns beyond the 20th century, *Earth System Science Data*, 10,
849 2329–2344, <https://doi.org/10.5194/essd-10-2329-2018>, 2018.](https://doi.org/10.5194/essd-10-2329-2018)

850 [Comas-Bru, L.](#), Rehfeld, K., Roesch, C., Amirnezhad-Mozhdehi, S., Harrison, S. P., Atsawawaranunt, K.,
851 Ahmad, S. M., Brahim, Y. A., Baker, A., Bosomworth, M., Breitenbach, S. F. M., Burstyn, Y., Columbu, A.,
852 Deininger, M., Demény, A., Dixon, B., Fohlmeister, J., Hatvani, I. G., Hu, J., Kaushal, N., Kern, Z., Labuhn,
853 I., Lechleitner, F. A., Lorrey, A., Martrat, B., Novello, V. F., Oster, J., Pérez-Mejías, C., Scholz, D., Scropton,
854 N., Sinha, N., Ward, B. M., Warken, S., Zhang, H., and SISAL Working Group members: SISALv2: a
855 comprehensive speleothem isotope database with multiple age–depth models, *Earth System Science*
856 *Data*, 12, 2579–2606, <https://doi.org/10.5194/essd-12-2579-2020>, 2020.

857 [Corella, J. P.](#), [Moreno, A.](#), [Morellón, M.](#), [Rull, V.](#), [Giralt, S.](#), [Rico, M. T.](#), [Pérez-Sanz, A.](#), and [Valero-Garcés,](#)
858 [B. L.](#): Climate and human impact on a meromictic lake during the last 6,000 years (Montcortès Lake,
859 Central Pyrenees, Spain), *Journal of Paleolimnology*, 46, 351–367, [https://doi.org/10.1007/s10933-010-](https://doi.org/10.1007/s10933-010-9443-3)
860 [9443-3](https://doi.org/10.1007/s10933-010-9443-3), 2011.

861 [Corella, J. P.](#), [Brauer, A.](#), [Mangili, C.](#), [Rull, V.](#), [Vegas-Villarúbia, T.](#), [Morellón, M.](#), and [Valero-Garcés, B. L.](#):
862 [The 1.5-ka varved record of Lake Montcortès \(southern Pyrenees, NE Spain\)](#), *Quaternary Research*, 78,
863 [323–332](https://doi.org/10.1016/j.yqres.2012.06.002), <https://doi.org/10.1016/j.yqres.2012.06.002>, 2012.

864 [Corella, J. P.](#), [Benito, G.](#), [Rodríguez Lloveras, X.](#), [Brauer, A.](#), and [Valero-Garcés, B. L.](#): Annually resolved
865 lake record of extreme hydro-meteorological events since AD 1347 in NE Iberian Peninsula, *Quaternary*
866 *Science Reviews*, 93, 77–90, <https://doi.org/10.1016/j.quascirev.2014.03.020>, 2014.

867 [Corella, J. P.](#), [Valero-Garcés, B. L.](#), [Vicente-Serrano, S. M.](#), [Brauer, A.](#), and [Benito, G.](#): Three millennia of
868 heavy rainfalls in Western Mediterranean: frequency, seasonality and atmospheric drivers, *Scientific*
869 *Reports*, 6, <https://doi.org/10.1038/srep38206>, 2016.

870 [Dessens, J.](#) and [Bücher, A.](#): Changes in minimum and maximum temperatures at the Pic du Midi in
871 relation with humidity and cloudiness, 1882–1984, *Atmospheric Research*, 37, 147–162,
872 [https://doi.org/10.1016/0169-8095\(94\)00075-0](https://doi.org/10.1016/0169-8095(94)00075-0), 1995.

873 [Edwards, R. L.](#), [Chen, J. H.](#), and [Wasserburg, G. J.](#): 238U–234U–230Th–232Th systematics and the precise
874 measurements of time over the past 500,000 years, *Earth and Planetary Science Letters*, 81, 175–192,
875 1987.

876 [Fohlmeister, J.](#): A statistical approach to construct composite climate records of dated archives,
877 *Quaternary Geochronology*, 14, 48–56, <https://doi.org/10.1016/j.quageo.2012.06.007>, 2012.

878 [Fohlmeister, J.](#), [Kromer, B.](#), and [Mangini, A.](#): The influence of soil organic matter age spectrum on the
879 reconstruction of atmospheric 14C levels via stalagmites, *Radiocarbon*, 53, 99–115,
880 <https://doi.org/10.1017/S003382220003438X>, 2011.

881 [Fohlmeister, J.](#), [Schroder-Ritzrau, A.](#), [Scholz, D.](#), [Spötl, C.](#), [Riechelmann, D. F. C.](#), [Mudelsee, M.](#),
882 [Wackerbarth, A.](#), [Gerdes, A.](#), [Riechelmann, S.](#), [Immenhauser, A.](#), [Richter, D. K.](#), and [Mangini, A.](#): Bunker
883 Cave stalagmites: an archive for central European Holocene climate variability, *Clim. Past*, 8, 1751–1764,
884 <https://doi.org/10.5194/cp-8-1751-2012>, 2012.

885 [García-Ruiz, J. M.](#), [Palacios, D.](#), [Andrés, N. de](#), [Valero-Garcés, B. L.](#), [López-Moreno, J. I.](#), and [Sanjuán, Y.](#):
886 Holocene and ‘Little Ice Age’ glacial activity in the Marboré Cirque, Monte Perdido Massif, Central
887 Spanish Pyrenees, *The Holocene*, 24, 1439–1452, <https://doi.org/10.1177/0959683614544053>, 2014.

888 [Genty, D.](#), [Vokal, B.](#), [Obelic, B.](#), and [Massault, M.](#): Bomb 14C time history recorded in two modern
889 stalagmites — importance for soil organic matter dynamics and bomb 14C distribution over continents,
890 *Earth and Planetary Science Letters*, 160, 795–809, [https://doi.org/10.1016/S0012-821X\(98\)00128-9](https://doi.org/10.1016/S0012-821X(98)00128-9),
891 1998.

892 [Genty, D.](#), [Blamart, D.](#), [Ghaleb, B.](#), [Plagnes, V.](#), [Causse, Ch.](#), [Bakalowicz, M.](#), [Zouari, K.](#), [Chkir, N.](#),
893 [Hellstrom, J.](#), [Wainer, K.](#), and [Bourges, F.](#): Timing and dynamics of the last deglaciation from European
894 and North African $\delta^{13}\text{C}$ stalagmite profiles—comparison with Chinese and South Hemisphere

895 stalagmites, *Quaternary Science Reviews*, 25, 2118–2142,
896 <https://doi.org/10.1016/j.quascirev.2006.01.030>, 2006.

897 Genty, D., Labuhn, I., Hoffmann, G., Danis, P. A., Mestre, O., Bourges, F., Wainer, K., Massault, M., Van
898 Exter, S., Régnier, E., Orengo, Ph., Falourd, S., and Minster, B.: Rainfall and cave water isotopic
899 relationships in two South-France sites, *Geochimica et Cosmochimica Acta*, 131, 323–343,
900 <https://doi.org/10.1016/j.gca.2014.01.043>, 2014.

901 Giménez, R., Bartolomé, M., Gázquez, F., Iglesias, M., and Moreno, A.: Underlying Climate Controls in
902 Triple Oxygen (16 O, 17 O, 18 O) and Hydrogen (1 H, 2 H) Isotopes Composition of Rainfall (Central
903 Pyrenees), *Front. Earth Sci.*, 9, <https://doi.org/10.3389/feart.2021.633698>, 2021.

904 González-Sampériz, P., Aranbarri, J., Pérez-Sanz, A., Gil-Romera, G., Moreno, A., Leunda, M., Sevilla-
905 Callejo, M., Corella, J. P., Morellón, M., Oliva, B., and Valero-Garcés, B.: Environmental and climate
906 change in the southern Central Pyrenees since the Last Glacial Maximum: A view from the lake records,
907 *CATENA*, 149, 668–688, 2017.

908 Goosse, H., Guiot, J., Mann, M. E., Dubinkina, S., and Sallaz-Damaz, Y.: The medieval climate anomaly in
909 Europe: Comparison of the summer and annual mean signals in two reconstructions and in simulations
910 with data assimilation, *Global and Planetary Change*, 84–85, 35–47,
911 <https://doi.org/10.1016/j.gloplacha.2011.07.002>, 2012.

912 Gray, L. J., Beer, J., Geller, M., Haigh, J. D., Lockwood, M., Matthes, K., Cubasch, U., Fleitmann, D.,
913 Harrison, G., Hood, L., Luterbacher, J., Meehl, G. A., Shindell, D., van Geel, B., and White, W.: Solar
914 influences on climate, *Rev. Geophys.*, 48, RG4001, 2010.

915 [Hammer, O., Harper, D. A. T., and Ryan, P. D.: PAST: Paleontological statistics software package for
916 education and data analysis. 4\(1\): 9pp., *Palaeontologia Electronica*, 4 \(1\), 9, 2001.](#)

917 Helama, S., Meriläinen, J., and Tuomenvirta, H.: Multicentennial megadrought in northern Europe
918 coincided with a global El Niño–Southern Oscillation drought pattern during the Medieval Climate
919 Anomaly, *Geology*, 37, 175–178, <https://doi.org/10.1130/G25329A.1>, 2009.

920 [Helama, S., Jones, P. D., and Briffa, K. R.: Dark Ages Cold Period: A literature review and directions for
921 future research, *The Holocene*, 27, 1600–1606, <https://doi.org/10.1177/0959683617693898>, 2017.](#)

922 [Hellstrom, J.: Rapid and accurate U/Th dating using parallel ion counting multi-collector ICP-MS, *Journal
923 of Analytical Atomic Spectrometry*, 18, 1346–1351, 2003.](#)

924 Hellstrom, J.: U–Th dating of speleothems with high initial ²³⁰Th using stratigraphical constraint,
925 *Quaternary Geochronology*, 1, 289–295, <https://doi.org/10.1016/j.quageo.2007.01.004>, 2006.

926 [Hernández, A., Sánchez-López, G., Pla-Rabes, S., Comas-Bru, L., Parnell, A., Cahill, N., Geyer, A., Trigo, R.
927 M., and Giral, S.: A 2,000-year Bayesian NAO reconstruction from the Iberian Peninsula, *Sci Rep*, 10,
928 14961, <https://doi.org/10.1038/s41598-020-71372-5>, 2020.](#)

929 Holzhauser, H., Magny, M., and Zumbühl, H. J.: Glacier and lake-level variations in west-central Europe
930 over the last 3500 years; The Holocene, <https://doi.org/10.1191/0959683605hl853ra>, 2016.

931 Hu, H.-M., Michel, V., Valensi, P., Mii, H.-S., Starnini, E., Zunino, M., and Shen, C.-C.: Stalagmite-Inferred
932 Climate in the Western Mediterranean during the Roman Warm Period, *Climate*, 10, 93,
933 <https://doi.org/10.3390/cli10070093>, 2022.

934 Hua, Q., McDonald, J., Redwood, D., Drysdale, R., Lee, S., Fallon, S., and Hellstrom, J.: Robust
935 chronological reconstruction for young speleothems using radiocarbon, *Quaternary Geochronology*, 14,
936 67–80, <https://doi.org/10.1016/j.quageo.2012.04.017>, 2012.

937 Hua, Q., Cook, D., Fohlmeister, J., Penny, D., Bishop, P., and Buckman, S.: Radiocarbon Dating of a
938 Speleothem Record of Paleoclimate for Angkor, Cambodia, *Radiocarbon*, 59, 1873–1890,
939 <https://doi.org/10.1017/RDC.2017.115>, 2017.

940 Hughes, P. D.: Little Ice Age glaciers and climate in the Mediterranean mountains: a new analysis, *CIG*,
941 44, 15, <https://doi.org/10.18172/cig.3362>, 2018.

942 Ilyashuk, E. A., Heiri, O., Ilyashuk, B. P., Koinig, K. A., and Psenner, R.: The Little Ice Age signature in a
943 700-year high-resolution chironomid record of summer temperatures in the Central Eastern Alps, *Clim*
944 *Dyn*, 52, 6953–6967, <https://doi.org/10.1007/s00382-018-4555-y>, 2019.

945 ~~Intergovernmental Panel on IPCC, 2021: Climate Change: Climate Change 2013 2021: The Physical~~
946 ~~Science Basis- Contribution of Working Group I Contribution to the IPCC Fifth Assessment Report,~~
947 ~~Cambridge University Press, Cambridge, 2014.~~

948 ~~IPCC to the Sixth Assessment Report of the Intergovernmental Panel on Climate Change, in: Climate~~
949 ~~Change 2021: The Physical Science Basis. Contribution of Working Group I [Masson-Delmotte, V., P. Zhai,~~
950 ~~A. Pirani, S.L. Connors, C. Péan, S. Berger, N. Caud, Y. Chen, L. Goldfarb, M. I., Gomis, M. Huang, K.~~
951 ~~Leitzell, E. Lonnoy, J.B.R. Matthews, T.K. Maycock, T. Waterfield, O. Yelekci, R. Yu, and B. Zhou (eds.)],~~
952 ~~Cambridge University Press, United Kingdom and New York, NY, USA, 2391, 2021~~
953 ~~[pp.doi:10.1017/9781009157896](https://doi.org/10.1017/9781009157896).~~

954 Jacob, D., Kotova, L., Teichmann, C., Sobolowski, S. P., Vautard, R., Donnelly, C., Koutroulis, A. G.,
955 Grillakis, M. G., Tسانis, I. K., Damm, A., Sakalli, A., and van Vliet, M. T. H.: Climate Impacts in Europe
956 Under +1.5°C Global Warming, *Earth’s Future*, 6, 264–285, <https://doi.org/10.1002/2017EF000710>,
957 2018.

958 Jiménez-Moreno, G., García-Alix, A., Hernández-Corbalán, M. D., Anderson, R. S., and Delgado-Huertas,
959 A.: Vegetation, fire, climate and human disturbance history in the southwestern Mediterranean area
960 during the late Holocene, *Quaternary Research*, 79, 110–122,
961 <https://doi.org/10.1016/j.yqres.2012.11.008>, 2013.

962 Konecky, B. L., McKay, N. P., Churakova (Sidorova), O. V., Comas-Bru, L., Dassié, E. P., DeLong, K. L.,
963 Falster, G. M., Fischer, M. J., Jones, M. D., Jonkers, L., Kaufman, D. S., Leduc, G., Managave, S. R.,
964 Martrat, B., Opel, T., Orsi, A. J., Partin, J. W., Sayani, H. R., Thomas, E. K., Thompson, D. M., Tyler, J. J.,
965 Abram, N. J., Atwood, A. R., Conroy, J. L., Kern, Z., Porter, T. J., Stevenson, S. L., von Gunten, L., and the
966 Iso2k Project Members: The Iso2k Database: A global compilation of paleo- $\delta^{18}\text{O}$ and $\delta^2\text{H}$ records to aid
967 understanding of Common Era climate, *Earth System Science Data Discussions*, 1–49,
968 <https://doi.org/10.5194/essd-2020-5>, 2020.

969 Lachniet, M. S.: Climatic and environmental controls on speleothem oxygen-isotope values, *Quaternary*
970 *Science Reviews*, 28, 412–432, 2009.

971 [Leunda, M., González-Sampériz, P., Gil-Romera, G., Bartolomé, M., Belmonte-Ribas, Á., Gómez-García,](https://doi.org/10.1111/1365-2745.13077)
972 [D., Kaltenrieder, P., Rubiales, J. M., Schwörer, C., Tinner, W., Morales-Molino, C., and Sancho, C.: Ice](https://doi.org/10.1111/1365-2745.13077)
973 [cave reveals environmental forcing of long-term Pyrenean tree line dynamics, *Journal of Ecology*, 107,](https://doi.org/10.1111/1365-2745.13077)
974 [814–828, <https://doi.org/10.1111/1365-2745.13077>, 2019.](https://doi.org/10.1111/1365-2745.13077)

975 López-Moreno, J. I., Revuelto, J., Rico, I., Chueca-Cía, J., Julián, A., Serreta, A., Serrano, E., Vicente-
976 Serrano, S. M., Azorin-Molina, C., Alonso-González, E., and García-Ruiz, J. M.: Thinning of the Monte
977 Perdido Glacier in the Spanish Pyrenees since 1981, *The Cryosphere*, 10, 681–694,
978 <https://doi.org/10.5194/tc-10-681-2016>, 2016.

979 López-Moreno, J. I., García-Ruiz, J. M., Vicente-Serrano, S. M., Alonso-González, E., Revuelto-Benedí, J.,
980 Rico, I., Izagirre, E., and Beguería-Portugués, S.: Critical discussion of: “A farewell to glaciers: Ecosystem
981 services loss in the Spanish Pyrenees,” *Journal of Environmental Management*, 275, 111247,
982 <https://doi.org/10.1016/j.jenvman.2020.111247>, 2020.

- 983 Lüning, S., Schulte, L., Garcés-Pastor, S., Danladi, I. b., and Gafka, M.: The Medieval Climate Anomaly in
984 the Mediterranean Region, *Paleoceanography and Paleoclimatology*, 34, 1625–1649,
985 <https://doi.org/10.1029/2019PA003734>, 2019.
- 986 Luterbacher, J., Werner, J. P., Smerdon, J. E., Fernández-Donado, L., González-Rouco, F. J., Barriopedro,
987 D., Ljungqvist, F. C., Büntgen, U., Zorita, E., Wagner, S., Esper, J., McCarroll, D., Toreti, A., Frank, D.,
988 Jungclauss, J. H., M Barriendos, Bertolin, C., Bothe, O., Brázdil, R., Camuffo, D., Dobrovolný, P., Gagen, M.,
989 García-Bustamante, E., Ge, Q., Gómez-Navarro, J. J., Guiot, J., Hao, Z., Hegerl, G. C., Holmgren, K.,
990 Klimenko, V. V., Martín-Chivelet, J., Pfister, C., N Roberts, Schindler, A., Schurer, A., Solomina, O.,
991 Gunten, L. von, Wahl, E., Wanner, H., Wetter, O., Xoplaki, E., Yuan, N., D Zanchettin, Zhang, H., and
992 Zerefos, C.: European summer temperatures since Roman times, *Environ. Res. Lett.*, 11, 024001,
993 <https://doi.org/10.1088/1748-9326/11/2/024001>, 2016.
- 994 Magny, M.: Orbital, ice-sheet, and possible solar forcing of Holocene lake-level fluctuations in west-
995 central Europe: A comment on Bleicher, *The Holocene*, <https://doi.org/10.1177/0959683613483627>,
996 2013.
- 997 Mangini, A., Spötl, C., and Verdes, P.: Reconstruction of temperature in the Central Alps during the past
998 2000 yr from a $\delta^{18}O$ stalagmite record, *Earth and Planetary Science Letters*, 235, 741–751,
999 <https://doi.org/10.1016/j.epsl.2005.05.010>, 2005.
- 1000 Mann, M. E.: Beyond the hockey stick: Climate lessons from the Common Era, *PNAS*, 118,
1001 <https://doi.org/10.1073/pnas.2112797118>, 2021.
- 1002 [Mann, M. E., Zhang, Z., Rutherford, S., Bradley, R. S., Hughes, M. K., Shindell, D., Ammann, C., Faluvegi,](#)
1003 [G., and Ni, F.: Global Signatures and Dynamical Origins of the Little Ice Age and Medieval Climate](#)
1004 [Anomaly, *Science*, 326, 1256–1260, 2009.](#)
- 1005 Margaritelli, G., Cacho, I., Català, A., Barra, M., Bellucci, L. G., Lubritto, C., Rettori, R., and Lirer, F.:
1006 Persistent warm Mediterranean surface waters during the Roman period, *Sci Rep*, 10, 10431,
1007 <https://doi.org/10.1038/s41598-020-67281-2>, 2020.
- 1008 Markowska, M., Fohlmeister, J., Treble, P. C., Baker, A., Andersen, M. S., and Hua, Q.: Modelling the 14C
1009 bomb-pulse in young speleothems using a soil carbon continuum model, *Geochimica et Cosmochimica*
1010 *Acta*, 261, 342–367, <https://doi.org/10.1016/j.gca.2019.04.029>, 2019.
- 1011 Martín-Chivelet, J., Muñoz-García, M. B., Edwards, R. L., Turrero, M. J., and Ortega, A. I.: Land surface
1012 temperature changes in Northern Iberia since 4000yrBP, based on $\delta^{13}C$ of speleothems, *Global and*
1013 *Planetary Change*, 77, 1–12, <https://doi.org/10.1016/j.gloplacha.2011.02.002>, 2011.
- 1014 Martín-Puertas, C., Valero-Garcés, B. L., Brauer, A., Mata, M. P., Delgado-Huertas, A., and Dulski, P.: The
1015 Iberian-Roman Humid Period (2600-1600 cal yr BP) in the Zoñar Lake varve record (Andalucía, southern
1016 Spain), *Quaternary Research*, 71, 108–120, 2009.
- 1017 Martín-Puertas, C., Matthes, K., Brauer, A., Muscheler, R., Hansen, F., Petrick, C., Aldahan, A., Possnert,
1018 G., and van Geel, B.: Regional atmospheric circulation shifts induced by a grand solar minimum, *Nature*
1019 *Geoscience*, <https://doi.org/10.1038/ngeo1460>, 2012.
- 1020 McCormick, M., Büntgen, U., Cane, M. A., Cook, E. R., Harper, K., Huybers, P., Litt, T., Manning, S. W.,
1021 Mayewski, P. A., More, A. F. M., Nicolussi, K., and Tegel, W.: Climate Change during and after the Roman
1022 Empire: Reconstructing the Past from Scientific and Historical Evidence, *The Journal of Interdisciplinary*
1023 *History*, 43, 169–220, https://doi.org/10.1162/JINH_a_00379, 2012.
- 1024 Morellón, M., Valero-Garcés, B., Vegas-Vilarrúbia, T., González-Sampériz, P., Romero, Ó., Delgado-
1025 Huertas, A., Mata, P., Moreno, A., Rico, M., and Corella, J. P.: Lateglacial and Holocene palaeohydrology
1026 in the western Mediterranean region: The Lake Estanya record (NE Spain), *Quaternary Science Reviews*,
1027 28, 2582–2599, 2009.

1028 Morellón, M., Valero-Garcés, B., González-Sampérez, P., Vegas-Vilarrúbia, T., Rubio, E., Rieradevall, M.,
1029 Delgado-Huertas, A., Mata, P., Romero, Ó., Engstrom, D. R., López-Vicente, M., Navas, A., and Soto, J.:
1030 Climate changes and human activities recorded in the sediments of Lake Estanya (NE Spain) during the
1031 Medieval Warm Period and Little Ice Age, *Journal of Paleolimnology*, 46, 423–452,
1032 <https://doi.org/10.1007/s10933-009-9346-3>, 2011.

1033 Morellón, M., Pérez-Sanz, A., Corella, J. P., Büntgen, U., Catalán, J., González-Sampérez, P., González-
1034 Trueba, J. J., López-Sáez, J. A., Moreno, A., Pla-Rabes, S., Saz-Sánchez, M. Á., Scussolini, P., Serrano, E.,
1035 Steinhilber, F., Stefanova, V., Vegas-Vilarrúbia, T., and Valero-Garcés, B.: A multi-proxy perspective on
1036 millennium-long climate variability in the Southern Pyrenees, *Clim. Past*, 8, 683–700,
1037 <https://doi.org/10.5194/cp-8-683-2012>, 2012.

1038 Moreno, A., Stoll, H. M., Jiménez-Sánchez, M., Cacho, I., Valero-Garcés, B., Ito, E., and Edwards, L. R.: A
1039 speleothem record of rapid climatic shifts during last glacial period from Northern Iberian Peninsula,
1040 *Global and Planetary Change*, 71, 218–231; doi:10.1016/j.gloplacha.2009.10.002, 2010.

1041 Moreno, A., Pérez, A., Frigola, J., Nieto-Moreno, V., Rodrigo-Gámiz, M., Martrat, B., González-Sampérez,
1042 P., Morellón, M., Martín-Puertas, C., Corella, J. P., Belmonte, Á., Sancho, C., Cacho, I., Herrera, G.,
1043 Canals, M., Grimalt, J. O., Jiménez-Espejo, F., Martínez-Ruiz, F., Vegas-Vilarrúbia, T., and Valero-Garcés,
1044 B. L.: The Medieval Climate Anomaly in the Iberian Peninsula reconstructed from marine and lake
1045 records, *Quaternary Science Reviews*, 43, 16–32, <https://doi.org/10.1016/j.quascirev.2012.04.007>,
1046 2012.

1047 Moreno, A., Sancho, C., Bartolomé, M., Oliva-Urcia, B., Delgado-Huertas, A., Estrela, M. J., Corell, D.,
1048 López-Moreno, J. I., and Cacho, I.: Climate controls on rainfall isotopes and their effects on cave drip
1049 water and speleothem growth: the case of Molinos cave (Teruel, NE Spain), *Clim Dyn*, 43, 221–241,
1050 <https://doi.org/10.1007/s00382-014-2140-6>, 2014.

1051 Moreno, A., Pérez-Mejías, C., Bartolomé, M., Sancho, C., Cacho, I., Stoll, H., Delgado-Huertas, A.,
1052 Hellstrom, J., Edwards, R. L., and Cheng, H.: New speleothem data from Molinos and Ejulve caves reveal
1053 Holocene hydrological variability in northeast Iberia, *Quaternary Research*, 1–11,
1054 <https://doi.org/10.1017/qua.2017.39>, 2017.

1055 Moreno, A., Iglesias, M., Azorín-Molina, C., Pérez-Mejías, C., Bartolomé, M., Sancho, C., Stoll, H., Cacho,
1056 I., Frigola, J., Osácar, C., Muñoz, A., Delgado-Huertas, A., Blade, I., and Vimeux, F.: Spatial variability of
1057 northern Iberian rainfall stable isotope values: Investigating climatic controls on daily and monthly
1058 timescales, *Atmospheric Chemistry and Physics Discussions*, 1–34, [https://doi.org/10.5194/acp-2020-](https://doi.org/10.5194/acp-2020-861)
1059 861, 2021a.

1060 Moreno, A., Bartolomé, M., López-Moreno, J. I., Pey, J., Corella, J. P., García-Orellana, J., Sancho, C.,
1061 Leunda, M., Gil-Romera, G., González-Sampérez, P., Pérez-Mejías, C., Navarro, F., Otero-García, J.,
1062 Lapazarán, J., Alonso-González, E., Cid, C., López-Martínez, J., Oliva-Urcia, B., Faria, S. H., Sierra, M. J.,
1063 Millán, R., Querol, X., Alastuey, A., and García-Ruiz, J. M.: The case of a southern European glacier which
1064 survived Roman and medieval warm periods but is disappearing under recent warming, *The Cryosphere*,
1065 15, 1157–1172, <https://doi.org/10.5194/tc-15-1157-2021>, 2021b.

1066 Morice, C. P., Kennedy, J. J., Rayner, N. A., Winn, J. P., Hogan, E., Killick, R. E., Dunn, R. J. H., Osborn, T. J.,
1067 Jones, P. D., and Simpson, I. R.: An Updated Assessment of Near-Surface Temperature Change From
1068 1850: The HadCRUT5 Data Set, *Journal of Geophysical Research: Atmospheres*, 126, e2019JD032361,
1069 <https://doi.org/10.1029/2019JD032361>, 2021.

1070 Naumann, G., Cammalleri, C., Mentaschi, L., and Feyen, L.: Increased economic drought impacts in
1071 Europe with anthropogenic warming, *Nat. Clim. Chang.*, 11, 485–491, [https://doi.org/10.1038/s41558-](https://doi.org/10.1038/s41558-021-01044-3)
1072 021-01044-3, 2021.

- 1073 Neukom, R., Steiger, N., Gómez-Navarro, J. J., Wang, J., and Werner, J. P.: No evidence for globally
1074 coherent warm and cold periods over the preindustrial Common Era, *Nature*, 571, 550–554,
1075 <https://doi.org/10.1038/s41586-019-1401-2>, 2019.
- 1076 Observatorio Pirenaico de Cambio Global: Executive summary report OPCC2: Climate change in the
1077 Pyrenees: impacts, vulnerability and adaptation, 2018.
- 1078 Oliva, M., Ruiz-Fernández, J., Barriendos, M., Benito, G., Cuadrat, J. M., Domínguez-Castro, F., García-
1079 Ruiz, J. M., Giralt, S., Gómez-Ortiz, A., Hernández, A., López-Costas, O., López-Moreno, J. I., López-Sáez,
1080 J. A., Martínez-Cortizas, A., Moreno, A., Prohom, M., Saz, M. A., Serrano, E., Tejedor, E., Trigo, R., Valero-
1081 Garcés, B., and Vicente-Serrano, S. M.: The Little Ice Age in Iberian mountains, *Earth-Science Reviews*,
1082 177, 175–208, <https://doi.org/10.1016/j.earscirev.2017.11.010>, 2018.
- 1083 [Ortega, P., Lehner, F., Swingedouw, D., Masson-Delmotte, V., Raible, C. C., Casado, M., and Yiou, P.: A
1084 model-tested North Atlantic Oscillation reconstruction for the past millennium. *Nature*, 523, 71–74,
1085 <https://doi.org/10.1038/nature14518>, 2015.](https://doi.org/10.1038/nature14518)
- 1086 PAGES 2k Consortium: Continental-scale temperature variability during the past two millennia, *Nature*
1087 *Geosci*, 6, 339–346, <https://doi.org/10.1038/ngeo1797>, 2013.
- 1088 PAGES Hydro2k Consortium: Comparing proxy and model estimates of hydroclimate variability and
1089 change over the Common Era, *Climate of the Past*, 13, 1851–1900, [https://doi.org/10.5194/cp-13-1851-](https://doi.org/10.5194/cp-13-1851-2017)
1090 2017, 2017.
- 1091 PAGES2k Consortium, Emile-Geay, J., McKay, N. P., Kaufman, D. S., Gunten, L. von, Wang, J., Anchukaitis,
1092 K. J., Abram, N. J., Addison, J. A., Curran, M. A. J., Evans, M. N., Henley, B. J., Hao, Z., Martrat, B.,
1093 McGregor, H. V., Neukom, R., Pederson, G. T., Stenni, B., Thirumalai, K., Werner, J. P., Xu, C., Divine, D.
1094 V., Dixon, B. C., Gergis, J., Mundo, I. A., Nakatsuka, T., Phipps, S. J., Routson, C. C., Steig, E. J., Tierney, J.
1095 E., Tyler, J. J., Allen, K. J., Bertler, N. A. N., Björklund, J., Chase, B. M., Chen, M.-T., Cook, E., Jong, R. de,
1096 DeLong, K. L., Dixon, D. A., Ekaykin, A. A., Ersek, V., Filipsson, H. L., Francus, P., Freund, M. B., Frezzotti,
1097 M., Gaire, N. P., Gajewski, K., Ge, Q., Goosse, H., Gornostaeva, A., Grosjean, M., Horiuchi, K., Hormes, A.,
1098 Husum, K., Isaksson, E., Kandasamy, S., Kawamura, K., Kilbourne, K. H., Koç, N., Leduc, G., Linderholm, H.
1099 W., Lorrey, A. M., Mikhalenko, V., Mortyn, P. G., Motoyama, H., Moy, A. D., Mulvaney, R., Munz, P. M.,
1100 Nash, D. J., Oerter, H., Opel, T., Orsi, A. J., Ovchinnikov, D. V., Porter, T. J., Roop, H. A., Saenger, C., Sano,
1101 M., Sauchyn, D., Saunders, K. M., Seidenkrantz, M.-S., Severi, M., Shao, X., Sicre, M.-A., Sigl, M., Sinclair,
1102 K., George, S. S., Jacques, J.-M. S., Thamban, M., Thapa, U. K., Thomas, E. R., Turney, C., Uemura, R.,
1103 Viau, A. E., Vladimirova, D. O., Wahl, E. R., White, J. W. C., Yu, Z., and Zinke, J.: A global multiproxy
1104 database for temperature reconstructions of the Common Era, *Scientific Data*, 4, sdata201788,
1105 <https://doi.org/10.1038/sdata.2017.88>, 2017.
- 1106 Peregrine, P. N.: Climate and social change at the start of the Late Antique Little Ice Age, *The Holocene*,
1107 30, 1643–1648, <https://doi.org/10.1177/0959683620941079>, 2020.
- 1108 Pérez-Mejías, C., Moreno, A., Sancho, C., Bartolomé, M., Stoll, H., Osácar, M. C., Cacho, I., and Delgado-
1109 Huertas, A.: Transference of isotopic signal from rainfall to dripwaters and farmed calcite in
1110 Mediterranean semi-arid karst, *Geochimica et Cosmochimica Acta*, 243, 66–98,
1111 <https://doi.org/10.1016/j.gca.2018.09.014>, 2018.
- 1112 [Pérez-Sanz, A., González-Samperiz, P., Valero-Garcés, B., Moreno, A., Morellón, M., Sancho, C.,
1113 Belmonte, A., Gil-Romera, G., Sevilla-Callejo, M., and Navas, A.: Clima y actividades humanas en la
1114 dinámica de la vegetación durante los últimos 2000 años en el Pirineo Central: el registro palinológico de
1115 la Basa de la Mora \(Macizo de Cotiella\), *Zubia*, 23, 17–38, 2011.](https://doi.org/10.1016/j.jgl.2011.03.001)
- 1116 Pérez-Zanón, N., Sigró, J., and Ashcroft, L.: Temperature and precipitation regional climate series over
1117 the central Pyrenees during 1910–2013, *International Journal of Climatology*, 37, 1922–1937,
1118 <https://doi.org/10.1002/joc.4823>, 2017.

1119 Pla, S. and Catalan, J.: Chrysophyte cysts from lake sediments reveal the submillennial winter/spring
1120 climate variability in the northwestern Mediterranean region throughout the Holocene, *Climate*
1121 *Dynamics*, 24, 263–278, <https://doi.org/10.1007/s00382-004-0482-1>, 2005.

1122 Pla-Rabes, S. and Catalan, J.: Deciphering chrysophyte responses to climate seasonality, *J Paleolimnol*,
1123 46, 139, <https://doi.org/10.1007/s10933-011-9529-6>, 2011.

1124 [Priestley, S. C., Treble, P. C., Griffiths, A. D., Baker, A., Abram, N. J., and Meredith, K. T.: Caves](#)
1125 [demonstrate decrease in rainfall recharge of southwest Australian groundwater is unprecedented for](#)
1126 [the last 800 years, *Commun Earth Environ*, 4, 1–12, <https://doi.org/10.1038/s43247-023-00858-7>, 2023.](#)

1127 Reimer, P.: Discussion: Reporting and Calibration of Post-Bomb 14C Data, *Radiocarbon*, 46, 1299–1304,
1128 <https://doi.org/10.1017/S003822200033154>, 2004.

1129 Rico, I., Izagirre, E., Serrano, E., and López-Moreno, J. I.: Superficie glaciaria actual en los Pirineos: Una
1130 actualización para 2016, *Pirineos*, 172, 029, <https://doi.org/10.3989/Pirineos.2017.172004>, 2017.

1131 [Riera, S., Lopez-Saez, J. A., and Julia, R.: Lake responses to historical land use changes in northern Spain:](#)
1132 [The contribution of non-pollen palynomorphs in a multiproxy study, *Review of Palaeobotany and*](#)
1133 [Palynology](#), 141, 127–137, 2006.

1134 [Rull, V., González-Sampériz, P., Corella, J. P., Morellón, M., and Giral, S.: Vegetation changes in the](#)
1135 [southern Pyrenean flank during the last millennium in relation to climate and human activities: the](#)
1136 [Montcortès lacustrine record, *J Paleolimnol*, 46, 387–404, <https://doi.org/10.1007/s10933-010-9444-2>,](#)
1137 [2011.](#)

1138 Sánchez-López, G., Hernández, A., Pla-Rabes, S., Trigo, R. M., Toro, M., Granados, I., Sáez, A., Masqué, P.,
1139 Pueyo, J. J., Rubio-Inglés, M. J., and Giral, S.: Climate reconstruction for the last two millennia in central
1140 Iberia: The role of East Atlantic (EA), North Atlantic Oscillation (NAO) and their interplay over the Iberian
1141 Peninsula, *Quaternary Science Reviews*, 149, 135–150, <https://doi.org/10.1016/j.quascirev.2016.07.021>,
1142 2016.

1143 Sancho, C., Belmonte, Á., Bartolomé, M., Moreno, A., Leunda, M., and López-Martínez, J.: Middle-to-late
1144 Holocene palaeoenvironmental reconstruction from the A294 ice-cave record (Central Pyrenees,
1145 northern Spain), *Earth and Planetary Science Letters*, 484, 135–144,
1146 <https://doi.org/10.1016/j.epsl.2017.12.027>, 2018.

1147 Scholz, D. and Hoffmann, D. L.: StalAge - An algorithm designed for construction of speleothem age
1148 models, *Quaternary Geochronology*, 6, 369–382, <https://doi.org/10.1016/j.quageo.2011.02.002>, 2011.

1149 [Scussolini, P., Vegas-Vilarrúbia, T., Rull, V., Corella, J. P., Valero-Garcés, B., and Gomà, J.: Middle and late](#)
1150 [Holocene climate change and human impact inferred from diatoms, algae and aquatic macrophyte](#)
1151 [pollen in sediments from Lake Montcortès \(NE Iberian Peninsula\), *Journal of Paleolimnology*, 46, 369–](#)
1152 [385, <https://doi.org/10.1007/s10933-011-9524-y>, 2011.](#)

1153 [Schurer, A. P., Tett, S. F. B., and Hegerl, G. C.: Small influence of solar variability on climate over the past](#)
1154 [millennium, *Nature Geosci.* 7, 104–108, <https://doi.org/10.1038/ngeo2040>, 2014.](#)

1155 Shen, C. C., Edwards, R. L., Cheng, H., Dorale, J. A., Thomas, R. B., Moran, S. B., Weinstein, S. E., and
1156 Edmonds, H. N.: Uranium and thorium isotopic and concentration measurements by magnetic sector
1157 inductively coupled plasma mass spectrometry, *Chemical Geology*, 185, 165–178, 2002.

1158 Shindell, D. T., Schmidt, G. A., Mann, M. E., Rind, D., and Waple, A.: benito, *Science*, 294, 2149, 2001.

1159 Sigl, M., Winstrup, M., McConnell, J. R., Welten, K. C., Plunkett, G., Ludlow, F., Büntgen, U., Caffee, M.,
1160 Chellman, N., Dahl-Jensen, D., Fischer, H., Kipfstuhl, S., Kostick, C., Maselli, O. J., Mekhaldi, F., Mulvaney,
1161 R., Muscheler, R., Pasteris, D. R., Pilcher, J. R., Salzer, M., Schüpbach, S., Steffensen, J. P., Vinther, B. M.,

1162 and Woodruff, T. E.: Timing and climate forcing of volcanic eruptions for the past 2,500 years, *Nature*,
1163 523, 543–549, <https://doi.org/10.1038/nature14565>, 2015.

1164 Spötl, C.: Long-term performance of the Gasbench isotope ratio mass spectrometry system for the
1165 stable isotope analysis of carbonate microsamples, *Rapid Commun. Mass Spectrom.*, 25, 1683–1685,
1166 <https://doi.org/10.1002/rcm.5037>, 2011.

1167 Steffen, W., Broadgate, W., Deutsch, L., Gaffney, O., and Ludwig, C.: The trajectory of the Anthropocene:
1168 The Great Acceleration, *The Anthropocene Review*, 2, 81–98,
1169 <https://doi.org/10.1177/2053019614564785>, 2015.

1170 Sundqvist, H. S., Holmgren, K., Moberg, A., Spötl, C., and Mangini, A.: Stable isotopes in a stalagmite
1171 from NW Sweden document environmental changes over the past 4000 years, *Boreas*, 39, 77–86,
1172 <https://doi.org/10.1111/j.1502-3885.2009.00099.x>, 2010.

1173 [Swingedouw, D., Terray, L., Cassou, C., Voldoire, A., Salas-Melia, D., and Servonnat, J.: Natural forcing of](https://doi.org/10.1007/s00382-010-0803-5)
1174 [climate during the last millennium: fingerprint of solar variability, *Climate Dynamics*, 36, 1349–1364,](https://doi.org/10.1007/s00382-010-0803-5)
1175 <https://doi.org/10.1007/s00382-010-0803-5>, 2011.

1176 Tadros, C. V., Markowska, M., Treble, P. C., Baker, A., Frisia, S., Adler, L., and Drysdale, R. N.: Recharge
1177 variability in Australia’s southeast alpine region derived from cave monitoring and modern stalagmite
1178 $\delta^{18}\text{O}$ records, *Quaternary Science Reviews*, 295, 107742,
1179 <https://doi.org/10.1016/j.quascirev.2022.107742>, 2022.

1180 Thatcher, D. L., Wanamaker, A. D., Denniston, R. F., Ummenhofer, C. C., Asmerom, Y., Polyak, V. J.,
1181 Cresswell-Clay, N., Hasiuk, F., Haws, J., and Gillikin, D. P.: Iberian hydroclimate variability and the Azores
1182 High during the last 1200 years: evidence from proxy records and climate model simulations, *Clim Dyn*,
1183 <https://doi.org/10.1007/s00382-022-06427-6>, 2022.

1184 Trachsel, M., Kamenik, C., Grosjean, M., McCarroll, D., Moberg, A., Brázdil, R., Büntgen, U., Dobrovolný,
1185 P., Esper, J., Frank, D. C., Friedrich, M., Glaser, R., Larocque-Tobler, I., Nicolussi, K., and Riemann, D.:
1186 Multi-archive summer temperature reconstruction for the European Alps, AD 1053–1996, *Quaternary*
1187 *Science Reviews*, 46, 66–79, <https://doi.org/10.1016/j.quascirev.2012.04.021>, 2012.

1188 [Treble, P. C., Baker, A., Abram, N. J., Hellstrom, J. C., Crawford, J., Gagan, M. K., Borsato, A., Griffiths, A.](https://doi.org/10.1038/s43247-022-00347-3)
1189 [D., Bajo, P., Markowska, M., Priestley, S. C., Hankin, S., and Paterson, D.: Ubiquitous karst hydrological](https://doi.org/10.1038/s43247-022-00347-3)
1190 [control on speleothem oxygen isotope variability in a global study, *Commun Earth Environ*, 3, 1–10,](https://doi.org/10.1038/s43247-022-00347-3)
1191 <https://doi.org/10.1038/s43247-022-00347-3>, 2022.

1192 Tremaine, D. M., Froelich, P. N., and Wang, Y.: Speleothem calcite farmed in situ: Modern calibration of
1193 $\delta^{18}\text{O}$ and $\delta^{13}\text{C}$ paleoclimate proxies in a continuously-monitored natural cave system, *Geochimica et*
1194 *Cosmochimica Acta*, 75, 4929–4950, <https://doi.org/10.1016/j.gca.2011.06.005>, 2011.

1195 [Trouet, V., Esper, J., Graham, N. E., Baker, A., Scourse, J. D., and Frank, D. C.: Persistent Positive North](https://doi.org/10.1016/j.sci.2009.06.005)
1196 [Atlantic Oscillation Mode Dominated the Medieval Climate Anomaly, *Science*, 324, 78–80, 2009.](https://doi.org/10.1016/j.sci.2009.06.005)

1197 [Trouet, V., Scourse, J. D., and Raible, C. C.: North Atlantic storminess and Atlantic Meridional](https://doi.org/10.1016/j.gloplacha.2011.10.003)
1198 [Overturning Circulation during the last Millennium: Reconciling contradictory proxy records of NAO](https://doi.org/10.1016/j.gloplacha.2011.10.003)
1199 [variability, *Global and Planetary Change*, 84–85, 48–55,](https://doi.org/10.1016/j.gloplacha.2011.10.003)
1200 <https://doi.org/10.1016/j.gloplacha.2011.10.003>, 2012.

1201 [Usoskin, I. G., Hulot, G., Gallet, Y., Roth, R., Licht, A., Joos, F., Kovaltsov, G. A., Thébault, E., and](https://doi.org/10.1051/0004-6361/201423391)
1202 [Khokhlov, A.: Evidence for distinct modes of solar activity, *A&A*, 562, L10, \[6361/201423391\]\(https://doi.org/10.1051/0004-
1203 <a href=\), 2014.](https://doi.org/10.1051/0004-6361/201423391)

1204 [Usoskin, I. G., Gallet, Y., Lopes, F., Kovaltsov, G. A., and Hulot, G.: Solar activity during the Holocene: the](#)
1205 [Hallstatt cycle and its consequence for grand minima and maxima, *A&A*, 587, A150,](#)
1206 <https://doi.org/10.1051/0004-6361/201527295>, 2016.

1207 Vegas-Vilarrúbia, T., Corella, J. P., Sigró, J., Rull, V., Dorado-Liñan, I., Valero-Garcés, B., and Gutiérrez-
1208 Merino, E.: Regional precipitation trends since 1500 CE reconstructed from calcite sublayers of a varved
1209 Mediterranean lake record (Central Pyrenees), *Science of The Total Environment*, 826, 153773,
1210 <https://doi.org/10.1016/j.scitotenv.2022.153773>, 2022.

1211 Vicente de Vera García, A., Mata-Campo, M. P., Pla, S., Vicente, E., Prego, R., Frugone-Álvarez, M.,
1212 Polanco-Martínez, J., Galofré, M., and Valero-Garcés, B. L.: Unprecedented recent regional increase in
1213 organic carbon and lithogenic fluxes in high altitude Pyrenean lakes, *Sci Rep*, 13, 8586,
1214 <https://doi.org/10.1038/s41598-023-35233-1>, 2023.

1215 Vidaller, I., Revuelto, J., Izagirre, E., Rojas-Heredia, F., Alonso-González, E., Gascoin, S., René, P., Berthier,
1216 E., Rico, I., Moreno, A., Serrano, E., Serreta, A., and López-Moreno, J. I.: Toward an Ice-Free Mountain
1217 Range: Demise of Pyrenean Glaciers During 2011–2020, *Geophys Res Lett*, 48,
1218 <https://doi.org/10.1029/2021GL094339>, 2021.

1219 Welte, C., Wacker, L., Hattendorf, B., Christl, M., Koch, J., Synal, H.-A., and Günther, D.: Novel Laser
1220 Ablation Sampling Device for the Rapid Radiocarbon Analysis of Carbonate Samples by Accelerator Mass
1221 Spectrometry, *Radiocarbon*, 58, 419–435, <https://doi.org/10.1017/RDC.2016.6>, 2016.

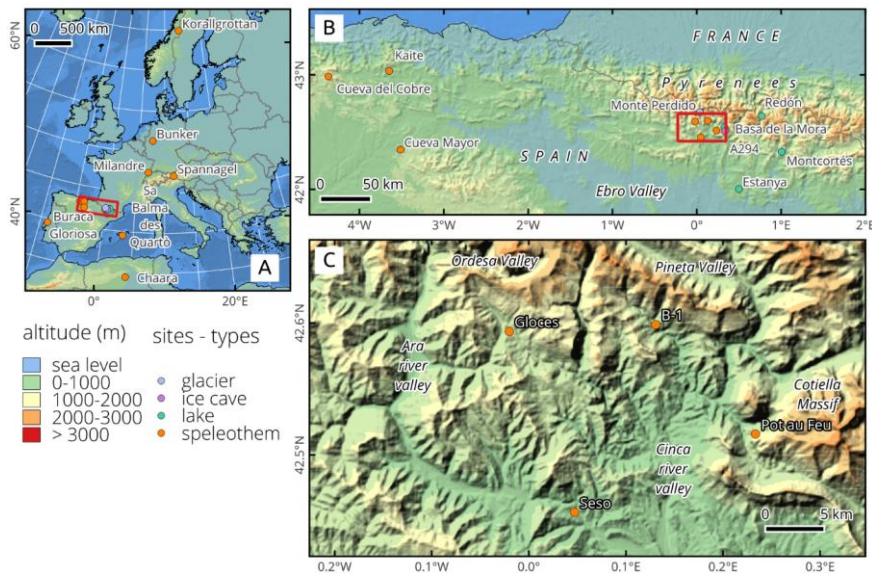
1222 Zawiska, I., Luoto, T. P., Nevalainen, L., Tylmann, W., Jensen, T. C., Obremaska, M., Słowiński, M.,
1223 Woszczyk, M., Schartau, A. K., and Walseng, B.: Climate variability and lake ecosystem responses in
1224 western Scandinavia (Norway) during the last Millennium, *Palaeogeography, Palaeoclimatology,*
1225 *Palaeoecology*, 466, 231–239, <https://doi.org/10.1016/j.palaeo.2016.11.034>, 2017.

1226

1227

1228 **Figure captions**

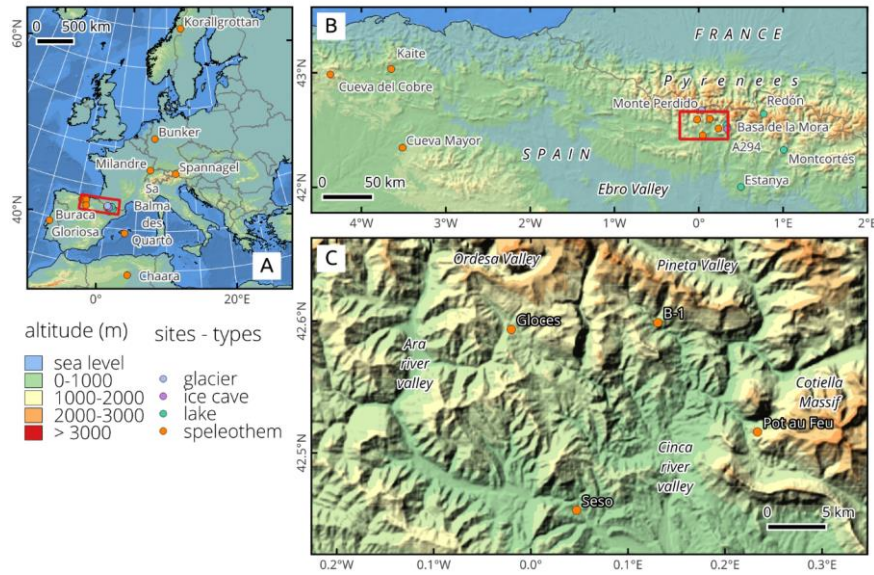
1229 **Figure 1.** **Aa)** Location of regional speleothem records covering last 2500 years to be compared with the
 1230 samples studied in the Pyrenees (red rectangle, enlarged in Fig. 1B). **Bb)** Location of caves (orange circles)
 1231 and other nearby records from northern Spain. See legend for the different types of available paleoclimate
 1232 archives. **Cc)** Location of the four studied caves in the Central Pyrenees of NE Spain in the vicinity of the
 1233 Ordesa and Monte Perdido National Park. Source base map: [digital elevation model and hillshade derived](#)
 1234 [from Mapzen Global Terrain, coastline, boundaries and geographic lines from NaturalEarthData.com](#)



1235

1236

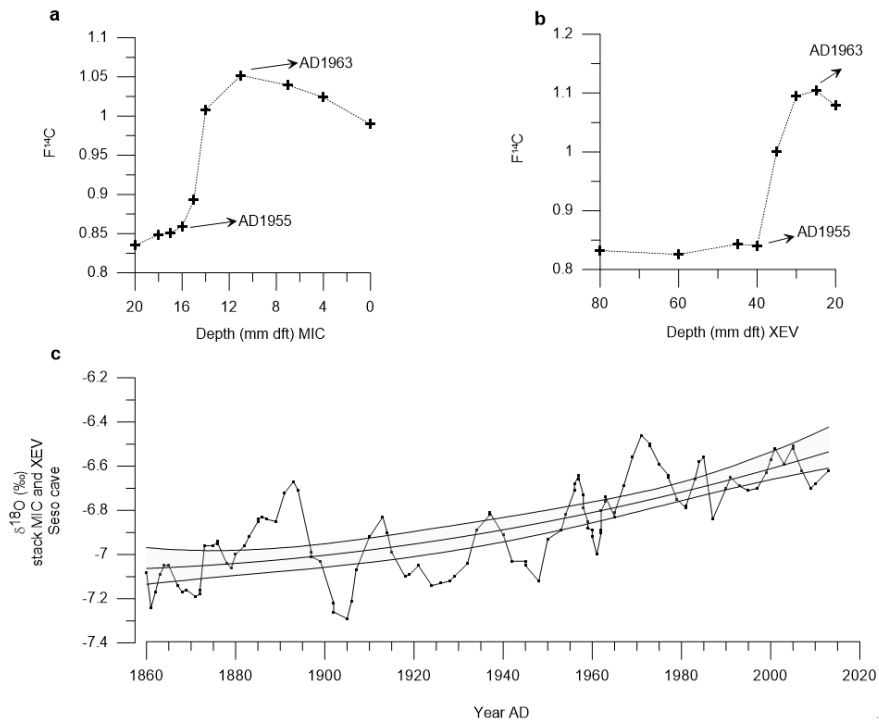
1237 **Figure 2.** $\delta^{14}\text{C}$ activity (expressed as F^{14}C)



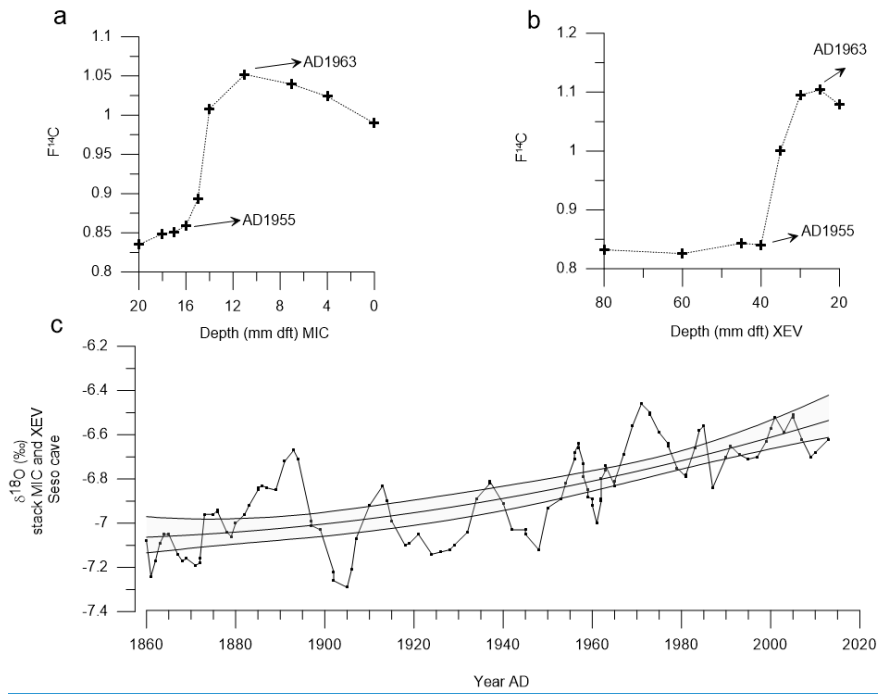
1238

1239

1240 **Figure 2.** ^{14}C activity (expressed as $F^{14}\text{C}$, following recommendations made in Reimer, 2004) of the top
1241 parts of stalagmites MIC (a) and XEV (b) from Seso Cave. The start of the increase in $F^{14}\text{C}$ and its
1242 maximum are recorded at 1955 and 1963 ADCE, respectively, in both stalagmites. c) Composite $\delta^{18}\text{O}$
1243 record using *Iscam* with data from MIC and XEV stalagmites.



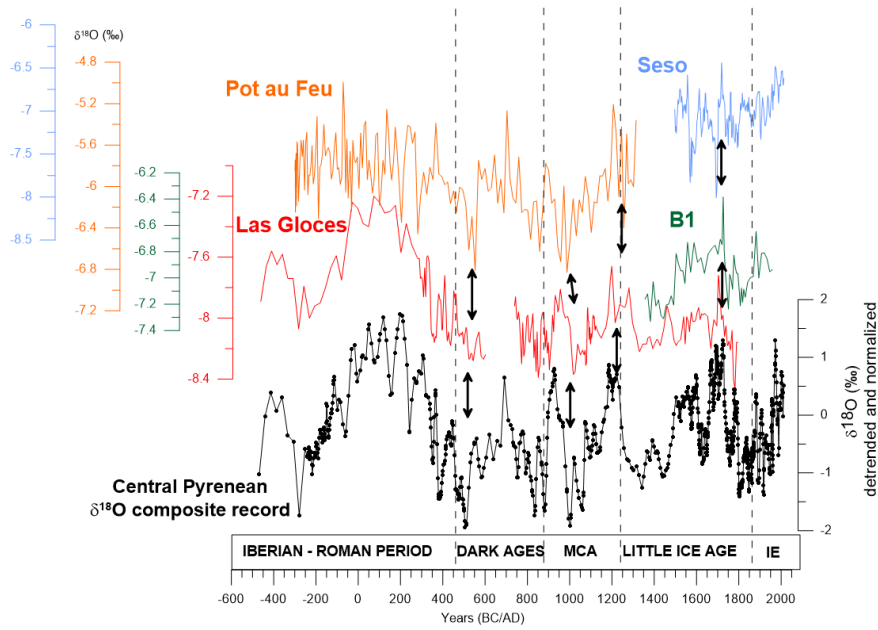
1244



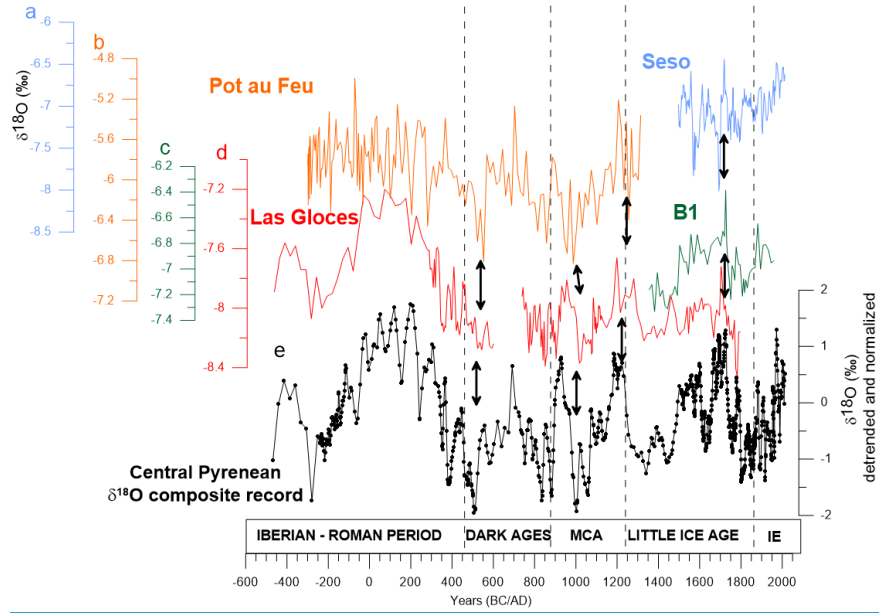
1245

1246

1247 **Figure 3.** Comparison of individual $\delta^{18}\text{O}$ records from four Pyrenean caves (orange, (a) Seso; (b) Pot au
 1248 Feu; blue, Seso; red, (c) B1 and (d) Las Gloces caves, and green, B1 cave) and (e) the composite $\delta^{18}\text{O}$ record
 1249 produced using *Iscam* (black curve) for the last 2500 years. Generating Seso and Las Gloces curves required
 1250 *Iscam* age modelling while Pot au Feu and B1 curves represent only one stalagmite, which age model was
 1251 produced by *StalAge* modelling. Black double arrows indicate intervals with patterns present in all records.
 1252 MCA: Medieval Climate Anomaly, IE: Industrial Era.



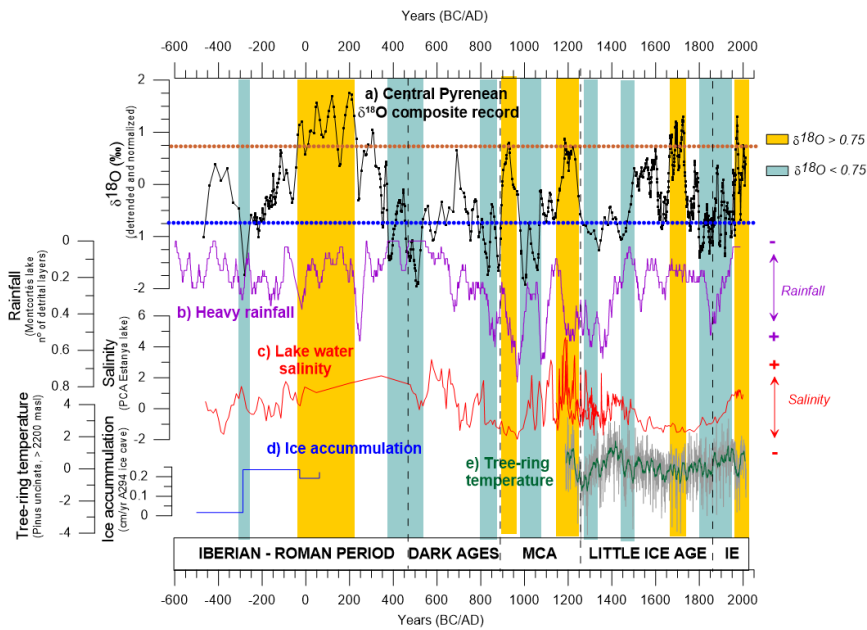
1253



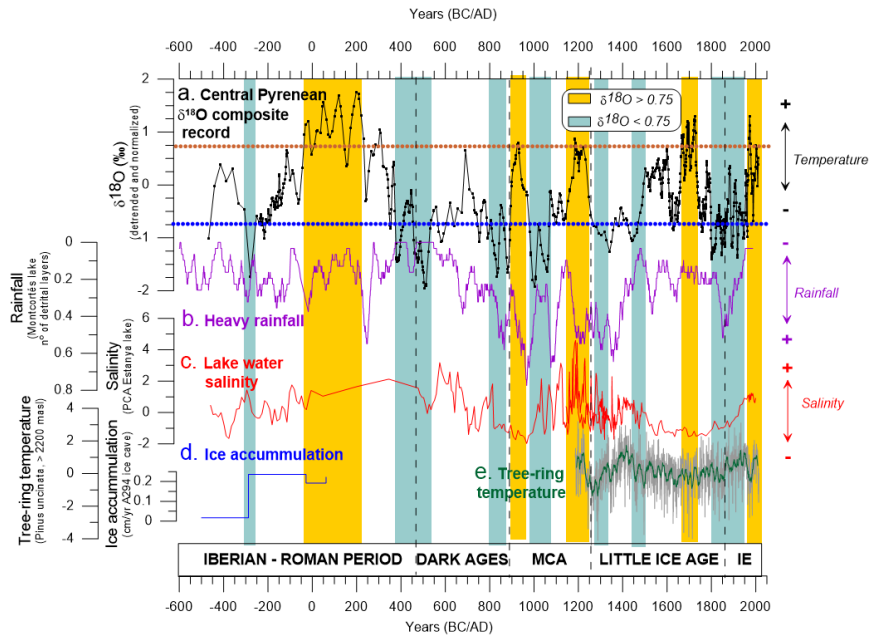
1254

1255

1256 **Figure 4.** a) Central Pyrenean $\delta^{18}\text{O}$ composite record for the last 2500 years based on eight stalagmites
 1257 from four caves. Blue bars mark intervals of $\delta^{18}\text{O}$ values below -0.75 , while yellow bars mark those with
 1258 $\delta^{18}\text{O}$ values above $+0.75$ (note this composite record was obtained from normalized records, so it varies
 1259 among -3 and 3 without possibility of direct translation to absolute $\delta^{18}\text{O}$ values). b) Rainfall reconstructed
 1260 from calcite layers from Montcortés lake in the Pre-Pyrenees (Corella et al., 2016). c) Salinity reconstructed
 1261 from geochemical data from Estanya lake in the Pre-Pyrenees (González-Sampérez et al., 2017; Morellón
 1262 et al., 2012, 2011). d) Snow and ice accumulation in ice cave A294 in the Cotiella massif of the Central
 1263 Pyrenees (Sancho et al., 2018), and e) Pyrenean temperature reconstruction based on tree-ring data
 1264 (Büntgen et al., 2017). MCA: Medieval Climate Anomaly, IE: Industrial Era.



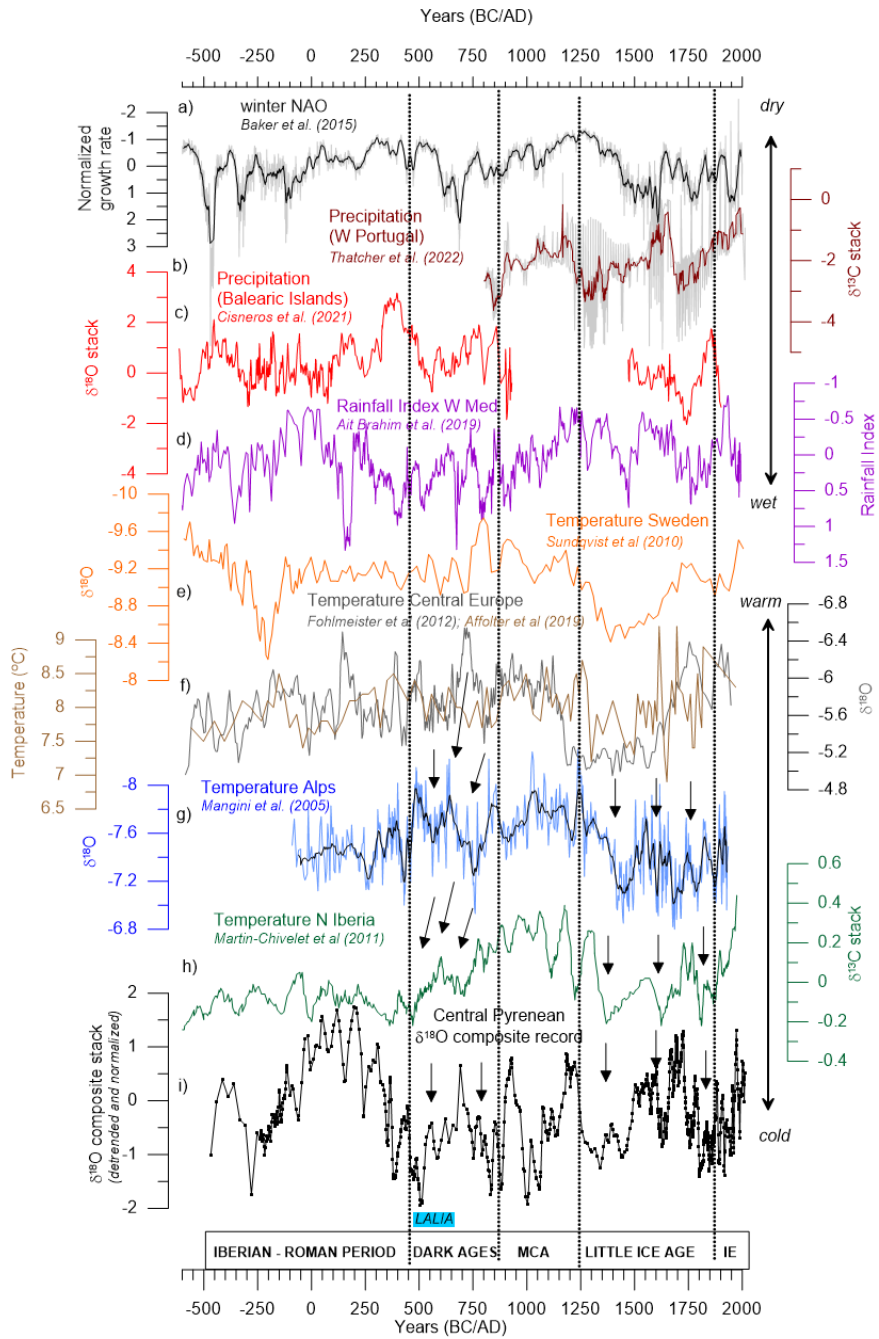
1265

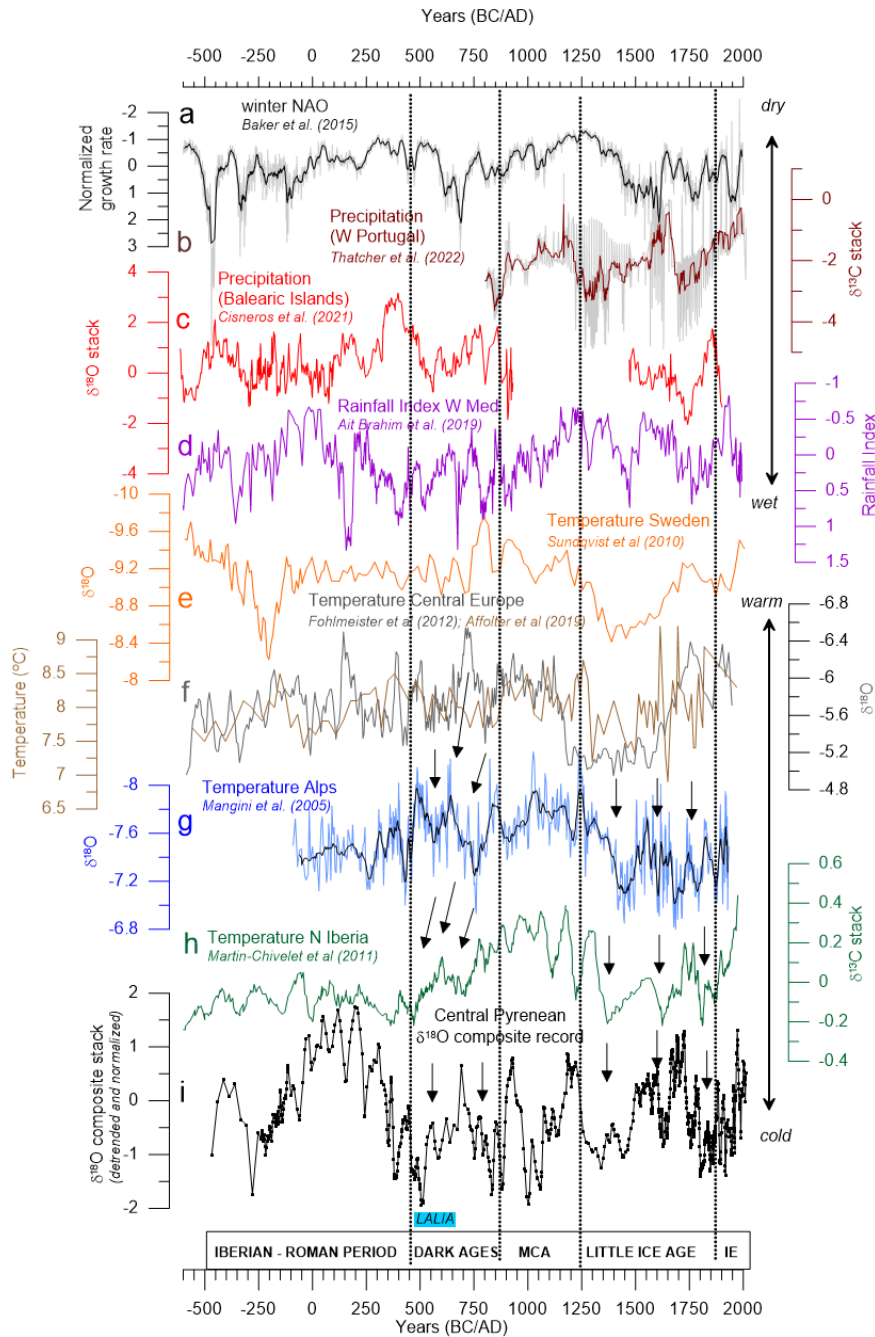


1266

1267

1268 **Figure 5.** Comparison of European and W Mediterranean speleothem records covering the last 2500 years.
1269 a) winter NAO reconstruction based on growth rate of Irish speleothems (Baker et al., 2015); b)
1270 precipitation variability reconstructed for W Portugal (Thatcher et al., 2022), c) Balearic Islands (Cisneros
1271 et al., 2021), and d) Morocco (Ait Brahim et al., 2019); temperature variation reconstructed from e) Sweden
1272 (Sundqvist et al., 2010), f) Central Europe (Affolter et al., 2019; Fohlmeister et al., 2012), g) Alps (Mangini
1273 et al., 2005) and h) Northern Iberia (Martín-Chivelet et al., 2011); i) Central Pyrenean $\delta^{18}\text{O}$ composite
1274 record (this study). Black arrows indicate intervals of well-reproduced patterns during the Dark Ages and
1275 the Little Ice Age cold intervals. MCA: Medieval Climate Anomaly, IE: Industrial Era.



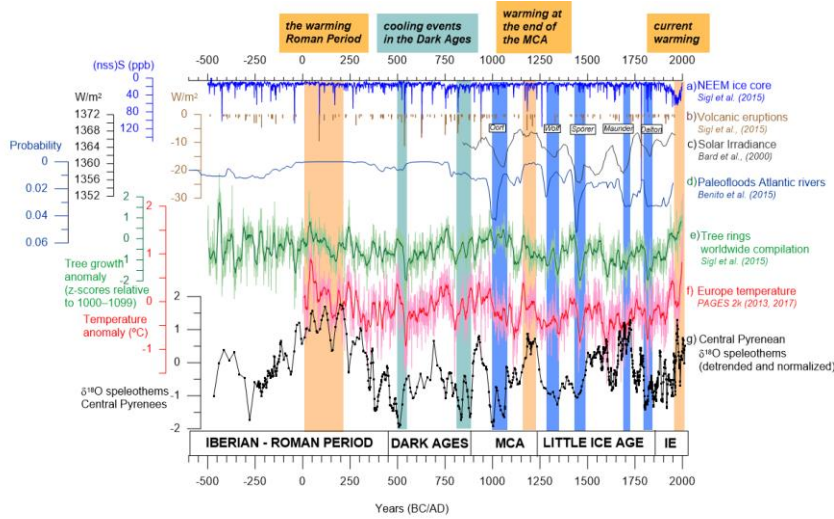


1277

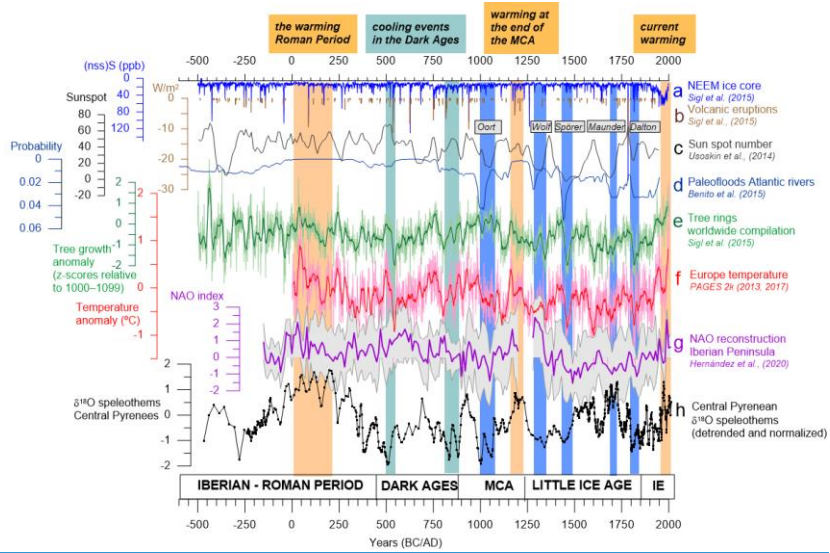
1278

1279 **Figure 6.** Global records and forcing mechanisms. a) volcanic forcing represented by the (nss)S (ppb) in
 1280 the NEEEM ice core (blue line); b) changes in the irradiance as a consequence of Northern Hemisphere
 1281 volcanic eruptions (Sigl et al., 2015) (brown bars); c) solar irradiance (Bard et al., 2000) sunspot numbers
 1282 (Usoskin et al., 2014); d) probability of paleofloods in European temperate regions (Benito et al., 2015); e)
 1283 worldwide tree-ring compilation (green line, running average width window = 15) (Sigl et al., 2015); f)
 1284 temperature reconstruction from Europe, compiled by the PAGES2k group (red line, running average width
 1285 window = 15) (PAGES 2k Consortium, 2013); g) the NAO reconstruction for the Central Iberian Peninsula
 1286 (purple line) and the 95% (light grey band) uncertainty intervals and h) Central Pyrenean $\delta^{18}\text{O}$ composite
 1287 record (this study). Light brown bars indicate warming periods during the Roman Period, the end of the
 1288 MCA and in recent decades. Light blue bands mark cooling events during the DA while dark blue bands
 1289 mark solar minima (Oort, Wolf, Spörer, Maunder and Dalton). MCA: Medieval Climate Anomaly, IE:
 1290 Industrial Era.

- Con formato: Inglés (Estados Unidos)
- Con formato: Inglés (Estados Unidos)
- Código de campo cambiado
- Con formato: Inglés (Estados Unidos)
- Código de campo cambiado
- Con formato: Inglés (Estados Unidos)
- Código de campo cambiado



1291



1292

1293

1294 **Table 1.** Sample characteristics

Cave	Sample ID	Length (cm)	Number of U-Th dates (used in StalAge)	Interval covered (years BC/AD BCE/CE in StalAge)	Sampling resolution (average years per isotope sample)	Comments
<i>Seso</i>	MIC	8.5	8	1718- 2010AD 2010 CE	3.8 years	Growth to present
	XEV	26	9	1501- 2013AD 2013 CE	1.9 years	Two growth periods, no hiatus. Growth to present
	CHA	8.5	3	1573- 1779AD 1779 CE	3.5 years	The uppermost 7 mm are not sampled
	CLA	10.5 (a hiatus at 8.5 cm)	4	1826- 1935AD 1935 CE	1.5 years	The uppermost 2 cm are not sampled
<i>Las Gloces</i>	ISA	13.5 (a hiatus at 7 cm)	7	346- 607AD 607 CE 845- 634AD 634 CE	11.4 years	In StalAge, one date is not included due to high error
	LUC	23.3 (a hiatus at 12.5 cm)	6	471BC -504AD 471BCE-504 CE 547- 1991AD 1991 CE	11.2 years	Really short hiatus
<i>B-1</i>	TAR	7.5 cm	8	1355- 1959AD 1959 CE	10.5 years	
<i>Pot au Feu</i>	JAR	80 cm	10	299BC - 1314AD299BCE- 1314 CE	10 years	

Tabla con formato

1295
1296

1297
1298
1299
1300
1301

Table 2. ²³⁰Th dating results of the eight stalagmites examined in this study (data from the University of Minnesota, University of Xi'an and University of Melbourne). Analytical errors are 2σ of the mean. The sample marked by a red asterisk was discarded due to the high error.

Sample ID	²³⁸ U (ppb)	²³² Th (ppb)	²³⁰ Th/ ²³² Th (0)	²³⁴ U (measured) (a)	²³⁰ Th/ ²³⁴ U (0)
Xca-0	451 ± 1	1292 ± 248	4.0 ± 0.1	45.3 ± 3.1	0.0066 ± 0.0001
Xca-5	351 ± 1	2675 ± 58	4.2 ± 0.2	43.3 ± 2.9	0.0021 ± 0.0001
Xca-8	299 ± 1	1597 ± 31	8.0	43.6 ± 3.1	0.0027 ± 0.0001
Xca-10	308 ± 1	798 ± 16	18 ± 1	41.5 ± 2.4	0.0025 ± 0.0001
Xca-15	267 ± 1	335 ± 11	25 ± 1	40.7 ± 2.7	0.0033 ± 0.0001
Xca-90	361 ± 1	340 ± 7	54 ± 2	41.0 ± 2.8	0.0033 ± 0.0001
Xca-210	299 ± 1	1445 ± 29	20 ± 1	42.8 ± 3.5	0.0029 ± 0.0002
Xca-240	277 ± 1	1738 ± 35	19 ± 1	43.4 ± 2.7	0.0072 ± 0.0002
Xca-280	339 ± 1	2499 ± 50	20 ± 0	41.7 ± 3.8	0.0086 ± 0.0001
Xca-0	303 ± 1	4623 ± 95	5 ± 0	48.9 ± 2.4	0.0027 ± 0.0001
Xca-20	441 ± 1	1166 ± 23	6 ± 1	48.3 ± 2.3	0.0009 ± 0.0002
Xca-5	412 ± 1	127 ± 3	73 ± 6	47.0 ± 2.3	0.0014 ± 0.0001
Xca-35	427 ± 1	708 ± 14	25 ± 1	45.2 ± 2.3	0.0025 ± 0.0001
Xca-48	417 ± 1	603 ± 12	34 ± 1	45.7 ± 3.0	0.0030 ± 0.0001
Xca-60	393 ± 1	1049 ± 21	23 ± 1	46.1 ± 3.8	0.0037 ± 0.0001
Xca-67	413 ± 1	3812 ± 77	9 ± 0	48.7 ± 2.9	0.0051 ± 0.0001
Xca-75	389 ± 1	25715 ± 517	4 ± 0	45.8 ± 2.5	0.0141 ± 0.0002
Xca-0	346 ± 1	332 ± 7	34 ± 2	37.1 ± 3.1	0.0020 ± 0.0001
Xca-25	368 ± 1	493 ± 10	32 ± 1	36.1 ± 2.9	0.0026 ± 0.0001
Xca-70	346 ± 1	1262 ± 25	17 ± 1	36.8 ± 2.4	0.0037 ± 0.0001
Xca-74	319 ± 1	226 ± 5	70 ± 3	38.6 ± 2.7	0.0030 ± 0.0001
Xca-0	393 ± 0.7	169 ± 3	116 ± 6	38.0 ± 2.0	0.0030 ± 0.0001
Xca-30	3429 ± 1.0	69 ± 1.2	47 ± 2	38.2 ± 3.0	0.0030 ± 0.0001
Xca-58	3481 ± 0.8	396 ± 8	81 ± 2	39.3 ± 2.7	0.0035 ± 0.0001
Las Chaves cave					
Ksa-0	1671 ± 0.3	431 ± 9	233 ± 5	146.3 ± 3.4	0.0282 ± 0.0003
Ksa-4	1193 ± 0.2	291 ± 6	221 ± 5	148.0 ± 4.1	0.0225 ± 0.0003
Ksa-4	1150 ± 0.1	905 ± 18	61 ± 2	151.0 ± 3.1	0.0289 ± 0.0004
Ksa-6	1077 ± 0.2	8322 ± 171	5 ± 1	150.8 ± 4.5	0.0253 ± 0.0004
Ksa-8	1084 ± 0.1	261 ± 5	142 ± 4	150.6 ± 3.6	0.0207 ± 0.0004
Ksa-11	693 ± 0.1	2977 ± 60	8 ± 1	150.3 ± 3.7	0.0201 ± 0.0006
Lac-0	113 ± 1	2380 ± 47	56 ± 1	189.9 ± 4	0.0469 ± 0.0005
Lac-5	88 ± 1	539 ± 11	127 ± 3	188.8 ± 4	0.0469 ± 0.0005
Lac-10	131 ± 0.2	388 ± 8	213 ± 5	172.6 ± 3.2	0.0382 ± 0.0003
Lac-11	81 ± 1	955 ± 19	50 ± 1	179.6 ± 5	0.0359 ± 0.0005
Lac-15	73 ± 0	282 ± 6	118 ± 3	178.3 ± 6	0.0279 ± 0.0005
Lac-18	72 ± 0	1477 ± 30	16 ± 1	170.5 ± 5	0.0202 ± 0.0005
Lac-22.5	139 ± 0	287 ± 6	47 ± 2	154 ± 3	0.0035 ± 0.0002
Bl-fence					
Bl-12.5: 5.6m	6083 ± 27	797 ± 16	49 ± 2	288.5 ± 2.5	0.0039 ± 0.0002
Bl-12.5: 4.4m	625 ± 32	201 ± 4	60 ± 14	258.5 ± 1.8	0.0019 ± 0.0001
Bl-12.5: 3.7m	1006 ± 47	616 ± 12	392 ± 9	262 ± 2.3	0.0016 ± 0.0001
Bl-12.5: 3.1m	8347 ± 31	10930 ± 219	20 ± 1	264 ± 1.4	0.0019 ± 0.0002
Bl-12.5: 2.6m	7424 ± 27	163 ± 33	156 ± 3	264 ± 1.5	0.0028 ± 0.0002
Bl-12.5: 1.6m	8318 ± 31	385 ± 8	102 ± 23	262 ± 2.0	0.0025 ± 0.0002
Bl-12.5: 1.0m	9499 ± 41	551 ± 11	290 ± 1.5	260 ± 1.5	0.0033 ± 0.0002
Bl-12.5: 0 m	8128 ± 33	649 ± 13	88 ± 18	260 ± 1.9	0.00428 ± 0.0002

1302

1303 U decay constants: $\lambda_{238} = 1.55125 \times 10^{-10}$ (Jaffey et al., 1971) and $\lambda_{234} = 2.82206 \times 10^{-6}$ (Cheng et al., 2013).

1304 Th decay constant: $\lambda_{230} = 9.1705 \times 10^{-6}$ (Cheng et al., 2013).

1305
$$* \delta^{234}U = \left(\frac{^{234}U}{^{238}U} \right)_{activity} - 1 \times 1000$$

1306
$$** \delta^{234}U_{initial} \text{ was calculated based on } ^{230}Th \text{ age (T), i.e., } \delta^{234}U_{initial} = \delta^{234}U_{measured} \times e^{-\lambda_{234}T}$$

1307 Corrected ²³⁰Th ages assume the initial ²³⁰Th/²³²Th atomic ratio of $4.4 \pm 2.2 \times 10^{-6}$. Those are the values

1308 for a material at secular equilibrium, with the bulk earth ²³²Th/²³⁸U value of 3.8. The errors are

1309 arbitrarily assumed to be 50%.

1310 ***B.P. stands for "Before Present" where the "Present" is defined as the year 1950 A.D.

1311

Sample	^{210}Po (ppb)	$^{210}\text{Po}/^{210}\text{Pb}$ (a)	$^{210}\text{Po}/^{210}\text{Pb}$ (a)	Point Pair curve		Age (yr BP) (b)	Age (yr BP) (b)	error	$^{210}\text{Po}/^{210}\text{Pb}$ build (c)
				$^{210}\text{Po}/^{210}\text{Pb}$ (a)	$^{210}\text{Po}/^{210}\text{Pb}$ (a)				
CEP775	109	0.022	1.570	0.004	2.6	158	746	-193	1.72
CEP787	NR	0.015	1.583	0.017	7.3	884	713	-179	1.86
CEP788	NR	0.014	1.580	0.015	7.1	890	712	-182	1.81
CEP789	NR	0.014	1.580	0.015	7.1	890	712	-182	1.81
CEP793	NR	0.030	1.533	0.001	5.8	217	1652	-253	1.56
CEP790	NR	0.029	1.533	0.003	8.6	204	1739	-140	1.55
CEP791	NR	0.033	1.534	0.006	7.1	217	1934	-145	1.57
CEP794	103	0.036	1.600	0.002	7.1	203	2060	-146	1.604
CEP796	NR	0.022	1.570	0.004	2.6	158	2221	-237	1.72
CEP790	NR	0.015	1.583	0.017	7.3	884	2099	-163	1.86

1313
1314
1315
1316

(a) Activity ratios determined after (Hellstrom, 2003) using the decay constants of (Cheng et al., 2000)
 (b) Age in kyr before present corrected for initial ²³⁰Th using eqn. 1 of (Hellstrom, 2006) and ²³⁰Th/²³²Th₀ of 0.9 ± 0.4
 (c) Initial ²³⁴U/²³⁸U calculated using corrected age

Sample ID	²³⁸ U (ppb)	²³⁵ U (ppt)	²³⁸ Th/ ²³² Th (atomic x10 ⁶)	²³⁸ U (measured) (°)	²³⁸ Th/ ²³² Th (corrected)	²³⁸ Th Age (yr) (uncorrected)	²³⁸ Th Age (yr) (corrected)	²³⁸ U/ ²³⁵ U (corrected)	²³⁸ Th Age (yr BP) (corrected)
Xer-0	431 ±1	12392 ±248	4.0 ±0.1	434.3 ±3.1	0.0066 ±0.0001	495 ±8	-52 ±387	454 ±3	-115 ±387
Xer-55	355 ±1	2875 ±58	4.2 ±0.2	434.3 ±2.9	0.0021 ±0.0001	159 ±8	-6 ±116	454 ±3	-69 ±116
Xer-85	299 ±1	1557 ±31	8 ±0	424.6 ±3.1	0.0027 ±0.0001	204 ±9	97 ±76	425 ±3	34 ±76
Xer-110	208 ±1	798 ±16	18 ±1	410.5 ±2.4	0.0029 ±0.0001	223 ±9	170 ±39	411 ±2	107 ±39
Xer-145	267 ±1	535 ±11	25 ±1	404.7 ±2.7	0.0030 ±0.0001	236 ±10	195 ±31	405 ±3	132 ±31
Xer-190	264 ±1	340 ±7	54 ±2	419.0 ±2.8	0.0043 ±0.0001	338 ±10	301 ±22	419 ±3	238 ±22
Xer-210	299 ±1	1445 ±29	20 ±1	420.8 ±2.5	0.0059 ±0.0002	452 ±12	353 ±71	421 ±3	290 ±71
Xer-280	277 ±1	1758 ±35	19 ±1	426.4 ±2.7	0.0072 ±0.0002	548 ±12	470 ±92	457 ±3	357 ±92
Xer-330	339 ±1	2459 ±50	2.0 ±0	414.7 ±2.8	0.0086 ±0.0001	667 ±10	517 ±106	415 ±3	454 ±106
Xer-410	505 ±1	4623 ±95	2 ±0	445.9 ±2.8	0.0027 ±0.0001	169 ±10	16 ±128	485 ±2	-46 ±128
Xer-440	470 ±1	1106 ±25	9 ±2	427.0 ±2.3	0.0019 ±0.0001	69 ±11	12 ±38	485 ±2	-46 ±38
Xer-50	413 ±1	1106 ±25	7 ±0	427.0 ±2.3	0.0019 ±0.0001	161 ±11	6 ±40	471 ±2	3 ±40
Xer-60	407 ±1	708 ±14	25 ±1	452.7 ±2.3	0.0025 ±0.0001	191 ±8	158 ±25	455 ±2	96 ±25
Xer-35	417 ±1	603 ±12	34 ±1	452.7 ±2.3	0.0025 ±0.0001	223 ±8	206 ±15	456 ±3	142 ±15
Xer-46	417 ±1	1049 ±21	23 ±1	461.4 ±3.8	0.0037 ±0.0001	274 ±8	242 ±24	462 ±4	179 ±24
Xer-60	395 ±1	3812 ±77	9 ±0	438.7 ±2.9	0.0051 ±0.0001	380 ±8	196 ±30	459 ±3	134 ±30
Xer-67	389 ±1	25715 ±517	4 ±0	438.0 ±2.5	0.0144 ±0.0002	1080 ±15	267 ±876	458 ±3	204 ±876
Xer-75	346 ±1	332 ±7	34 ±2	371.5 ±3.1	0.0020 ±0.0001	158 ±9	138 ±17	372 ±3	75 ±17
Xer-25	368 ±1	493 ±10	32 ±1	367.1 ±2.9	0.0026 ±0.0001	204 ±8	176 ±22	367 ±3	113 ±22
Xer-70	346 ±1	1262 ±25	17 ±1	367.8 ±2.4	0.0037 ±0.0001	298 ±8	221 ±56	368 ±2	158 ±56
Xer-74	319 ±1	226 ±5	70 ±5	368.6 ±2.7	0.0050 ±0.0001	240 ±9	225 ±14	369 ±2	162 ±14
Xer-30	3930 ±0.7	169 ±3	116 ±6	381.0 ±2.0	0.0050 ±0.0001	259 ±11	230 ±13	381 ±2	168 ±13
Xer-50	3429 ±1.0	609 ±12	47 ±2	381.2 ±2.0	0.0050 ±0.0001	398 ±12	300 ±29	382 ±3	298 ±29
Xer-58	3481 ±0.8	596 ±8	84 ±2	381.3 ±2.7	0.0058 ±0.0001	457 ±9	424 ±19	383 ±3	372 ±19
Las Grottes cave									
Las-0	1451 ±0.3	451 ±2	333 ±5	1465.3 ±3.4	0.0022 ±0.0001	130 ±14	166 ±26	1473 ±3	166 ±26
Las-1	1193 ±0.2	291 ±2	221 ±2	1467.0 ±3.1	0.0020 ±0.0001	110 ±14	166 ±26	1493 ±3	130 ±14
Las-45	1150 ±0.1	905 ±18	61 ±2	1510.8 ±3.1	0.0039 ±0.0004	1262 ±19	1171 ±67	1516 ±3	1108 ±67
Las-6	1077 ±0.2	852 ±17	5 ±1	1504.8 ±3.5	0.0033 ±0.0004	1107 ±20	185 ±63	1506 ±3	122 ±63
Las-8	1084 ±0.1	261 ±5	142 ±4	1504.6 ±3.6	0.0027 ±0.0004	905 ±17	877 ±26	1508 ±3	814 ±26
Las-11	692 ±0.1	2977 ±60	8 ±1	1505.3 ±3.7	0.0201 ±0.0006	877 ±26	379 ±383	1507 ±4	316 ±383
Las-10	113 ±1	2350 ±47	56 ±1	1859 ±4	0.0699 ±0.0006	269 ±23	2483 ±150	1872 ±4	2420 ±150
Las-55	88 ±1	539 ±11	127 ±3	1848 ±4	0.0469 ±0.0005	1806 ±18	1744 ±47	1857 ±4	1681 ±47
Las-10	131 ±0.2	388 ±8	213 ±5	1721.6 ±3.2	0.0382 ±0.0003	1540 ±16	1808 ±27	1729 ±3	1445 ±27
Las-11	81 ±1	95 ±19	50 ±1	1796 ±5	0.0359 ±0.0006	1407 ±23	1284 ±90	1803 ±5	1221 ±90
Las-15	73 ±0	282 ±6	118 ±3	1783 ±6	0.0279 ±0.0006	1098 ±22	1057 ±36	1789 ±6	994 ±36
Las-18	72 ±0	1477 ±50	16 ±1	1705 ±5	0.0202 ±0.0005	250 ±11	597 ±158	1708 ±5	534 ±158
Las-22	139 ±0	287 ±6	47 ±2	1524 ±5	0.0058 ±0.0002	810 ±22	216 ±50	1555 ±5	163 ±50
Balnear									
Bal-125: 56 mm	6083 ±27	797 ±16	49 ±2	238.5 ±2.5	0.0059 ±0.0002	59 ±3	54 ±5	239 ±2	9 ±5
Bal-125: 44 mm	6492 ±32	201 ±4	630 ±14	226.8 ±1.8	0.0119 ±0.0001	184 ±2	182 ±2	236 ±2	130 ±2
Bal-125: 57 mm	10059 ±41	616 ±19	392 ±9	228.1 ±2.3	0.0146 ±0.0001	224 ±2	182 ±2	236 ±2	189 ±2
Bal-125: 32 mm	754 ±51	1639 ±33	15 ±1	229.5 ±1.9	0.0058 ±0.0002	47 ±2	229 ±2	236 ±2	130 ±2
Bal-125: 52 mm	151 ±1	1663 ±33	15 ±1	294.3 ±1.5	0.0028 ±0.0001	32 ±3	312 ±28	295 ±1	240 ±27
Bal-125: 16 mm	838 ±31	385 ±8	1052 ±23	293.2 ±1.0	0.0029 ±0.0002	45 ±4	456 ±4	296 ±2	303 ±4
Bal-125: 10 mm	949 ±41	551 ±11	961 ±20	290.9 ±1.5	0.0038 ±0.0002	521 ±4	519 ±4	291 ±2	484 ±4
Bal-125: 0 mm	8128 ±33	649 ±15	884 ±18	290.2 ±1.9	0.0043 ±0.0002	660 ±4	657 ±5	291 ±2	584 ±5

U decay constants: $\lambda_{238} = 1.55125 \times 10^{-10}$ (Jaffar et al., 1971) and $\lambda_{235} = 2.82206 \times 10^{-10}$ (Cheng et al., 2013). The decay constant: $\lambda_{234} = 9.1705 \times 10^{-10}$ (Cheng et al., 2013).
 $^{238}\text{U} = (^{238}\text{U}/^{235}\text{U})_{\text{activity}} - 1 \times 10^{100}$.
 $^{238}\text{Th}/^{232}\text{Th}$ was calculated based on ^{238}Th age (T) i.e. $^{238}\text{Th}/^{232}\text{Th} = (^{238}\text{Th}/^{232}\text{Th})_{\text{present}} \times e^{-\lambda_{238} T}$.
 Corrected ^{238}Th ages assume the initial $^{238}\text{Th}/^{232}\text{Th}$ atomic ratio of $4.4 \pm 2.2 \times 10^{-6}$. Those are the values for a material at secular equilibrium, with the bulk earth $^{238}\text{Th}/^{232}\text{Th}$ value of 3.8. The errors are arbitrarily assumed to be 50%.
 **B.P. stands for "Before Present" where the "Present" is defined as the year 1950 A.D.

1317
1318

Sample	^{238}U (ppb)	$^{238}\text{Th}/^{238}\text{U}$	$^{235}\text{U}/^{238}\text{U}$	Pot and Fea cave			^{238}Th Age (yr) uncorrected	Age (yr BP) (b)	error	$^{238}\text{U}/^{238}\text{U}$ Initial (c)
				$^{232}\text{Th}/^{238}\text{U}$	$^{230}\text{Th}/^{238}\text{U}$	$^{230}\text{Th}/^{232}\text{Th}$				
CT-PP 7.5	109	0.022	1.570	0.0084	(a)	2.6	1508	746 ±193	1.572	
CT-PP 47	NR	0.013	1.563	0.0017	(a)	7.3	884	733 ±79	1.565	
CT-PP 95	NR	0.014	1.580	0.0015	(a)	9.1	956	822 ±82	1.581	
CT-PP 205	95	0.019	1.565	0.0017	(a)	11.0	1330	1176 ±68	1.567	
CT-PP 335	NR	0.030	1.533	0.0051	(a)	5.8	2117	1652 ±253	1.536	
CT-PP 400	131	0.029	1.533	0.0033	(a)	8.6	2041	1739 ±140	1.535	
CT-PP 510	NR	0.033	1.534	0.0046	(a)	7.1	2347	1934 ±145	1.537	
CT-PP 640	103	0.036	1.600	0.0052	(a)	7.1	2503	2060 ±146	1.604	
CT-PP 740	109	0.022	1.570	0.0084	(a)	2.6	1508	2221 ±217	1.572	
CT-PP 790	NR	0.013	1.563	0.0017	(a)	7.3	884	2099 ±463	1.565	

(a) Activity ratios determined after Helstrom (2003) using the decay constants of (Cheng et al., 2000)

(b) Age in kyr before present corrected for initial ^{230}Th using eqn. 1 of (Helstrom, 2006) and $[\text{Th}/\text{U}]_0$ of 0.9 ± 0.4

(c) Initial $[\text{Th}/\text{U}]_0$ calculated using corrected age

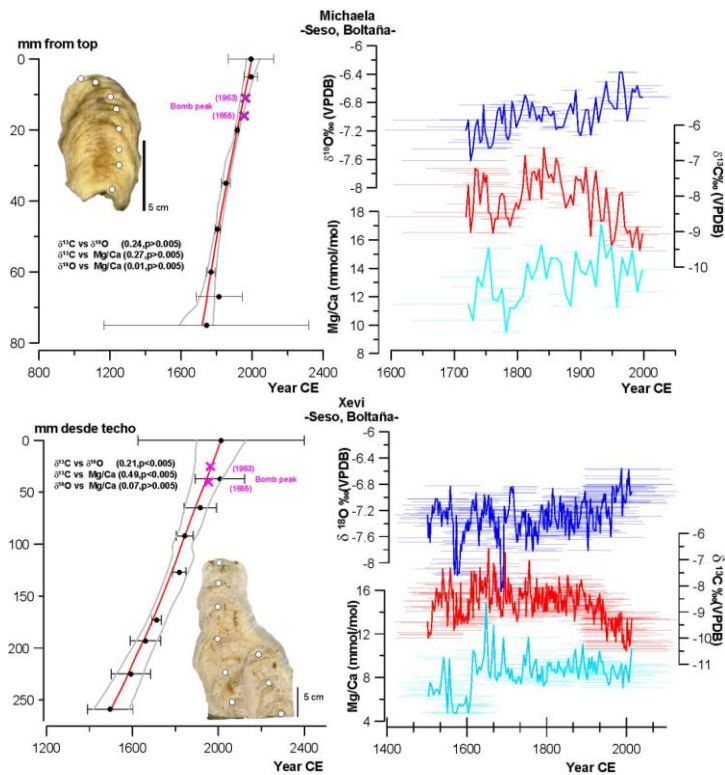
1319
1320
1321
1322

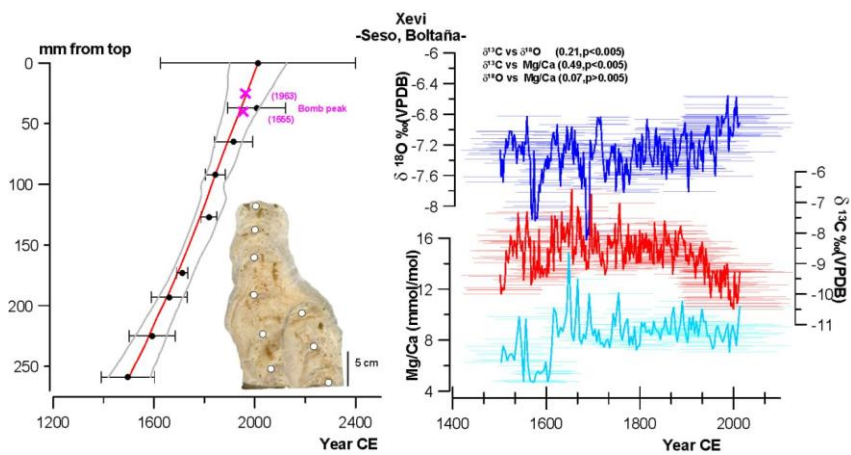
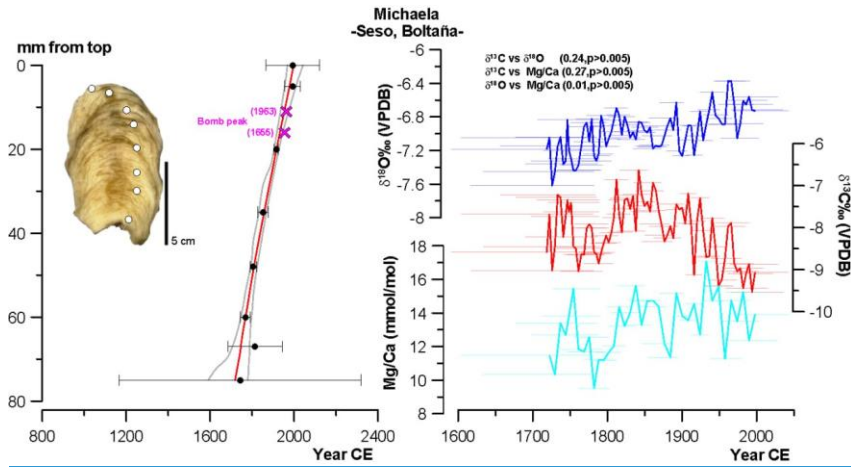
1323

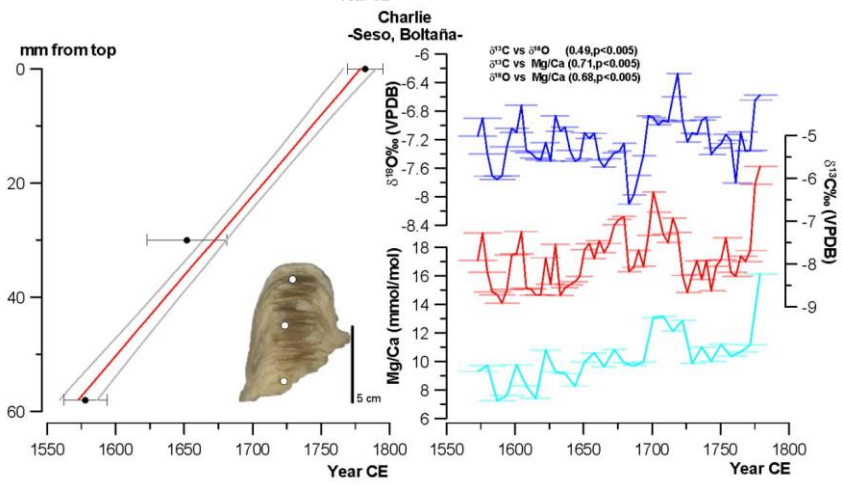
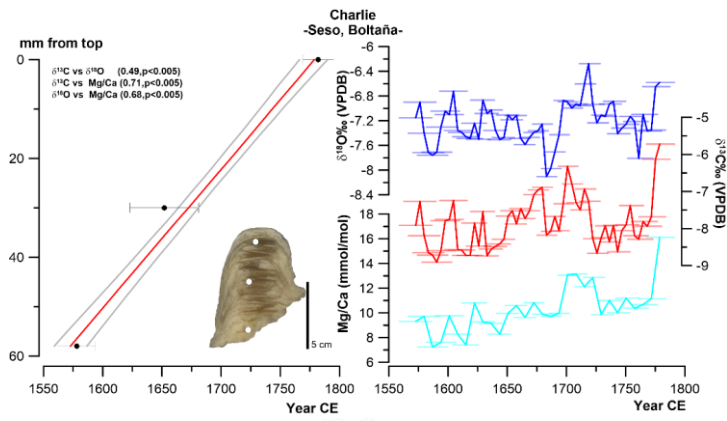
1324 **Appendix A**

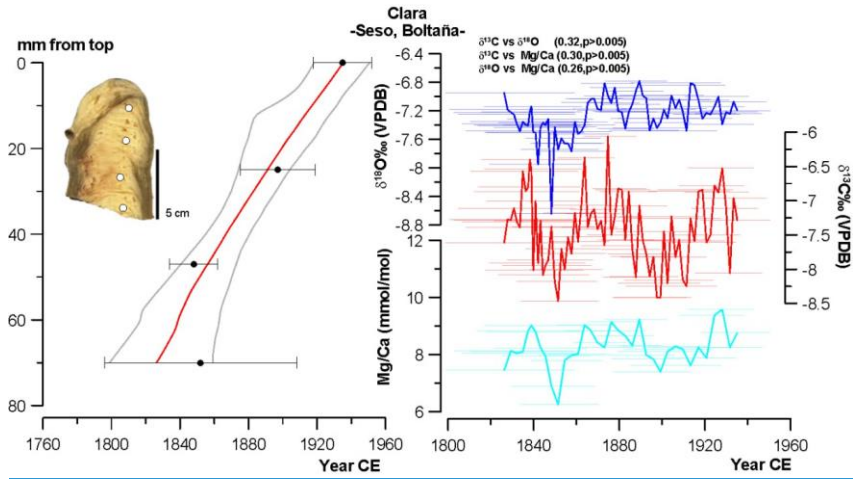
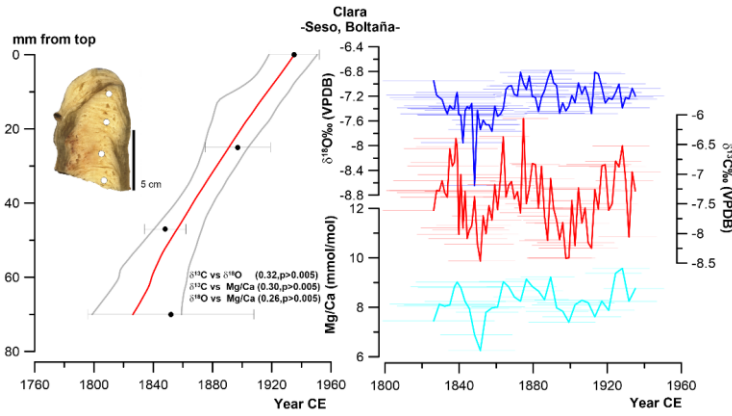
1325 **Figure A1.** Polished slabs, age-depth model using StalAge (left) and proxy profiles versus age (right) for
1326 the stalagmites used in this study arranged by cave (Aa. Seso, Bb. Las Gloces, Cc. B1, and Dd. Pot au Feu
1327 caves). Correlation coefficients among the three proxies are indicated based on Pearson correlation.
1328 Horizontal lines represent the age error for every data point, following StalAge uncertainty.

1329 Aa- Seso cave









1330 B

1331

1332

1333

1334

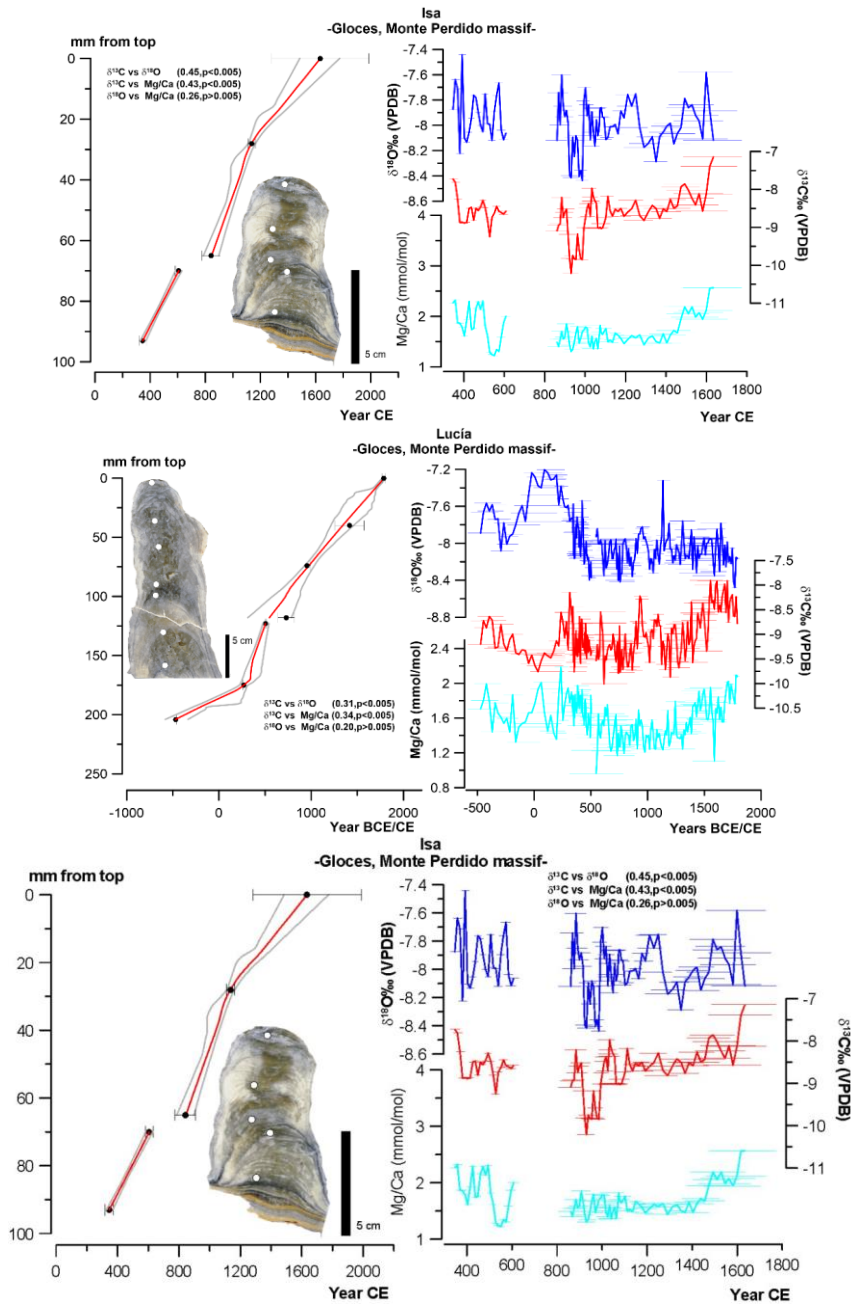
1335

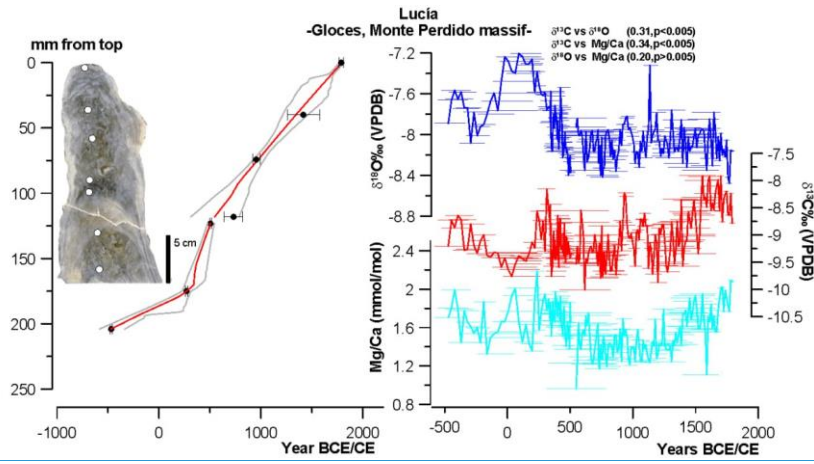
1336

1337

1338

1339 [b](#). Las Gloces cave





1340 e

1341

1342

1343

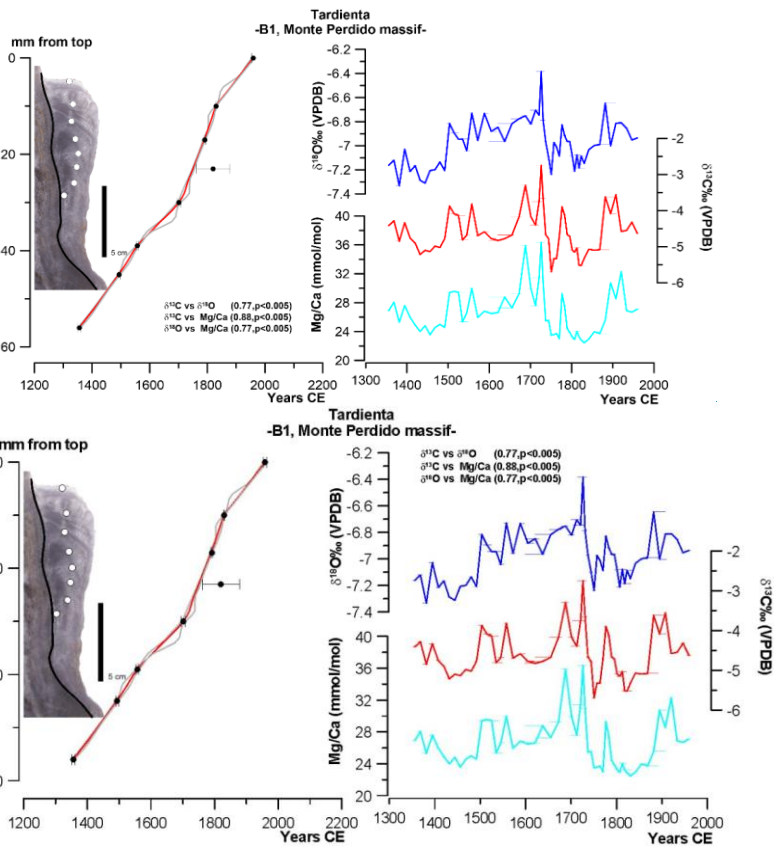
1344

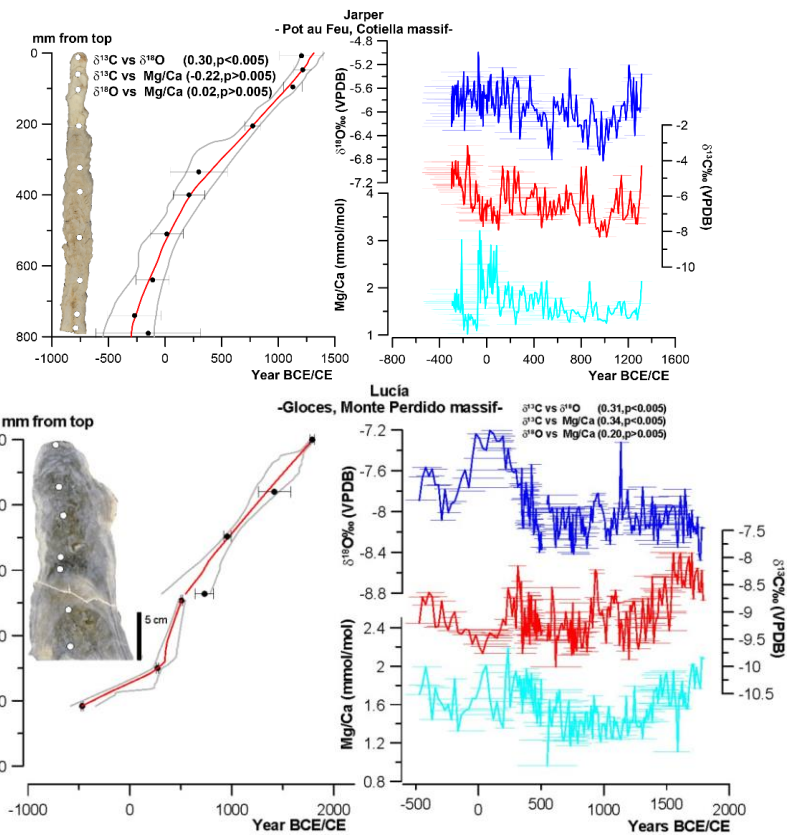
1345

1346

1347

1348 c. B1 cave





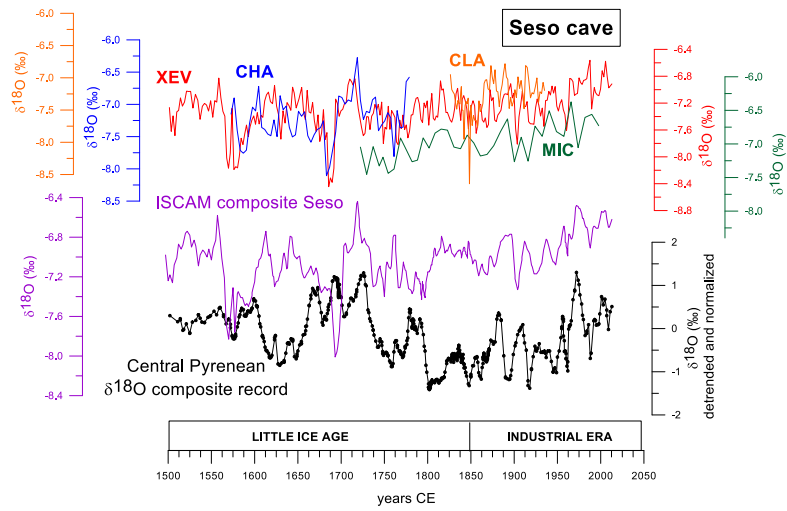
1350

1351

1352

1353 **Figure A2.** Construction of the composite $\delta^{18}\text{O}$ record for Seso cave. In the upper graph, the individual
1354 $\delta^{18}\text{O}$ profiles of the four Seso stalagmites are presented, using their StalAge models (XEV in red, CHA in
1355 blue, CLA in orange and MIC in green). Some records overlap (mostly between XEV and CHA and XEV
1356 and MIC). The composite $\delta^{18}\text{O}$ record for Seso cave is shown in purple on the same y-axis as the individual
1357 curves. The Central Pyrenees $\delta^{18}\text{O}$ composite record is shown at the bottom of the graph.

1358

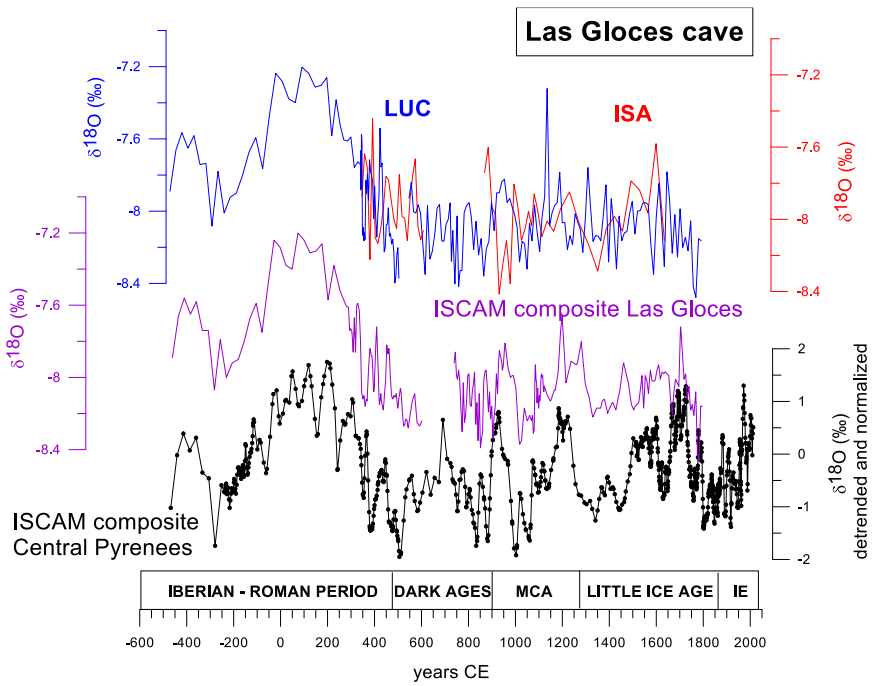


1359

1360

1361 **Figure A3.** Construction of the composite $\delta^{18}\text{O}$ record for Las Gloces cave. In the upper graph, the $\delta^{18}\text{O}$
1362 profiles of the two Las Gloces stalagmites are presented, using their StalAge models (ISA in red and LUC
1363 in blue). The composite $\delta^{18}\text{O}$ record for this cave is shown in purple curve on the same y-axis as the
1364 individual curves. The Central Pyrenees $\delta^{18}\text{O}$ composite record is shown at the bottom of the graph. MCA:
1365 Medieval Climate Anomaly, IE: Industrial Era.

1366

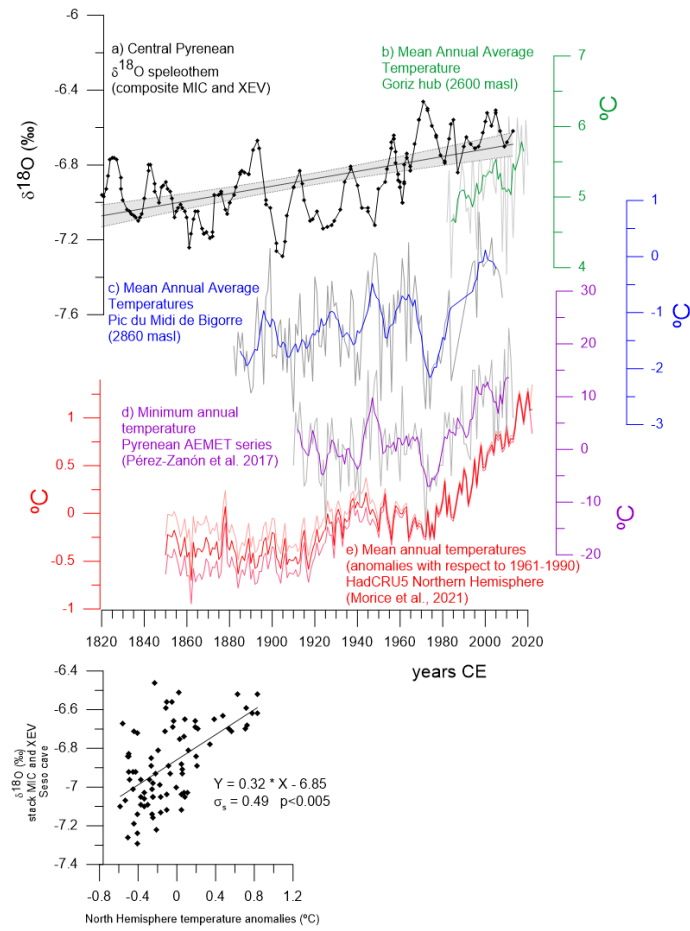


1367

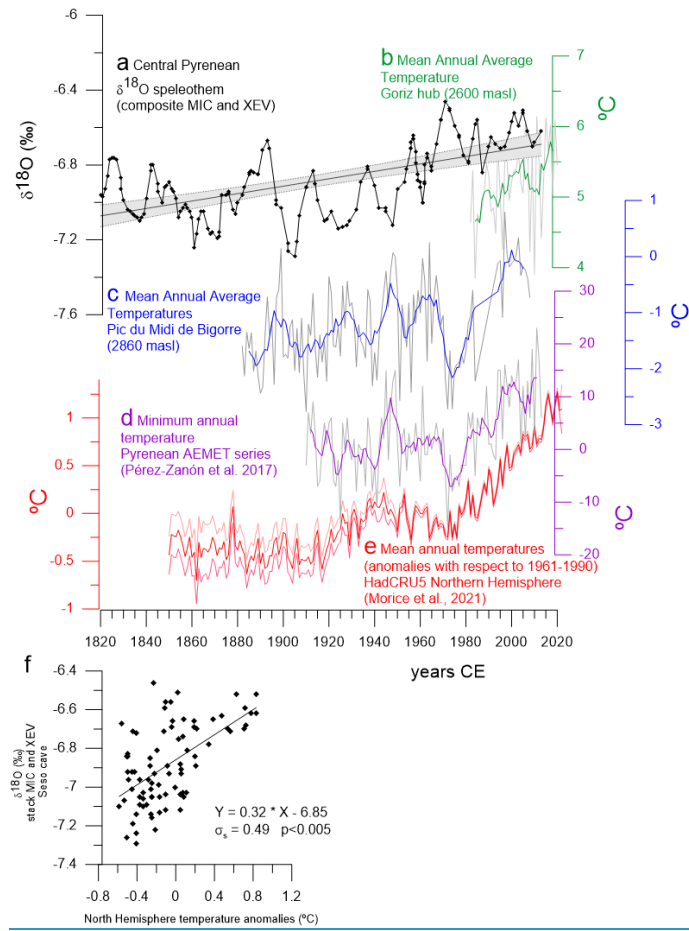
1368

1369

1370 **Figure A4.** Correlation of (a) composite $\delta^{18}\text{O}$ record from MIC and XEV stalagmites with instrumental
 1371 temperature records at local, regional and global levels. (b) Mean Annual Average Temperature (MAAT)
 1372 from Goriz hub (AEMET data); (c) MAAT from Pic du Midi de Bigorre (Bücher and Dessens, 1991;
 1373 Dessens and Bücher, 1995); (d) Minimum Annual Temperature from the Pyrenees from AEMET series
 1374 (Pérez-Zanón et al., 2017) and (e) MAAT anomalies (respect to 1961-1990 years) using the HadCRUT
 1375 5.0.1.0. dataset (Morice et al., 2021). At the bottom, $\delta^{18}\text{O}$ values of the Pyrenees composite record (in a)
 1376 compared to North Hemisphere mean annual temperatures (in e) showing a significant correlation.



1377



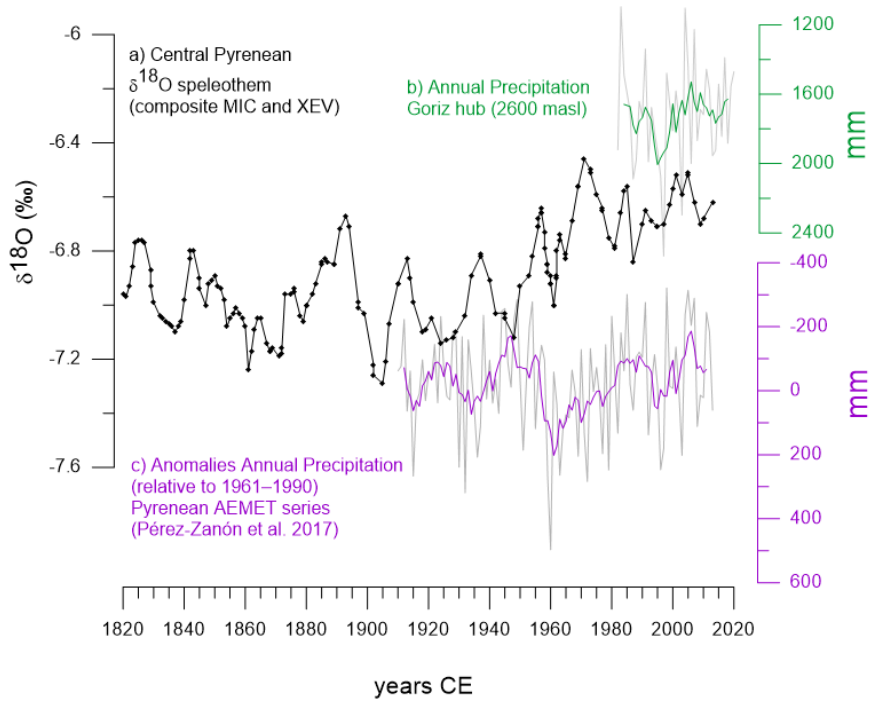
1378

1379

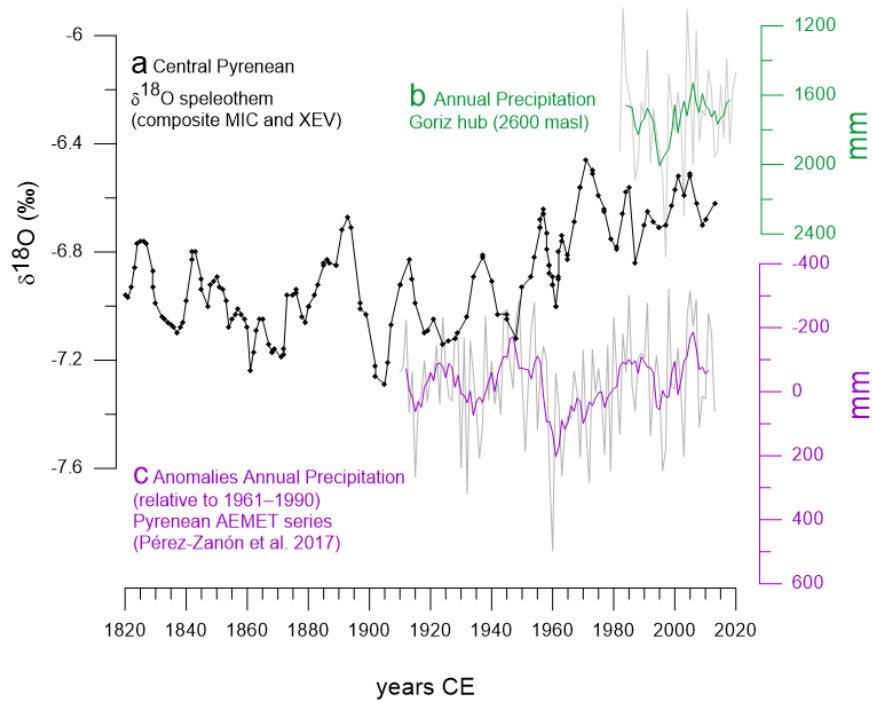
1380

1381 **Figure A5.** Correlation of (a) composite $\delta^{18}\text{O}$ record from MIC and XEV stalagmites with instrumental
1382 precipitation records at regional levels. (b) Annual precipitation from Goriz hub (AEMET data) and (c)
1383 Precipitation anomalies from the Pyrenees from AEMET series (respect to 1961-1990 years) (Bücher and
1384 Dessens, 1991; Dessens and Bücher, 1995). No significant correlation is observed.

1385



1386



1387

1388